# THE VERTICAL DISTRIBUTION OF COPEPODS IN BEDFORD BASIN AND ITS RELATIONSHIP WITH PHYSICAL VARIABLES WITH PARTICULAR EMPHASIS ON SMALL-SCALE TURBULENCE

by

Candace Deanne Smith

Submitted in partial fulfillment of the requirements
for the degree of Master of Science

at

Dalhousie University
Halifax, Nova Scotia
October 2012

DALHOUSIE UNIVERSITY

DEPARTMENT OF OCEANOGRAPHY

The undersigned hereby certify that they have read and recommend to the Faculty of Graduate Studies for acceptance a thesis entitled "THE VERTICAL DISTRIBUTION OF COPEPODS IN BEDFORD BASIN AND ITS RELATIONSHIP WITH PHYSICAL VARIABLES WITH PARTICULAR EMPHASIS ON SMALL-SCALE TURBULENCE" by Candace Deanne Smith in partial fulfillment of the requirements for the degree of Master of Science.

Dated: October 26, 2012

External Examiner: _____

Supervisor: _____

Readers: _____

_____

DALHOUSIE UNIVERSITY

DATE: October 26, 2012

AUTHOR: Candace Deanne Smith

TITLE: THE VERTICAL DISTRIBUTION OF COPEPODS IN BEDFORD BASIN AND ITS RELATIONSHIP WITH PHYSICAL VARIABLES WITH PARTICULAR EMPHASIS ON SMALL-SCALE TURBULENCE

DEPARTMENT OR SCHOOL: Department of Oceanography

DEGREE: M.Sc. CONVOCATION: May YEAR: 2013



_____

Signature of Author

*To my parents and my John, who always believed I could do anything, especially in those moments when I didn't.*

# TABLE OF CONTENTS

# LIST OF TABLES

# LIST OF FIGURES

# ABSTRACT

In the autumn of 2010 a novel free-falling profiler was deployed in attempt to measure, quantify and understand the vertical distribution of copepods in Bedford Basin, with particular emphasis on the effects of small-scale turbulence. Coincident measurements of high-resolution copepod abundance, depth, temperature, salinity, density, buoyancy frequency and turbulent dissipation rates were collected. Data for light, tide and winds were also available on a larger space and time scale. The results suggest that the distribution of copepods in Bedford Basin is not affected by turbulence and is mainly controlled by temperature, salinity and density, while the large scale copepod abundance is controlled by light and tides.

# List of Abbreviations and Symbols Used

| Roman symbol | Description | Units |
|---|---|---|
| $C_k$ | Kolmogorov constant | unitless |
| $D$ | depth bin | $\mathrm{m}$ |
| $\frac{D}{Dt}$ | material derivative | $1/\mathrm{s}$ |
| $d$ | degrees of freedom | unitless |
| $\frac{\partial u'}{\partial z}$ | vertical gradient of turbulent fluctuations in x direction | $1/\mathrm{s}$ |
| $\frac{d\vec{u}}{dt}$ | local acceleration | $\mathrm{m/s^2}$ |
| $E(k)$ | energy in wavenumber space | $\mathrm{m^3/s^2}$ |
| $E_e$ | scaling energy in wavenumber space | unitless |
| $E_i$ | expected number of observations in bin $i$ | unitless |
| $e'_{ij}$ | strain rate for turbulent fluctuations (tensor notation) | $\mathrm{m/s^2}$ |
| $g$ | acceleration due to gravity | $\mathrm{m/s^2}$ |
| $k$ | wavenumber | $\mathrm{cpm}$ |
| $L$ | characteristic length scale | $\mathrm{m}$ |
| $L^*$ | copepod prosome length | $\mathrm{mm}$ |
| $k_c$ | wavenumber at length scale c | $\mathrm{cpm}$ |
| $k_\eta$ | Kolmogorov wavenumber | $\mathrm{cpm}$ |
| $N$ | number of frames per metre | $\mathrm{frames/m}$ |
| $N^2$ | buoyancy frequency | $1/\mathrm{s^2}$ |
| $O_i$ | observations in bin $i$ | unitless |
| $P$ | pressure | $\mathrm{Pa}$ |
| $\overline{P}$ | pressure of mean flow | $\mathrm{Pa}$ |
| $p'$ | pressure of flow from turbulent fluctuations | $\mathrm{Pa}$ |
| $R^2$ | coefficient of determination | unitless |
| $R_a^2$ | adjusted coefficient of determination | unitless |
| $Re$ | Reynold's number | unitless |
| $S_{obs}(k)$ | shear signal | $\mathrm{s^{-2}cpm^{-1}}$ |
| $S_{th}(k)$ | noise signal | $\mathrm{s^{-2}cpm^{-1}}$ |

| Roman symbol | Description | Units |
|---|---|---|
| $T_0$ | temperature of total flow | °C |
| $T'$ | temperature of flow from turbulent fluctuations | °C |
| $\overline{T}$ | temperature of mean flow | °C |
| $U$ | characteristic velocity | $\mathrm{m/s}$ |
| $u$ | velocity shear | $\mathrm{m/s}$ |
| $u'$ | velocity due to turbulent fluctuations | $\mathrm{m/s}$ |
| $\vec{u}$ | velocity of flow (vector in 3 dimensions) | $\mathrm{m/s}$ |
| $\tilde{u}$ | velocity of total flow | $\mathrm{m/s}$ |
| $\overline{u}$ | velocity of mean flow | $\mathrm{m/s}$ |
| $V$ | value of variable in depth bin D | ex: °C |
| $V\_S$ | volume of water sampled per metre | $\mathrm{m}^3$ |
| $v$ | Kolmogorov velocity | $\mathrm{m/s}$ |
| $v\_camera$ | volume sampled by camera per frame | $\mathrm{m}^3$ |
| $W$ | width of copepod | $\mathrm{mm}$ |
| $\overline{w}$ | mean velocity in z-direction | $\mathrm{m/s}$ |
| $x_i$ | $i^{th}$ $x$ value (tensor notation) | $\mathrm{m}$ |
| $y$ | ratio of shear to Nasmyth signals | unitless |
| $\overline{y}$ | mean of $y$ | unitless |

| Greek symbol | Description | Units |
|---|---|---|
| $\alpha$ | thermal expansion coefficient | 1/ °C |
| $\beta$ | energy constant | unitless |
| $\delta_{i3}$ | Kronecker delta (tensor notation) | unitless |
| $\varepsilon$ | turbulent dissipation rate | $\mathrm{W/kg}$ |
| $\eta$ | Kolmogorov length scale | $\mathrm{m}$ |
| $\mu$ | dynamic viscosity of water | $\mathrm{Pas}$ |
| $\nu$ | dynamic viscosity | $\mathrm{m}^2/\mathrm{s}$ |
| $\rho$ | density | $\mathrm{kg/m}^3$ |
| $\rho_0$ | average density of seawater | $\mathrm{kg/m}^3$ |
| $\rho'$ | density of flow from turbulent fluctuations | $\mathrm{kg/m}^3$ |
| $\phi(k)$ | energy in wavenumber space | $\mathrm{s}^{-2}/\mathrm{cpm}$ |
| $\phi_i$ | shear energy in wavenumber space | $\mathrm{s}^{-2}/\mathrm{cpm}$ |

| Greek symbol | Description | Units |
|---|---|---|
| $\phi_s$ | Nasmyth spectra in wavenumber space | $\mathrm{s}^{-2}/\mathrm{cpm}$ |
| $\chi^2$ | Chi-sqaured test statistic | unitless |
| $\Omega$ | angular velocity due to Coriolis force | 1/s |

| Abbreviations | |
|---|---|
| C.G.S | Coast Guard Ship |
| cpm | Cycles Per Metre |
| CT | Conductivity, Temperature |
| DVM | Diel Vertical Migration |
| GPS | Global Positioning System |
| MAD | Median Absolute Deviation |
| MATLAB | MATrix LABoratory |
| MD | Mean Depth |
| O($10^n$) | Order of magnitude |
| psu | Practical Salinity Units |
| ROI | Region Of Interest |
| SNR | Signal to Noise Ratio |
| UTC | Coordinated Universal Time |
| VMP | Vertical Microstructure Profiler |
| VMP/VPR | Vertical Microstructure Profiler and Video Plankton Recorder |
| VPR | Video Plankton Recorder |

# ACKNOWLEDGEMENTS

I would first like to thank my sampling team, Walter Judge and Matt Hatcher, who along with me and a lot of patience, had to learn the ins and outs of the VMP/VPR. Thanks goes out to Ed Horne for finding me sampling time in Bedford Basin, as well as others who helped from BIO: Kevin Pauly, Jeff Spry, and Rick Starr and Chuck Hamilton of the *Sigma T*. Even though the data were not used in this thesis I would like to thank the Captain and Crew of the *Dominion Victory* for hosting my first cruise as part of the Taggart Lab. Many thanks to my colleagues (and now my friends), who helped me with everything from analysing copepods to using LaTex to helping me debunk statistics: Franciska Broell, Mike Brown, Dr. Kim Davies, Mathieu Dever Colette Feehan, Dr. Simon Higginson, Jenna Hare, Michelle Lloyd, Beth MacEachern, Justine McMillan, Dr. Paul Mattern, Dr. Eric Oliver, Dr. Clark Richards, Shiliang Shan, Tara Tapics and Jessica Wong. Thanks to Jackie Hurst for her administrative support, moral support and chocolate-fix-needed support. Thanks to Daniel Morrison for saving my data and thesis on at least three different occasions. Thanks to Barry Ruddick for insights during my proposal stage. Thanks to Dr. Ian McLaren for help with copepod analysis. I'd like to thank my brother TJ and his girlfriend Courtney for making my nephew Nash, without whom I would not have smiled in the past few months finishing my thesis. Thanks to my parents for their on-going support of me becoming a professional student. Thanks to my boyfriend John MaGee who had to listen to me complain about MATLAB, turbulence and copepods for three years.

Thanks to Dan Kelley and Chris Taggart for all their support, insights, help and questions with regards to my thesis over the years.

Especial thanks to three of my closest friends and classmates who started this journey with me: Lindsay Brager, Will Burt and Mike Fraser, who not only helped me get through classes but who have been there with me every step of the way. This would not have been possible without their support, as well as their mutual agony.

Finally, I can not thank Tetjana enough for everything. For this opportunity, for the support, advice and criticisms, for thoroughly reading my thesis (many times) while on sabbatical, for her patience with me and every other duty she has went above and beyond to fulfil as an advisor.

# CHAPTER 1

# INTRODUCTION

## 1.1 Motivation

The ocean is a vast and complex environment, governed by physical, biological and chemical processes across a range of space and time scales. To fully understand the ocean at large scales, focus must be placed on studying the small scales and determining how the small scale processes affect the large scale properties of the ocean. An important question, with possible impacts on transoceanic ecosystems, is the relationship between zooplankton and their physical environment. Much of the study of biophysical relationships has focused on copepods, the most abundant animal in the ocean (*Johnson and Allen*, 2005), which are a key component of many marine food webs. Copepods live in a dynamic, three-dimensional world, with the vertical dimension possibly the most important (*Clarke*, 1934). Thus I question which physical factors affect the vertical distribution and abundance of copepods.

My tool of choice is the Vertical Microstructure Profiler/ Video Plankton Recorder (VMP/VPR), a novel instrument that captures images of plankton within the water column, as well as high-frequency physical data: depth, temperature, salinity, density, buoyancy frequency and turbulent dissipation rates. Based on the measurement capabilities of this new instrument and past literature, an explorative study of the vertical distribution of copepods based on local physical factors has been completed with the intention to determine how the distribution of copepods may be influenced by a suite of physical factors. Particular focus was placed on determining if turbulent dissipation rates have an effect on the distribution of copepods because this instrument is designed to study the biophysical relationship between zooplankton and turbulence and many recent studies focus on this particular relationship.

Along with the depth, temperature, salinity, density and turbulence measurements, other potential physical factors, such as light, winds and tides have been included in this study based on 1) the availability of these data and 2) past literature linking these variables to the vertical distribution of copepods.

## 1.2 Turbulence

There has been much discussion in the literature on how turbulence affects copepods since *Rothschild and Osborn* (1988) suggested that heightened turbulence would cause more encounters between zooplankton and their prey or mates, hence more feeding and mating opportunities. Before summarizing the current literature on how turbulence effects the vertical distribution of copepods, I provide a review of turbulence theory and how it is measured in the ocean.

Small-scale turbulence is classically approached by considering energy transfer. Turbulence spans a broad length scale, from large oceanic eddies to a microscale. This project is focused on the small-scale end of the energy spectrum since these are the scales most likely to affect the vertical distribution of copepods. Eddies can be considered the largest scale of oceanic turbulence (up to O$(10^5)$ m scales) and have the most energy. Without an external force to supply the eddy with energy, it will decay via an energy cascade from the large eddy scale to a small length scale called the Kolmogorov length scale ($\eta$). There is negligible variability in the velocity at scales smaller than $\eta$ because at $\eta$, the turbulent kinetic energy of the eddies is dissipated into heat by the viscosity of the water. Kolomogorov related the Kolmogorov length scale, $\eta$, to both $\varepsilon$ and the viscosity $\nu$:

$$\eta = \left(\frac{\nu^3}{\varepsilon}\right)^{1/4} \tag{1.1}$$

Where $\nu$ is the kinematic viscosity ($\mathrm{m}^2/\mathrm{s}$). The rate that energy is transferred from kinetic to internal, per unit mass, is called the turbulent dissipation rate, $\varepsilon$, and is used to quantify turbulence. Assuming isotropy, the turbulent dissipation rate is calculated via Equation 1.2.

$$\varepsilon = \frac{15}{2}\nu\overline{\left(\frac{\partial u'}{\partial z}\right)^2} \tag{1.2}$$

Where $u'$ is the turbulent velocity of the flow ($\mathrm{m/s}$), which is zero meaned. Hence the $\overline{\left(\frac{\partial u'}{\partial z}\right)^2}$ term is the variance in the turbulent shear. The units of $\varepsilon$ are $\mathrm{W/kg}$. Shear microstructure, i.e. the $\frac{\partial u'}{\partial z}$ term in $\overline{\left(\frac{\partial u'}{\partial z}\right)^2}$, has been measured successfully in the ocean via two methods: the hot-film anemometer and the shear probe (*Lueck et al.*, 2002). For this project, two shear probes were used.

Refer to Appendix A for a more detailed mathematical treatment of Equation 1.2 (*Kundu and Cohen* (2008) and *Baumert et al.* (2005)).

### 1.2.1 The Turbulent Energy Spectrum

At the large eddy scale, turbulent energy is produced (through breaking waves, winds, etc.) and at the Kolmogorov length scale, the turbulent energy is dissipated. The range in between is called the inertial subrange (*Kundu and Cohen*, 2008). Kolmogorov concluded that the 3-dimensional representation of the turbulent energy spectrum has the form:

$$E(k) = C_k \varepsilon^{2/3} k^{-5/3} \tag{1.3}$$

where $E(k)$ is the energy in the spectrum, in wavenumber space, $C_k$ is the Kolmogorov constant, determined experimentally to be between $1.4$ and $2.2$ and $k$ is the wavenumber associated with the length scale ($l$) of the eddy ($l = \frac{2\pi}{k}$). Equation 1.3 is Kolmogorov's famous $\frac{-5}{3}$ law and is shown graphically in Figure 1.1.

The low wavenumber range represents the large length scale of turbulence, the eddies. The energy spectrum at low wavenumbers is separated from the wavenumbers in the inertial sub-range via $k_c$. High wavenumbers represent the smallest scales of turbulence $\eta$, and the inertial sub-range is the slowly-varying curve (labelled $k^{-5/3}$ in Figure 1.1) connecting the two extremes.

For his PhD dissertation, *Nasmyth* (1970) conducted two experiments using velocity microstructure to compare with Kolmogorov's energy spectrum for isotropic turbulence (Equation 1.3). Nasmyth used velocity microstructure probes to calculate $\varepsilon$, whereas my study used data from shear probes. Nasmyth's work led to an empirical wave energy spectrum for turbulence energy that is now used to verify and correct poorly resolved shear measurements. Further discussion of this method is found in Chapter 2.

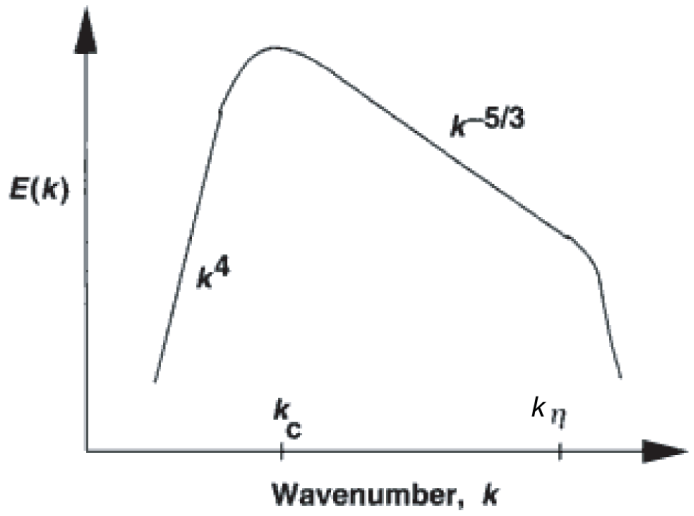


Figure 1.1: The turbulent energy spectrum from *Baumert et al.* (2005). The x-axis represents the wavenumber, $k = 2\pi/L$, where $L$ is the length scale of an eddy. The y-axis represents the energy spectrum at wavenumber $k$. From low wavenumbers up to $k_c$ ($k_c$ separates the energy at the large eddy scale from the energy in the inertial sub-range), $E(k)$ increases as a function of $k^4$. From $k_c$ to $k_\eta$ ($k_\eta$ separates the energy at the dissipation scales from the energy in the inertial sub-range), $E(k)$ changes as a function of $k^{\frac{-5}{3}}$. The Kolmogorov wavenumber is $k_\eta = \frac{2\pi}{\eta}$, where $\eta = (\frac{\varepsilon}{\nu^3})^{1/4}$ is the Kolmogorov length scale.

## 1.3 The Copepods of Bedford Basin

Here I discuss the five most abundant copepod species in Bedford Basin and review the factors that have been shown to affect the vertical distribution of those five species.

The dominant copepod species in Bedford Basin are *Pseudocalanus minutus*, *Oithona similis*, *Acartia hudsonica*, *Temora longicornis* and *Eurytemora herdmani* (*Li and Harrison*, 2008).

Out of the five most abundant copepod species in Bedford Basin, *Oithona similis* is the smallest, between 0.4 - 0.5 $\mathrm{mm}$ (males) and 0.5 - 0.6 $\mathrm{mm}$ (females) in length. *O. similis* are sink-and-hop swimmers, and are known as relatively weak swimmers. They feed by waiting motionlessly for motile prey. Copepods that feed this way are known as ambush predators (*Johnson and Allen*, 2005).

*Acartia hudsonica* is a small copepod (1 - 1.3 $\mathrm{mm}$ females and 1 - 1.1 $\mathrm{mm}$ males) and are vertical migrators. Adults can feed both on immobile particles (via suspension

feeding using currents) and on microzooplankton (ambush feeding). Their swimming style is normally sink-and-hop (like *O. similis*) (*Johnson and Allen*, 2005).

*Pseudocalanus minutus* is a mainly herbivorous copepod species, again a small copepod, with females 0.9 - 1.5 $\mathrm{mm}$ and males 0.8 - 1.2 $\mathrm{mm}$. *P. minutus* are propulsion swimmers that occasionally leap or jump as an escape reaction and they suspension feed using feeding currents (*Johnson and Allen*, 2005).

*Eurytemora herdmani* is another filter feeding copepod whose swimming style is presumably similar to other filter feeders via propulsion. Females of this species tend to be between 1.5 - 1.6 $\mathrm{mm}$ and males 1.2 - 1.5 $\mathrm{mm}$ (*Johnson and Allen*, 2005).

*Temora longicornis* is a relatively large copepod for Bedford Basin; females are usually 1 - 1.5 $\mathrm{mm}$ and males 1 - 1.8 $\mathrm{mm}$. They filter feed and also propulsion swim with infrequent jumps during escapes (*Johnson and Allen*, 2005).

Diel vertical migration (DVM) has been studied and reported for all five of the dominant species in Bedford Basin: *A. hudsonica* (*Bollens et al.*, 1994), *T. longicornis* (*Dam and Peterson*, 1993), *P. minutus* (*Frost and Bollens*, 1992), *E. herdmani* (*McLaren*, 1963) and *O. similis* (*Pinkerton et al.*). Copepods that exhibit DVM behaviour stay at depth during the day, presumably to avoid predators that use vision to feed, and return to the surface at night to feed (*Corkett and McLaren*, 1978). The main sources of the copepod population in Bedford Basin are local production and currents, generated by tides or winds, carrying copepods into the basin. Some of the main sinks for the Bedford Basin copepod population are mortality (including grazing by predators) and currents carrying copepods out of the basin.

### 1.3.1 The Factors that Affect Vertical Distribution of Copepods in Bedford Basin

Previous observational evidence suggests the vertical distribution of copepods in Bedford Basin will be affected by predation (causing DVM via a response to light), feeding, salinity, temperature and turbulence.

#### 1.3.1.1 Predation, Depth and Light

The most common form of predator avoidance by copepods is diel vertical migration (DVM). If copepods exhibit DVM, their vertical distribution will be altered on a daily basis, usually triggered by sunlight. *Bollens et al.* (1994) conducted a field manipulation

experiment testing the effect of predator avoidance, light cues and chemical cues on the vertical migration of *A. hudsonica*. This study showed that *A. hudsonica* displayed DVM triggered by light but chemical cues from predators did not induce escape reactions.

Other factors can cause a change in the vertical distribution of copepods. *Corkett and McLaren* (1978) reviewed two other vertical migration patterns of *Pseudocalanus* spp. The first was ontogenetic migration, where younger nauplii stages are concentrated deeper in the water column and copepodites (the copepod stage between nauplii and adult) are more commonly found near the surface. They also summarized seasonal vertical distributions, where copepods stay at depth over a season after feeding (active diapause), which is now well known in *Pseudocalanus* spp.

#### 1.3.1.2 Food Distribution and Feeding

The location and abundance of copepods' food source may also affect their vertical distribution. In a field experiment located near Nova Scotia's southern shelf break, *Herman et al.* (1981) sampled copepod species: *Calanus finmarchicus*, *Metridia lucens*, *Pseudocalanus minutus* and *Clausocalanus arcuicornis* as well as chlorophyll (Chl a, indicative of phytoplankton distributions, the main food source of copepods), temperature, salinity and depth. They concluded that copepods are distributed within 10 $\mathrm{m}$ of the maximum chlorophyll gradient (though not at the maximum), suggesting that the vertical distribution of copepods may be affected by their food distribution. *Dam and Peterson* (1993) also tested whether copepods were distributed with respect to their food source using in-situ measurements of *T. longicornis* distributions in Long Island Sound, United States. They saw no clear relationship between the vertical distribution of chlorophyll and *T. longicornis* distributions.

Other studies have been conducted to determine if copepods react to food distributions based on the dissolved chemical signature left by phytoplankton in the water. Copepods that use feeding currents respond to chemical cues from their prey. This was shown in laboratory experiments by *Poulet and Marsot* (1978) for both *E. herdmani* and *A. hudsonica* and by *Buskey* (1984) for *P. minutus*. In another laboratory experiment, however, *Svensen and Kiørboe* (2000), showed that the hop-and-sink swimmer *O. similis* did not respond to chemical cues from food, suggesting that hop-and-sink swimmers do not benefit from chemical cues from prey.

#### 1.3.1.3 Water Mass Properties

Many field studies focus on the relationship between the vertical distribution of copepods and the vertical distribution of water mass properties. In one of the papers summarized by *Corkett and McLaren* (1978), it was suggested that *Pseudocalanus* spp. avoid waters with temperatures greater than 23 °C, suggesting temperature plays an important role in their vertical distribution.

Most of the abundant Bedford Basin species prefer high salinity waters. *Jeffries* (1962) suggested *E. herdmani* are numerically dominant in waters with salinity greater than 10 ppt. *Johnson and Allen* (2005) state both *A. hudsonica* and *O. similis* prefer 'high salinity water' though they do not quantify high salinity.

*Reiss et al.* (2002) sampled the vertical distribution of copepods (*Centropages sp.*, *Pseudocalanus sp.*, *Paracalanus sp.*, *Clausocalanus sp.*, *Microcalanus sp.*, *Microstella norvegica* and *Temora longicornis*) along with data pertaining to stratification and mixing. They concluded that the vertical distribution of copepods is highly correlated with the pycnocline depth, suggesting that density is important to vertical distribution of copepods. In another field study in the southern part of the Kattegat between Denmark and Sweden, *Tiselius et al.* observed a relationship between the vertical distribution of copepods and density. Most of the copepods found were *Oithona* spp. and the depths of both of the adult and copepodite stages were correlated with the pycnocline depth (copepodites found just above the pycnocline and adults within the pycnocline).

Conversely, *Gallager et al.* (2004) in a field program conducted on George's Bank, observed that *Pseudocalanus* spp.were always located well below a buoyancy frequency of $N^2 = 1.25 \cdot 10^{-4}\ 1/\mathrm{s}^2$, suggesting these species avoided relatively high buoyancy frequencies. Since $N^2 = g^2 \frac{\partial \rho_o}{\partial p}$ is a measure of pycnocline strength, this suggests *Pseudocalanus* spp. were avoiding the pycnocline.

#### 1.3.1.4 Effects of Turbulence on the Vertical Distribution of Copepods

**Theoretical effects of turbulence on the vertical distribution of copepods**

*Rothschild and Osborn* (1988) hypothesized that encounter rates between predators and prey would increase in higher levels of turbulence. As zooplankton would encounter more prey in high turbulence environments, they would find more to eat in the same absolute prey concentration.

Subsequently, authours suggested that very high rates of turbulence would not allow sufficient time for zooplankton to react, thus removing any benefit from higher encounter rates. This led to the idea of an Optimal Production Window (from *Cury and Roy* (1989)), which is illustrated in Figure 1.2. The peak of the curve represents the level of turbulence that will optimize population production. For copepods, this level would allow the most effective feeding and/or mating encounters, hence their population production would be at a maximum. Levels of turbulence higher than the Optimal Production Window could limit the ability of copepods to react to food or mates and lower turbulence levels could decrease encounter rates with prey or mates, in both cases lowering the production.

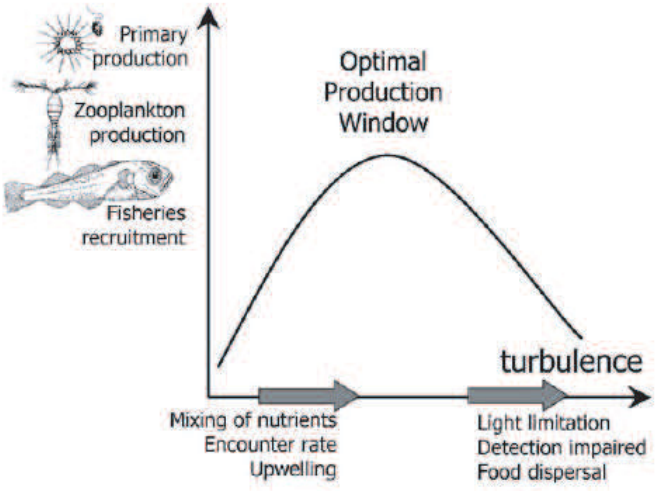


Figure 1.2: Optimal turbulence window idea as summarized in *Visser and Stips* (2002). The x-axis represents increasing turbulence (theoretical). The y-axis represents the population production for plankton. The theory predicts that the production will follow a dome-shaped curve as turbulence increases. At low turbulence, there would be less encounters between copepods and their mate or food, hence less overall production. At high turbulence, the copepods' detection of mates or food would be impaired, lowering the production. Theory suggests that there is an optimal turbulence window (at the peak of the curve) where copepods would have the highest population production, where turbulence is intermediate.

**In situ observations of effects of turbulence on the vertical distribution of copepods**

In a field study designed to study how the vertical distribution of copepods changes based on whether the water column is stratified or homogenized, *Lagadeuc et al.* (1997) concluded that copepods were not evenly distributed throughout the water column when the

water column is mixed (relatively high $\varepsilon$). During both stratification and homogenization of the water column, the zooplankton were stratified. During a wind event that occurred whilst sampling, the water column became homogenized from mixing (heightened turbulence). Following nixing, nauplii stages of copepods, stratified during water column stratification, became evenly distributed within the water column. The adult stages of the copepods, however, remained stratified. *O. similis* did not change its vertical position between the stratified and mixed water column, while *T. longicornis* and *Pseudocalanus* spp. migrated downwards, to a position that was less mixed (relatively lower $\varepsilon$). Though they suggest that some copepods react negatively to increased winds (and turbulence), they recommend complimentary studies to clarify which mechanisms control the vertical distribution of copepods.

*Incze et al.* (2001) inferred that copepods avoided turbulence levels higher than they had experienced before a storm ensued. Initially, they found copepod species *Temora spp., Oithona spp., Pseusocalanus spp.* and *Calanus finamarhicus* concentrated in the surface layer (10-15 $\mathrm{m}$ deep) at a turbulent dissipation rate of $\varepsilon = 10^{-8}\ \mathrm{W/kg}$. After a storm the dissipation rate in the surface layer increased to $\varepsilon = 10^{-6}\ \mathrm{W/kg}$ due to mixing of the surface waters. At that time, adult copepods were found deeper in the water column at a depth where $\varepsilon = 10^{-8}\ \mathrm{W/kg}$. From this, it was concluded that the copepods were avoiding depths of high turbulence.

*Reiss et al.* (2002) sampled turbulent dissipation rates using the vertical microstructure profiler "EPSONDE" and sampled copepods with a BIONESS net tow system on the Western Bank of the Scotian Shelf. They measured dissipation rates between $\varepsilon = 10^{-5}\ \mathrm{W/kg}$ and $\varepsilon = 3 \cdot 10^{-9}\ \mathrm{W/kg}$. The copepods sampled include *Oithona spp.*, calanoid genera (*Centropages sp.*, *Paracalanus sp.*, *Clausocalanus sp.*, *Pseudocalanus sp.* and *Microcalanus sp.*), *Microsetella norvegia* and *Temora longicornis*. Unlike earlier authours, they concluded that there was not a significant relationship between vertical distribution of copepods and turbulent dissipation rates.

**Laboratory observations of turbulence on the vertical distribution of copepods**

To test *Incze et al.* (2001)'s hypothesis that copepods avoid high levels of turbulence, *Yen et al.* (2008) conducted a laboratory experiment to observe whether copepods actively avoid high turbulence (by swimming) instead of migrating for other reasons, such as searching for food. Using a method designed by *Webster et al.* (2004), they set up known,

isotropic and homogeneous turbulence levels in a tank. They placed the copepod species *Acartia hudsonica*, *Calanus finmarchicus* and *Temora longicornis* in the tank and gradually increased the turbulence from $\varepsilon = 0\ \mathrm{W/kg}$ to $\varepsilon = 2.5 \cdot 10^{-4}\ \mathrm{W/kg}$. They observed copepod transport velocities and found that as dissipation rates increased, most *A.hudsonica* and *C. finmarchicus* moved faster out of the region of high turbulence (than when there was no turbulence), while *T. longicornis* did not change their velocity. From this, they inferred that *A.hudsonica* and *C. finmarchicus* actively avoided regions with high turbulent dissipation rates by swimming, but *T. longicornis* did not respond to any turbulence level tested.

**My Field Study**

Despite much theoretical, laboratory and field research on the effects of turbulence on copepods, there is no clear, definite relationship between vertical copepod distributions and local turbulence levels. Reliable, in situ, coincident measurements of both copepod distributions and turbulence are needed to establish if such a relationship exists. To this end, a new biophysical profiler, which can collect high-resolution turbulence and copepod data was deployed in Bedford Basin as a novel approach to this problem. These data will be used along with depth, temperature, salinity and density, buoyancy frequency, wind, tidal and light data to determine if the distribution of copepods in Bedford Basin is related to the copepods' physical environment.

## 1.4 Sample Site

Bedford Basin (Figure 1.3) was a convenient location that provided a range of dissipation rates and known copepod populations (*Li and Harrison*, 2008) to explore the relationship between vertical copepod distribution and local turbulent dissipation rates.

Bedford Basin is a semi-enclosed estuary (*Fader and Miller*, 2008) that is connected to the open sea via 400 $\mathrm{m}$ long narrows (*Li and Harrison*, 2008). Bedford Basin is 6 $\mathrm{km}$ long from mouth to end and 4 $\mathrm{km}$ across (*Shan et al.*, 2011), with a surface area of 16.8 $\mathrm{km}^2$. At high tide, the basin is 71 $\mathrm{m}$ deep at its maximum, with a maximum tidal range of 2.1 $\mathrm{m}$ (*Gregory et al.*, 1993). The daily tidal flushing of Bedford Basin may be advecting copepods into and out of Bedford Basin via the narrows.

Bedford Basin has a two-layer estuarine circulation. There is a sill that connects Bedford Basin to the narrows, mixing the water as the tide flows into the basin (*Syvitski et al.*, 1995),

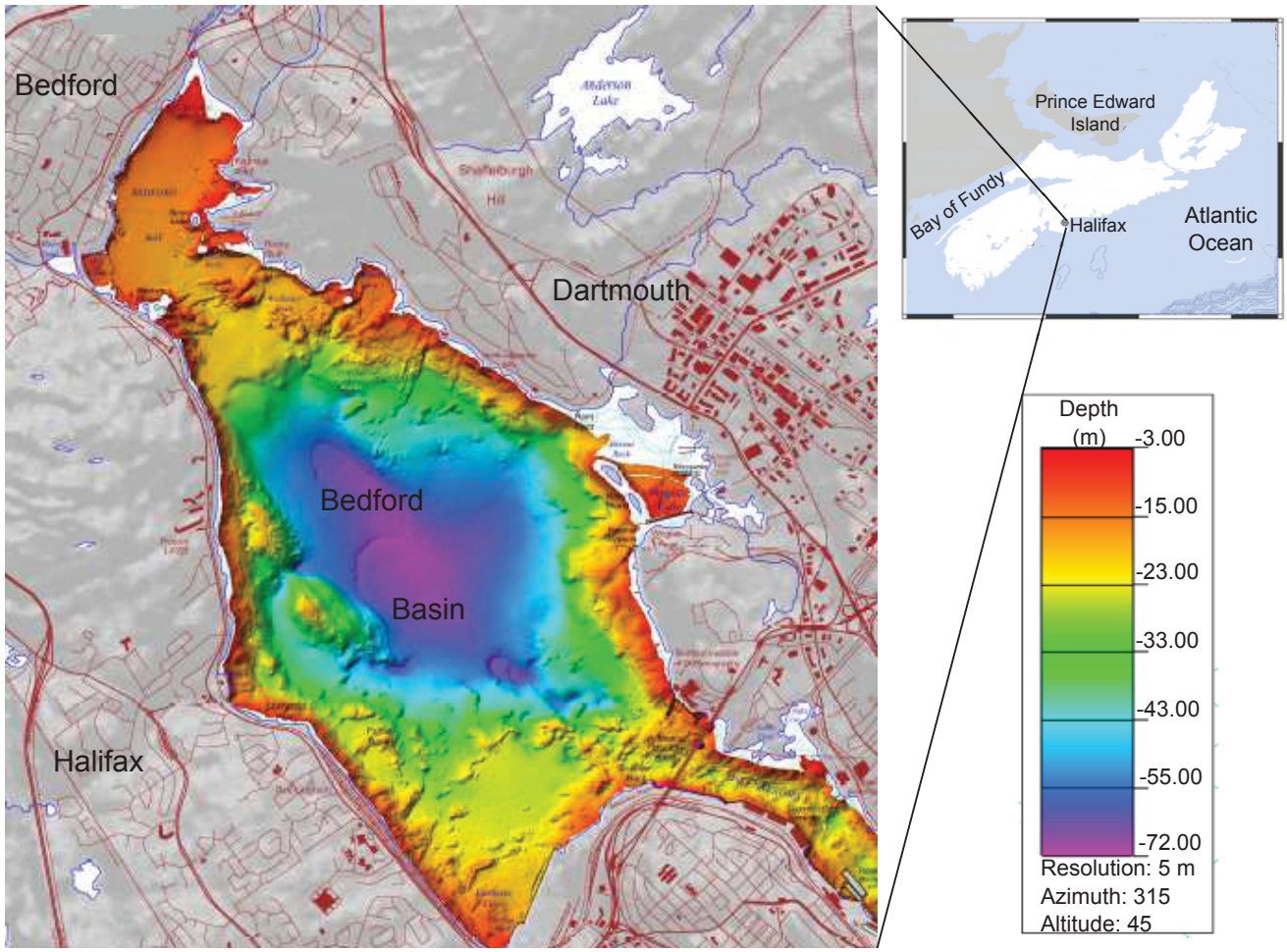


Figure 1.3: A bathymetric map of Bedford Basin modified from a figure created in *Fader and Miller* (2008).

generating turbulence. Fresher, lower density surface waters flow out of the basin, into the narrows and into the open ocean while denser, saltier oceanic waters flow into the basin (*Li and Harrison*, 2008). Mixing at the interface between the two layers causes the upper fresher layer to become saltier and the bottom layer to become fresher (*Fader and Miller*, 2008). The mean surface layer outflow is weak, only 0.2 $\mathrm{cm/s}$, but varies with the tides and winds (*Li and Harrison*, 2008). This two layer system can be enhanced by stronger vertical stratification (usually in the summer) or by wind stress and direction. In the winter, the dominant wind direction over the basin is from the northwest, with average speeds around 5.4 $\mathrm{m/s}$. In summertime, the winds blow mainly from the southwest and average winds about 3.9 $\mathrm{m/s}$ (*Shan et al.*, 2011). Heightened winds can generate turbulence due

to increased mixing, hence it may be expected that this seasonal wind change can affect the vertical distribution of copepods in Bedford Basin.

Both the estuarine circulation and stratification depend strongly on the freshwater input into Bedford Basin (*Syvitski et al.*, 1995). The main source of freshwater input into Bedford Basin is from the Sackville River at the head of the basin. Its average discharge is 5 $\mathrm{m}^3/\mathrm{s}$, though this number varies throughout the seasons (*Fader and Miller*, 2008) and is at a maximum between April and June due to ice and snow melt (*Shan et al.*, 2011). The seasonal vertical stratification in Bedford Basin is determined mainly by temperature as the weekly average values of stratification are highly correlated with temperature (*Li and Harrison*, 2008). The inter-annual variations are determined by the surface salinity. The surface salinity in Bedford Basin varies on a monthly basis, reaching a maximum in March at $30.8\ psu$ and a minimum in December at $27.5\ psu$ (*Shan et al.*, 2011). There are two low salinity periods in the upper 5 $\mathrm{m}$: one from April to June and the other from October to December (*Shan*, 2010). If salinity affects the distribution of copepods in Bedford Basin, I expect the freshwater input to change the horizontal distribution of copepods (i.e. less near the Sackville River). Since stratification may be important in determining the vertical distribution of copepods, I expect to see that buoyancy frequency affects the vertical distribution of copepods.

Another major feature of Bedford Basin is a seasonal deep water flushing. Ekman transport from the Scotian Shelf causes the replacement of deep waters in Bedford Basin with saltier shelf waters, a process that is heightened during the storm season. This process has been observed yearly for decades (*Platt et al.*, 1972). It is important to be aware of this process when sampling because the copepod population (and abundance) in Bedford Basin may change due to this flushing.

In Bedford Basin, the total phytoplankton biomass reaches a maximum in the spring during the phytoplankton bloom, during the weakest stratification. Less precipitation in the summer results in less river discharge, hence surface waters become saltier reducing stratification as the water column becomes more uniformly saline. Other tracers such as $\mathrm{NO}^{-3}$ will also be more uniform with depth, which allows for higher phytoplankton growth. The combination of low temperatures and weak stratification allows for conditions favourable for diatom growth and bloom in springtime. The high temperature, high stratification conditions in late summer provide an environment for flagellated phytoplankton

bloom (*Li and Harrison*, 2008). Since food may effect the vertical distribution of copepods in Bedford Basin, it is important to be aware of the variation throughout seasons. The Bedford Basin Plankton Monitoring Program sampled phytoplankton at 5 $\mathrm{m}$ depth. During the times I sampled Bedford Basin in autumn 2010, the peak phytoplankton concentration was $6.3 \cdot 10^4$ $\mathrm{cells/mL}$ and the minimum was $6.3 \cdot 10^3$ $\mathrm{cells/mL}$. The peak phytoplankton concentration in Bedford Basin for all of 2010 was $\sim 1.8 \cdot 10^5$ $\mathrm{cells/mL}$ in mid-July and the minimum in February was $2.5 \cdot 10^3$ $\mathrm{cells/mL}$.

## 1.5 Objectives

**Vertical Distributions of Copepods**

*Null-Hypothesis 1a: There is no relationship between the vertical distribution of copepods ($animals/m^3$) and the small-scale (1 $\mathrm{m}$) 1) vertical distribution of temperature ($^\circ C$), 2) vertical distribution of salinity ($\mathrm{g/kg}$) 3) vertical distribution of density ($\mathrm{kg/m^3}$), 4) vertical distribution of buoyancy frequency squared ($N^2$) or 5) vertical distribution of turbulent dissipation rates ($\mathrm{W/kg}$)*

*Null Hypothesis 1b: There is no difference between the abundance of copepods found within the pycnocline compared to the abundance of copepods below the pycnocline*

*Null Hypothesis 1c: There is no relationship between the mean copepod depth ($\mathrm{m}$) and the 1) mean thermocline depth ($\mathrm{m}$), 2) mean halocline depth ($\mathrm{m}$), 3) mean buoyancy frequency depth ($\mathrm{m}$) or 4) the mean dissipation depth ($\mathrm{m}$)*

My main objective is to determine if there is a predictable relationship between the vertical distribution of copepods and the physical factors in the copepods' environment. In particular, are copepods distributed throughout the water column with respect to any of these physical factors? Based on the literature review, temperature, salinity, buoyancy frequency, turbulence, light and food appear to affect the vertical distribution of the copepod species found in Bedford Basin.

From the VMP observations, I have profiles of physical data including depth, temperature, salinity, density, buoyancy frequency and turbulent dissipation rates. The VPR collected images of copepods during free-fall, hence the abundance of copepods in the vertical direction is known. Combining these two high-resolution datasets allowed me to test whether the distribution of the physical variables change with respect to the number of copepods, allowing examination of how the vertical distribution of copepods is affected by

these physical variables on a relatively small scale.

I also compared the mean thermocline, halocline, buoyancy frequency and dissipation depths for each sample period to the mean copepod depth to determine if the mean vertical distribution of copepods changes among sample periods.

**Variation in Copepod Presence between Sample Periods**

*Null Hypothesis 2: There is no relationship between the vertically integrated copepod abundance and average values of 1) temperature (°C), 2) salinity (*$\mathrm{g/kg}$*), 3) density (*$\mathrm{kg/m^3}$*), 4) buoyancy frequency squared (*$N^2$*), 5) turbulent dissipation rates (*$\mathrm{W/kg}$*), 6) wind (*$\mathrm{m/s}$*), 7) tidal cycle (time) or 8) daylight (unitless).*

The high-resolution physical variables were averaged over depth and time for each sample period (i.e. 19 October, 26 October, 03 November, 04 November and 30 November). Data for tides, winds and daylight were available near Bedford Basin on all sample days during the sample period. This analysis helped determine whether the large scale dynamics of Bedford Basin had any effect on the abundance of copepods. For the copepod data, a sample ratio (SR) was calculated for the sample period based on the number of copepod observations divided by the total number of observations from that sample period ($SR = \frac{number\ of\ copepods}{number\ of\ total\ observations}$)..

**Impact:**

Many recent studies have focused on the biophysical relationship between copepods and turbulence. This is the first time an instrument like the VMP/VPR has been used to examine copepod-turbulence relationships. High resolution, coincident, in situ observations of depth, temperature, salinity, density, buoyancy frequency, dissipation rates *and* copepod abundance are novel. Additionally, most studies assume turbulence affects copepod behaviour and that copepods are affected by turbulence on a species-by-species basis (i.e. a species of copepod will react to a heightened dissipation rate differently than another species). For this project, I take a different approach, using the copepod abundance ($animals/m^3$) and copepod presence to quantify the copepod data and do not attempt to quantify their behaviour or their species.

In situ measurements are needed to test the consistency of the results from previous studies; for example *Incze et al.* conclude that more observations are needed to determine whether it is turbulence or other factors causing the zooplankton to vertically migrate. The relationship between copepods and turbulence is not well understood and no general

consensus on their relationship has been reached.

My main objective adds much needed new data to the field and attempts to approach the question in a novel direction, giving reliable, high-resolution measurements of copepods and turbulence.

# CHAPTER 2

# METHODS

## 2.1 Field Work in Bedford Basin

The observations for this project were collected in Bedford Basin (Figure 1.3), adjacent to Halifax, Nova Scotia, on Canada's east coast. Sampling occurred on 19 October, 26 October, 03 November, 04 November and 30 November in the autumn of 2010 aboard the *C.G.S Sigma T*. The aim of this field work was to observe copepods as a taxonomic group in a range of turbulent conditions. I assume any differences in the copepod distributions are not due to changes in species composition. Different tidal phases were sampled to observe a range of dissipation rates generated by the tide flowing into the Basin. Most sampling was done at the mouth of the Basin where dissipation rates are elevated as the tide flows over the sill. Each sampling day resulted in $\sim$ 2 hours worth of data.

## 2.2 Vertical Microstructure Profiler/Video Plankton Recorder

The Vertical Microstructure Profiler/ Video Plankton Recorder (VMP/VPR) collects coincident measurements of turbulent dissipation rates and images of plankton within the water column (*Ross*, 2013; submitted). It combines a VMP (from Rockland Scientific International Incorporated) with a VPR (from Seascan Incorporated) that are mechanically connected but electronically separate. The VMP is an autonomous free-falling vertical profiler designed to measure high-resolution data from two shear probes, as well as conductivity and temperature (CT) data from Seabird sensors. The shear, accelerometer and pressure data are sampled at 512 Hz and the CT data are sampled at 64 Hz. The Video

Plankton Recorder (VPR) is an underwater video microscope system designed for rapid quantification of plankton taxonomic composition and abundance. The hardware consists of a camera facing a strobe light. The camera captured images at 15 Hz synchronized with the strobe light, that creates an 8-inch diameter cone of light in front of the camera. As it falls, the instrument records shear microstructure measurements, images of plankton, high resolution pressure, 3-axis accelerometery, as well as the Seabird CT data.

The VMP/VPR is deployed from of a ship drifting with its engines turned off for safety of the instrument. The VMP/VPR is lowered just below the surface, usually 5-10 $\mathrm{m}$ deep, to avoid signal contamination from the ship and then free-falls at a constant rate, nominally 0.6 $\mathrm{m/s}$. Once the instrument reaches the chosen depth, it is stopped, brought back to 5 $\mathrm{m}$ below the surface and re-deployed (starting a new cast).

Each sample day in Bedford Basin resulted in 12-23 casts. Repeated casts allow more statistical evidence to understand the vertical distribution of turbulence and copepods. The VMP and VPR data were recorded on separate computers, with respect to the computer's clock, giving two different time stamps. Since the two computer clocks did not have exactly the same time, a GPS signal was shared by both computers to synchronize the times.

## 2.3 Tide, Wind and Sunlight Data

Tidal data for this project were generated from the tide program, WebTide, a Government of Canada Tidal Prediction Model designed to predict tidal elevations and currents along Canada's coasts (*Greenberg et al.*, 1993). WebTide contains several local datasets for certain water bodies, including Halifax Harbour (thus Bedford Basin). The Halifax Harbour WebTide program combines tide tables from the Department of Fisheries and Oceanography with tidal current predictions from a linear, harmonic, finite element model developed at the Bedford Institute of Oceanography (*Greenberg et al.*, 1993 and *Greenberg*, 1999). The dataset generated from WebTide included tidal elevations for Bedford Basin every 15 minutes for the entire sample day.

Wind data were from the Government of Canada website from a weather station located on Bedford Basin (Climate ID: 8200573) (*WeatherOffice*, 2010). These data were reported on an hourly basis as the highest wind velocity observed that hour, hence it is a coarse measurement. The local time, wind speed and wind direction were used to quantify the

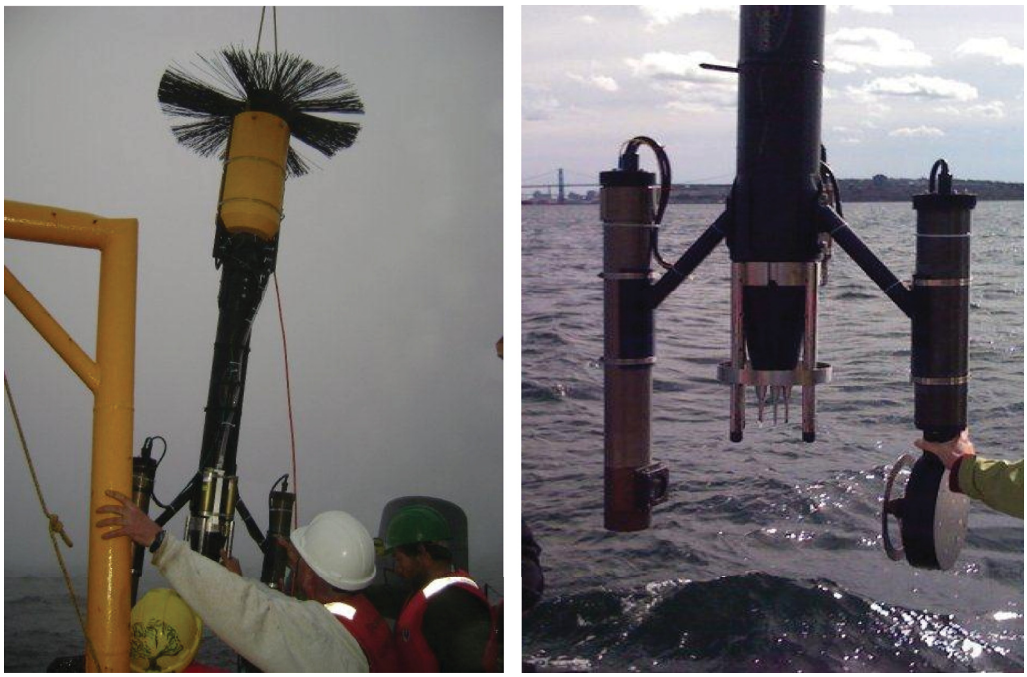

Figure 2.1: The Vertical Microstructure Profiler/Video Plankton Recorder in the field. The left panel shows the VMP/VPR deployment. The right panel shows a close-up of the tip of the instrument. The two outer arms are parts of the VPR hardware, the camera (left) and the strobe light (right). The centre of the right panel shows the shear probes, protected by a nose guard.

hourly wind data.

The sunrise and sunset times were retrieved from the National Research Council Canada's website (*NationalResearchCouncil*, 2010).

## 2.4 Analysis

### 2.4.1 VMP Analysis

Analysing the VMP data begins with identifying the start and end time of the instrument's free-fall from the GPS in Coordinated Universal Time (UTC). The instrument collected data before it started to free-fall, creating some data that should not be used in the analysis, hence the free-fall start and stop times were calculated based on the slope of the depth vs. time plot (Figure 2.2). For each cast, the difference in the UTC time and the computer time for each data point was recorded and then averaged, giving the mean time difference between the UTC time and the computer time. The mean difference was subtracted from

the computer clock so that all data were in UTC time.

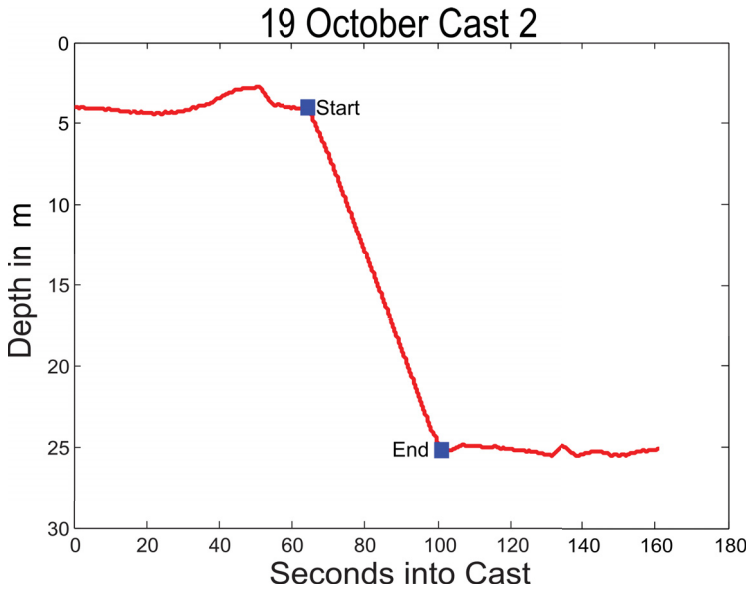


Figure 2.2: An example from one cast that highlights the free-fall pattern of the VMP/VPR. The x-axis is the time in seconds since the instrument started recording data. The y-axis is the depth in metres. The plot shows the vertical position of the instrument through time. From $\sim$ 0 to 60 seconds, the instrument is not yet falling at a constant rate and is nearly stationary near the surface ($\sim 5$ m). From $\sim$ 60 to 100 seconds, the curve is smooth and straight, indicating that the profiler free-falls at a constant rate. From $\sim$ 100 to 160 seconds, the profiler is stationary at the bottom of the profile ($\sim 25$ m). The start and end points are highlighted by the blue squares.

The next step was to convert the shear data from the VMP into physical units. The sensing element in the shear probe is a piezo-ceramic bimorph beam. When this beam feels a cross force, usually a turbulent velocity fluctuation $u'$, it generates an electrical charge. Once calibrated, the voltage from the electrical charge gives $\frac{\partial u'}{\partial z}$ (see *Oakey and Elliott* (1982) and *Ross* (2013), submitted). The turbulent dissipation rate, $\varepsilon$, can then be calculated (Figure 2.3) using Equation 1.2. A dissipation rate, $\varepsilon$, was calculated from the shear data (Figure 2.3, left panel) for each 1 m depth bins because this was the smallest reliable scale that dissipation measurements could be calculated. First, the shear data were despiked using the local variance of the signal and a low pass filter to remove any instances when particles hit the probe. The 1 m segments of shear data were converted into a spatial gradient using the mean free-fall velocity in that segment and the Fourier transform of the 1 m segment of shear data was calculated. Empirically calculated transfer

functions between the three-axis accelerometer data were used to remove vibrations from the instrument as it free-falls (*Goodman et al.*, 2006). A polynomial curve was fitted to the shear spectrum to find the cut-off wavenumber $k_{co}$ (i.e. the point where the background noise from the instrument dominates the shear signal, shown by the triangle in Figure 2.4). The dissipation rate, $\varepsilon$ was calculated by integrating from $\phi(k_{min})$ (the energy at the minimum wavenumber in the spectrum) up to $\phi(k_{co})$ (the energy at $k_{co}$). As the shear signal was only integrated up to $k_{co}$, $\varepsilon$ is underestimated because the signal from beyond $k_{co}$ is left out. Therefore, I used the Nasmyth spectra based on the initial $\varepsilon$ estimate to correct for the missing shear data and estimated a new $\varepsilon$. I repeated this process until the $\varepsilon$ estimates converged (Figure 2.3 right panel).

Some shear measurements were non-turbulent, hence the shear data were also compared to the Nasmyth spectra (Figure 2.4) to verify that the shear spectra followed the form expected for turbulence. A median absolute deviation (MAD) was used to compare the the shears and the expected Nasmyth curve (*Ruddick et al.*, 2000). The MAD is a measure of how closely the signal follows the theoretical curve over the observed wavenumber range:

$$MAD = \frac{\sum_{i=1}^{n} |y - \overline{y}|}{n}, \tag{2.1}$$

where $y = \phi_i/\phi_s$, where $\phi_i$ is the shear in wavenumber space and $\phi_s$ is the Nasmyth spectra, $\overline{y}$ is the mean of $y$ and $n$ is the number of $k$ in the spectrum up to $k_{co}$. Any $\varepsilon$ with $MAD > 1.5$ was rejected.

To ensure the shear signal is not dominated by noise, a threshold for signal-to-noise (SNR) was also set. A linear fit was used to model the increasing noise (from $\phi(k_{co})$ to $\phi_{max}$, the maximum of the energy) and the subsequent decreasing noise (from $\phi_{max}$ to $\phi(k_{max})$, the energy at the maximum wavenumber). The SNR was calculated as:

$$SNR = \frac{\sum_{i=1}^{n} S_{obs}(k)}{\sum_{i=1}^{n} S_{th}(k)} \tag{2.2}$$

Where $S_{obs}(k)$ is the observed shear signal in wavenumber space, in this case the shear measurements up to the cut-off, $S_{th}(k)$ is the theoretical signal, in this case, the noise and$n$

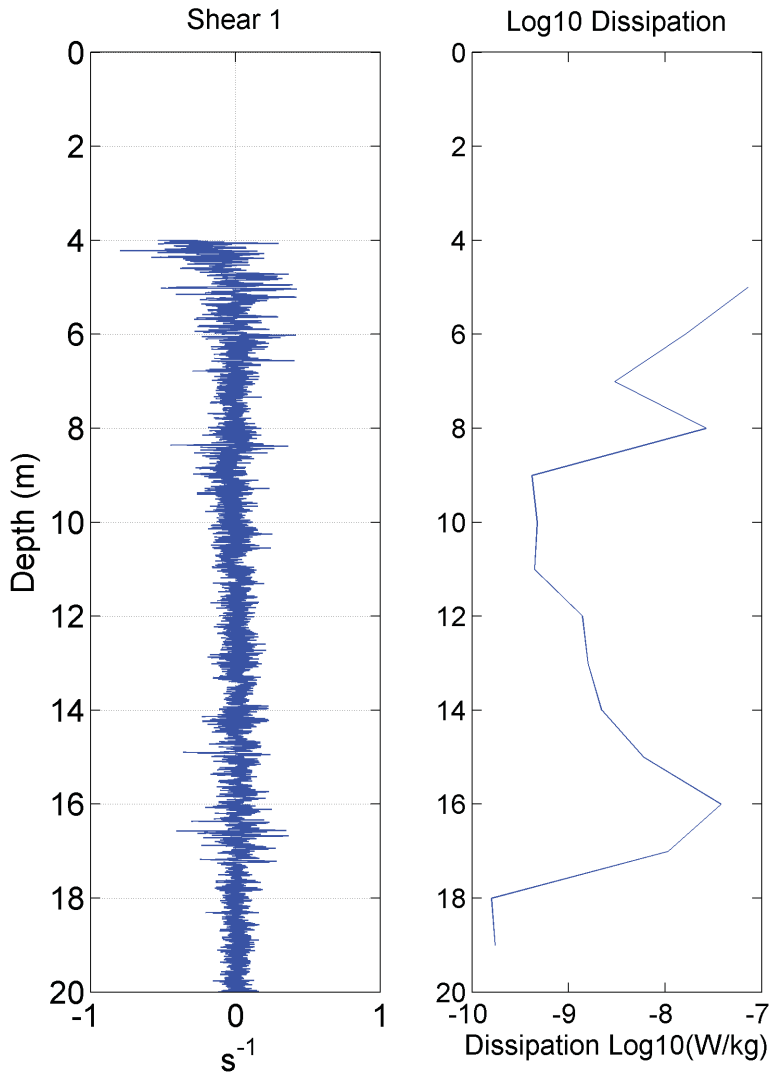


Figure 2.3: Shear data from Cast 6 on 30 November in Bedford Basin. The left hand panel displays the raw shear signal for the first 20 $\mathrm{m}$ of the record. The x-axis is the shear data $(1/\mathrm{s})$ and the y-axis is the depth in metres. The shear curve has high-frequency variability centred around 0. The right panel is the $log_{10}$ turbulent dissipation rate calculated from Equation 1.2. The x-axis is $log_{10}$ turbulent dissipation rate ($log_{10}$ $\mathrm{W/kg}$). The y-axis is depth in metres. The dissipation rates were calculated on a 1 $\mathrm{m}$ depth scale, much lower resolution than the 512 Hz sample rate for the shear data ($O(100)$ observations per 1 $\mathrm{m}$ bin).

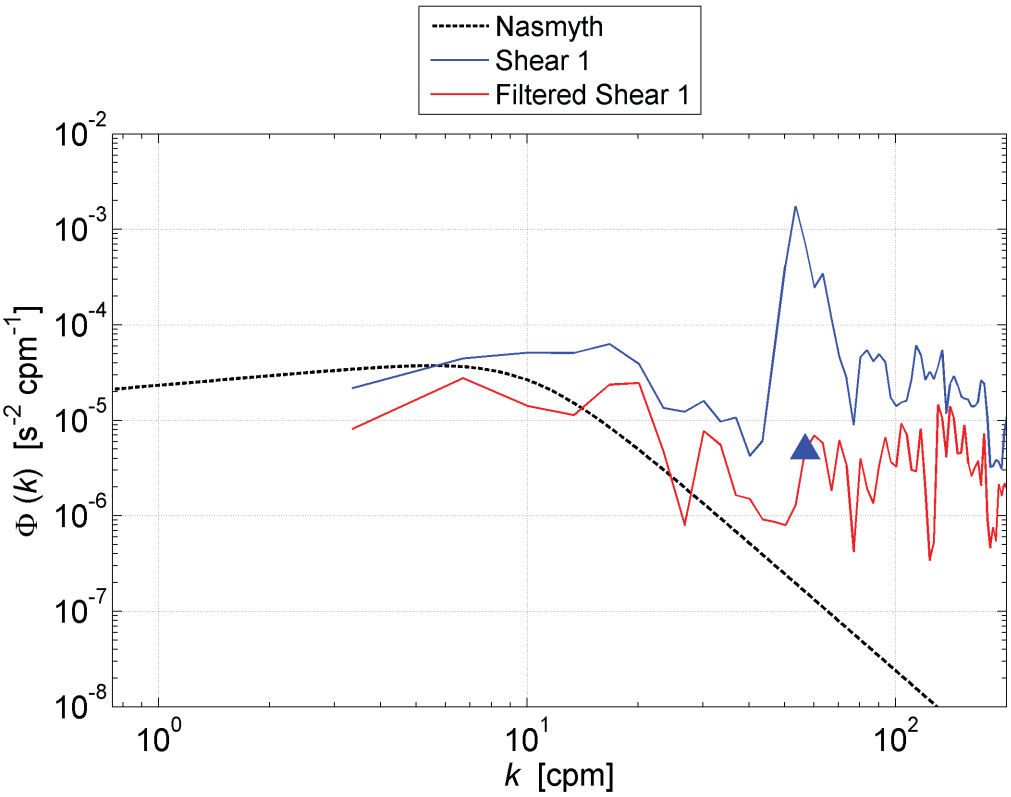


Figure 2.4: Turbulence-induced shear curves in wavenumber space for 14-15 $\mathrm{m}$ of Cast 6 on 30 November. The x-axis is $k$, the wavenumber in cycles per metre (cpm). The y-axis represents the energy in wavenumber space. The black curve is the Nasmyth spectrum, the curve the shear is expected to follow if the shear is generated by turbulence. The blue curve represents the raw shear data (same data as left panel of Figure 2.3). The red curve represents the filtered shear data. The triangle represents the cut-off wavenumber for the calculation of $\varepsilon$. The dissipation rate is calculated via Equation 1.2 from the beginning of the filtered shear data (red curve) up to the cut-off $k$ and is estimated based on the Nasmyth curve (black curve) from the cut-off and onwards for the remaining wavenumbers.

is the number of $k$ in the spectrum up to $k_{co}$. For Bedford Basin, any dissipation rate that had a $SNR < 2$ was rejected.

The Gibbs Seawater package for MATLAB was used to calculate temperature, salinity, density and buoyancy frequency from the measurements of T and C made by the Seabird sensors and pressure (*McDougall and Barker*, 2011). This package uses the 'Thermodynamic Equation of Seawater-2010', and it uses absolute rather than practical salinity. Absolute salinity is calculated from pressure, latitude and longitude (as well as conductivity and temperature used to calculate practical salinity).

Since the turbulent dissipation rates were calculated for $1\ \mathrm{m}$ depth bins, the depth, temperature, salinity and density were averaged into $1\ \mathrm{m}$ bins as well. The squared buoyancy frequency was calculated from these averaged data using $N^2 = g^2 \frac{\partial \rho_o}{\partial p}$.

In summary, for each cast, there were six physical variables calculated on a $1\ \mathrm{m}$ depth scale: depth, temperature, salinity, density, buoyancy frequency and turbulent dissipation rate. A temperature-salinity plot was created by contouring the density anomaly, $\sigma_t = density - 1000\ \mathrm{kg/m^3}$. Each $1\ \mathrm{m}$ data point for each sample period was plotted for temperature and salinity (Figure 3.7).

### 2.4.2 VPR Analysis

Analysis of the VPR data starts with running the raw, proprietary video data through AutoDeck, a program used to extract clear images of copepods. AutoDeck selects regions of interest (ROIs) from each frame, determined by settings specifying thresholds for light intensities and gradients.

Five settings are important to determine if an image meets the requirements to be deemed a ROI: High Segmentation Threshold, Sobel Focus, Standard Deviation Focus, Minimum Blob Size and Minimum Join Distance. The High Segmentation Threshold checks whether an image is bright enough to be considered a ROI. ROIs that pass this threshold are placed into rectangular boxes and are deemed 'blobs'. The Sobel Focus controls the light gradient analysis and analyses the boxed blobs for well-defined edges. If the light gradient within the box is strong enough, the blob is passed to the Standard Deviation control. This setting assesses the variance of the image by calculating the standard deviation of the mean high frequency content of the pixel light intensities in the boxed area. The Minimum Blob Size sets the smallest number of pixels a boxed blob can contain to be saved. The Minimum Join Distance is used to cluster small boxes together into one large box. This setting

merges two objects into one for pixel distances smaller than the set value. AutoDeck uses the Growth Scale to specify how the images are saved. This setting allows the user to save the area around an the ROI box. This is useful in detecting smaller details around an object, such as a copepod's antenna. If the boxed blob passes the Standard Deviation control, the image is augmented by the Growth Scale and is saved as a full resolution ROI.

Optimizing for clear images of copepods in Bedford Basin yielded the settings: Low Segmentation Threshold $= 0$, High Segmentation Threshold $= 150$, Sobel Focus $= 31$, Standard Deviation Focus $= 1$, Growth Scale $= 250\%$ Minimum Blob Size $= 10$ and Minimum Join Distance $= 1$.

The VPR camera was set to a nominal field of view of 24 x 24 $\mathrm{mm}$ for this study. A calibration was performed to determine the sampling volume of the camera for this setting. A set of calibration images were created by moving a plate with evenly distributed light-coloured refractive circles from the camera following the optical axis towards the strobe light. The calibration file was run through AutoDeck using the optimized copepod settings to give the number of frames in focus as the plate is moving. The depth of view of the camera was calculated by using the speed of the plate (1.83 $\mathrm{mm/s}$) and the number of in-focus frames. For this project, the average sampling volume of the camera was 574 $\mathrm{mm}^2$ (field of view for each frame 23.96 $\mathrm{mm}$ by 23.96 $\mathrm{mm}$) and the depth of view was 86.6 $\mathrm{mm}$. The volume sampled per metre was calculated as $V\_S = \frac{\Delta z}{W_{profiler}} \cdot f\_camera \cdot v\_camera$, where $\Delta z = 1$ m, $W_{profiler} \simeq 0.6$ $\mathrm{m/s}$ (free-fall velocity of profiler), $f\_camera$ = 15 Hz (images captured per second) and $v\_camera = 0.024$ m $\cdot 0.024$ m $\cdot 0.086$ m $= 4.98 \cdot 10^{-5}$ $\mathrm{m}^3$ (volume of each image captured). The sample volume per metre was $\sim 1 \cdot 10^{-3}$ $\mathrm{m}^3$ and varied little. Given that the vertical dimension of the field of view is 0.024 $\mathrm{m}$ and one image was collected every $\frac{0.6 \text{ m/s}}{15\ Hz} = 0.04$ m, the images were not overlapping.

Each clear image of a copepod can have 'fields' attached to it (more details about what constituents a clear image are found in Section 2.4.2). Since my sampling technique was using video data, I did not assign life stage information to the copepods, so the analysis presented is for copepodite and adult stages since the two are indistinguishable in video format. Even though the literature suggests that turbulence affects copepod distributions on a species-specific basis, I pool across all species since the species in Bedford Basin are all relatively small ($< 1.8$ $\mathrm{mm}^2$) and most ($>= 80\%$) of the observed were *Pseudocalanus* spp..

Each ROI contains an image of one copepod only. The name of each copepod ROI is a time stamp from the VPR computer in milliseconds of day and corresponds to a UTC time in hh:mm:ss format from the GPS. As with the time data from the VMP, the difference between the two times for each data point was recorded and then averaged over the entire cast, giving the mean time difference between the UTC and desktop time. Each copepod ROI was given the UTC time stamp in hh:mm:ss.ms format as a field. Since each UTC time data point corresponds to a depth data point, each copepod ROI was given a depth, as well as temperature, salinity, density, buoyancy frequency and dissipation, as a field, if the depth was in the free-fall range. The time since low tide (tidal phase) was added to each copepod ROI as well. Any copepod with a depth outside of the free-fall range was removed for the remaining analysis.

Four of the five sample days were sampled solely in daylight and one was sampled pre- and post-dawn. Each copepod observed during daylight were given a field 'light $= 1$' and those sampled pre-dawn were given the field 'light $= 0$', from the sunrise and sunset data (*NationalResearchCouncil*, 2010).

The copepod data were also binned into a $1\ \mathrm{m}$ depth scale resulting in number of copepods per metre, with values that ranged between 0 and 4 copepods. The copepod abundance data were calculated as the number of copepods observed (0, 1, 2, 3 or 4) in each $1\ \mathrm{m}$ bin over the volume sampled per metre. Based on the small sample volume of the VPR, the copepod abundance data increases in steps of $\sim 800\ \frac{animals}{\mathrm{m}^3}$.

A dataset for a sample period contains copepod presence, depth, temperature, salinity, density, buoyancy frequency and dissipation on a $1\ \mathrm{m}$ depth scale and a second dataset for each copepod observed in free-fall. Each copepod datum contains: ROI identifier, depth bin (the $1\ \mathrm{m}$ depth bin the copepod was observed in), depth (actual depth within the metre ex: $5.2\ \mathrm{m}$), temperature ($^\circ$C), salinity ($\mathrm{g/kg}$), density ($\mathrm{kg/m^3}$), buoyancy frequency squared ($1/\mathrm{s}^2$), the average in geometric space of the dissipations from each shear probe, the time since low tide (decimal hours) and light (unitless).

### 2.4.3 Data Analysis: Vertical Distributions

To test my main hypothesis that the vertical distribution of copepods is not affected by physical variables in Bedford Basin, I compared the vertical distribution of the physical variables over all times to the vertical distribution of the physical variables during copepod presence.

To determine whether 1) the physical variables cover a broad range of values, 2) the copepod distribution of physical variables covered the same range of values as the overall distribution, and 3) there appeared to be any relationships between variables, the data of all observations were compared with observations during copepod presence. This was initially accomplished by plotting the distributions in physical variable space using data density plots (Figure 2.5) of the high-resolution data. In order to examine the potential effect of variables on the copepod abundance, I quantified the copepod observations in a way that was not sensitive to the number and depths of the profiles collected in a given sampling period by using a sample ratio (SR), which is the number of copepods sampled divided by the number of total observations ($SR = \frac{number\ of\ copepods}{number\ of\ total\ observations}$) for a particular pixel in the panels of Figure 2.5 (i.e. particular combination of physical variable and depth). An example is shown in Figure 2.6.

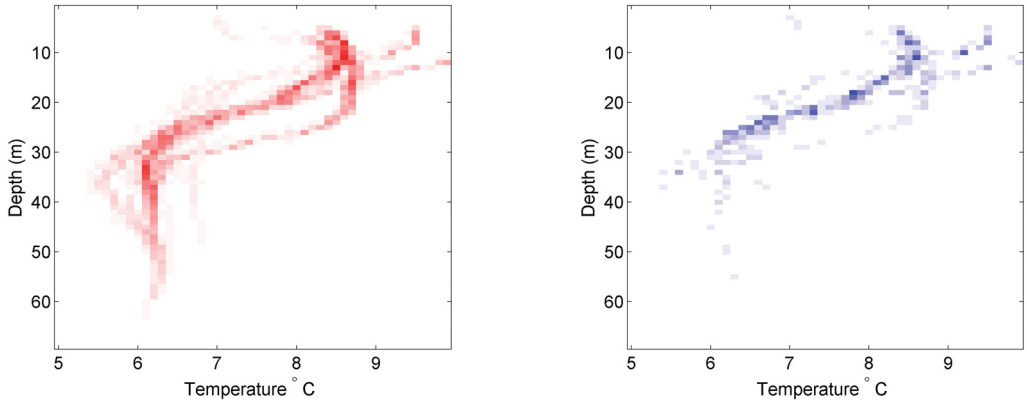


Figure 2.5: Data density plots for the depth vs. temperature data. The left panel shows all the observations. The x-axis is the temperature (in °C) and the y-axis is the depth in metres. The right panel shows the observations with copepods present (a subset of the left panel). For each panel, each pixel represents the number of data points found in that range. The darker the colour means there are data points found there. The lighter the points, the fewer data points are found there.

To examine the potential effect of each physical variable on the distribution of copepods separately, the distribution of all observations of a particular physical variable (e.g. temperature) was compared to the distribution of that variable observations with copepods present. The all observations data and the data during copepod presence were placed into bins (e.g for temperature 5 °C, 5.5 °C, ..., 10 °C) and each bin of the all observations distribution was scaled by $\left(\frac{n_{c\_obs}}{n_{t\_obs}}\right)$, where $n_{t\_obs}$ is the total number of observations of a

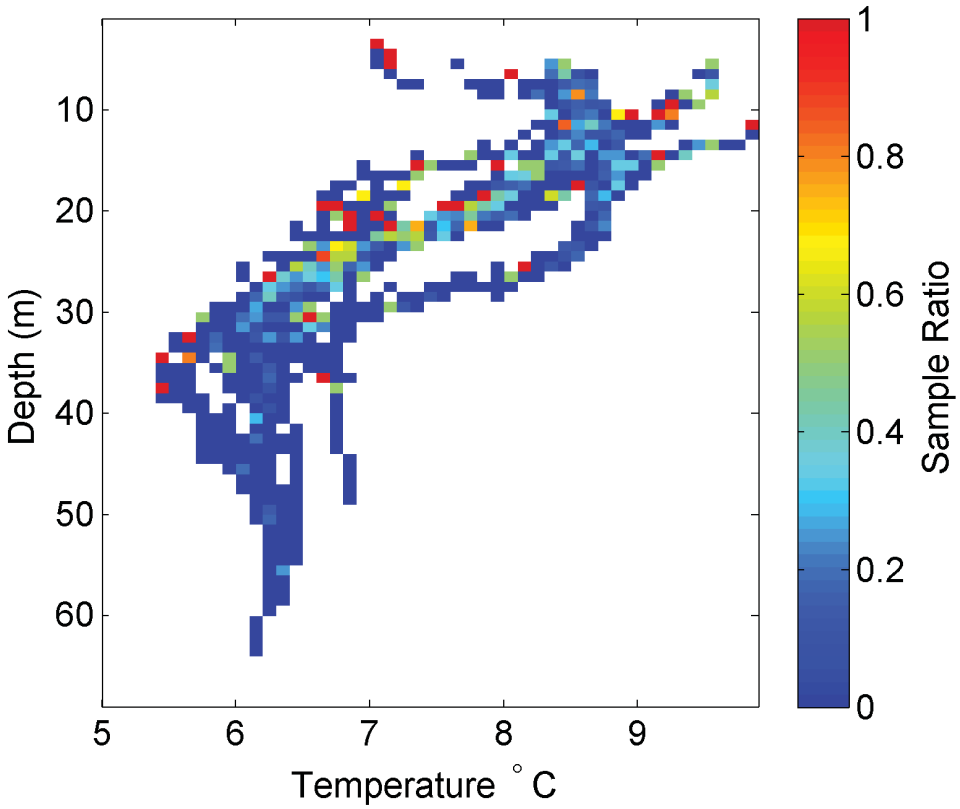


Figure 2.6: SR density plots for temperature vs. depth. The x-axis is temperature (°C) and the y-axis is depth in metres. The colour map represents the sample ratio ($SR = \frac{number\ of\ copepods}{number\ of\ total\ observations}$). The deep blue represents values of temperature and depth that were sampled, but where there were no copepod observations. As the figure colours transitions from blue to red, the relative number of copepod observations to total observations increases, providing information about the distribution of copepods in depth and temperature space. The white areas represent no observations (e.g there are no observations of 5 °C in waters at 10 m depth).

| Temperature Bin | Observations (all) | Observations (copepod presence) | Observations (all scaled) |
|---|---|---|---|
| 6 | 50 | 7 | 11.66 |
| 6.5 | 271 | 75 | 63.17 |
| 7 | 205 | 52 | 47.79 |
| 7.5 | 157 | 47 | 36.61 |
| 8 | 273 | 69 | 63.64 |
| 8.5 | 687 | 120 | 160.15 |
| 9 | 171 | 33 | 39.86 |
| 9.5 | 59 | 27 | 13.75 |
| 10 | 96 | 29 | 22.37 |
| Sum | $n_{t\_obs} = 1969$ | $n_{c\_obs} = 459$ | 459 |

Table 2.1: Column 1 shows the bins for the temperature. Columns 2 and 3 represent the number of observations found in those bins for all observations and the observations during copepod presence, respectively. Column 4 is the all observations scaled to the total number of copepod observations.

particular variable, $n_{c\_obs}$ is the number of observations of that variable when copepods are present (Table 2.1 shows an example for temperature). This new distribution will be referred to as the 'expected distribution'. As a reminder, the hypothesis is that no physical data will affect the vertical distribution of copepods. From this, it is expected that the copepod presence distribution will be the same as the expected distribution.

The second part of the first hypothesis was to determine if the copepod abundance was different in the pycnocline compared to below the pycnocline. For each sample period, I estimated the depth of the bottom of the pycnocline and calculated the copepod sample ratio (SR) in the pycnocline and below the pycnocline and compared the values. The bottom of the pycnocline for each sample period was selected based on the turning point of the slope of the density vs. depth plot. The data was plotted (Figure 2.7) and I manually selected the turning point.

The third part of the first hypothesis was to determine if the copepod depth changes based on the depth of any physical variable overall between sample periods. For each variable, I calculated a 'characteristic sample period depth'. The characteristic sample period depth for the copepod, buoyancy frequency and dissipation were weighted mean depths and were calculated via:

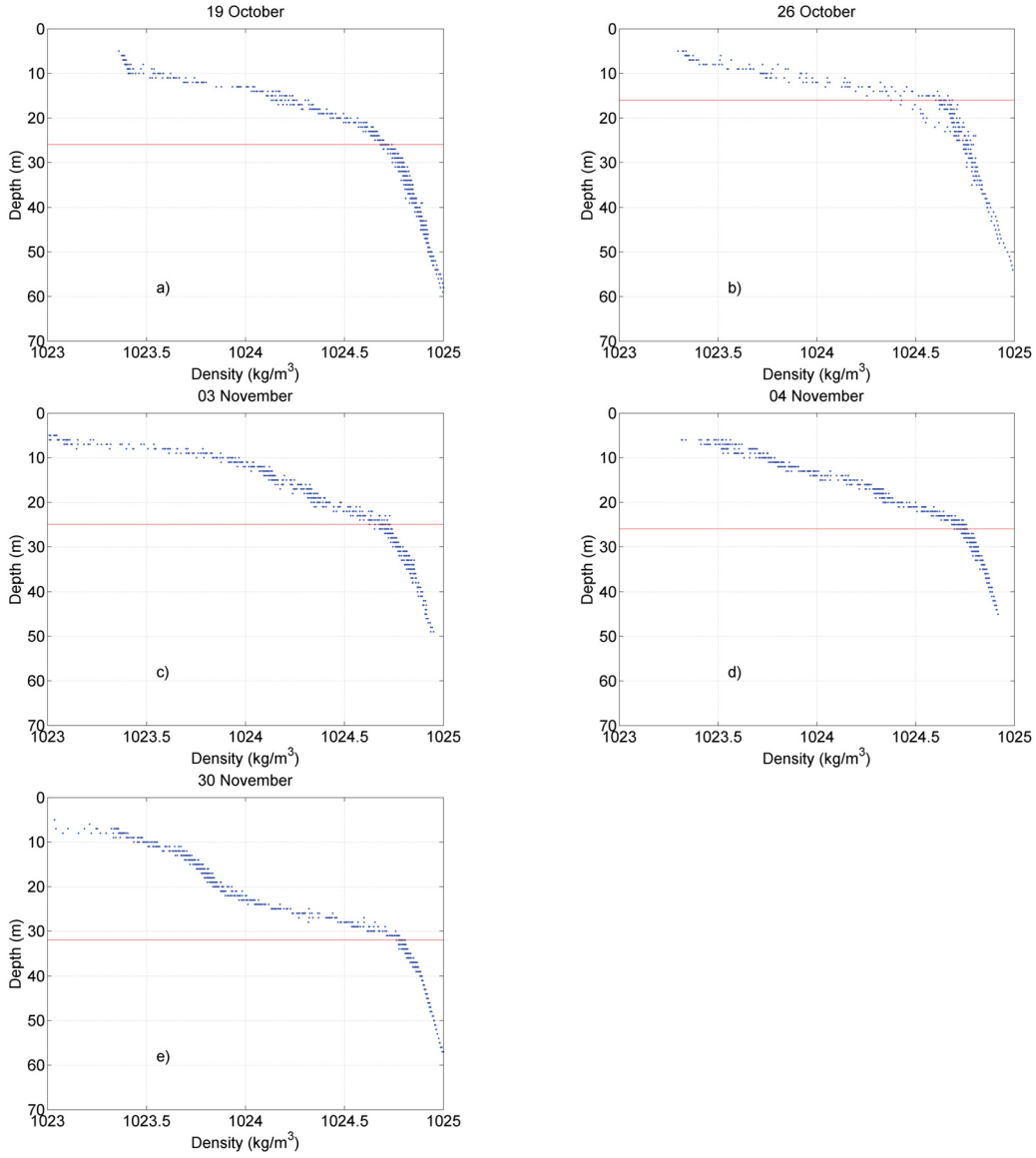


Figure 2.7: The pycnocline depths on a) 19 October, b) 26 October, c) 03 November, d) 04 November and e) 30 November showing the distribution of the sampled depths. The x-axis represent the density found in Bedford Basin, ranging from just under 1023.5 to 1025 $\mathrm{kg/m^3}$. The blue dots represent the distribution of depths and density sampled. The red line shows the bottom of the pycnocline depth near a) 26 $\mathrm{m}$, b) 16 $\mathrm{m}$, c) 25 $\mathrm{m}$, d) 26 $\mathrm{m}$ and e) 32 $\mathrm{m}$.

$$WMD = \frac{\sum_{i=1}^{n}(D_i V_i)}{\sum_{i=1}^{n} V_i}, \tag{2.3}$$

where WMD is the weighted mean depth in $\mathrm{m}$, D is the depth bin and V is the value of the variable (copepod abundance, buoyancy frequency or dissipation) at depth D. These data are summed over the number of depth bins per cast, $n$ and the overbar denotes the mean of this value over all casts for one sample period. The mean thermocline and halocline depths over the number of casts for each sample period were used as the characteristic sample period depths for the temperature and salinity data. The WMD thermocline and halocline depths were defined by calculating the depth of the greatest difference in each temperature and salinity for each cast and averaging these depths over each sample period. The copepod WMD was compared to the thermocline depth, halocline depth, buoyancy frequency WMD and dissipation WMD separately via a simple linear regression.

To test whether light affects the vertical distribution of copepods via DVM, I used a binned sample ratio (SR) to compare the vertical distribution of copepods during daytime to the vertical distribution of copepods during pre-dawn twilight. The depth observations for all sample periods and the copepod presence data for all sample periods were sorted into 2 $\mathrm{m}$ depth bins for both sampling during daytime and sampling during night-time. The number of copepod presence observations from each depth bin were divided by the number of total observations in the same bin (i.e if I observed 2 copepods between 7-9 $\mathrm{m}$ and I sampled the 7-9 $\mathrm{m}$ bin 20 times during the night, the binned SR = 2/20 = 0.1 for the depth bin centred at 8 $\mathrm{m}$ depth).

#### 2.4.3.1 Statistical Tests

**Chi-squared Test** The distributions of the physical variables with copepod presence can be statistically compared to the distribution for the expected distribution, using a $\chi^2$ test (*Zar*, 1999). The $\chi^2$ goodness-of-fit tests the null hypothesis that the observed frequency is the same as an expected frequency, i.e., the distribution with copepod presence is the same as the distribution with all data observations. The test statistic is computed as $\chi^2 = \sum_{i=1}^{n} \frac{(O_i - E_i)^2}{E_i}$. Where n is the degrees of freedom, $O_i$ is the number of observations in bin $i$ and $E_i$ is the number of expected observations in bin $i$. The probability of the null

hypothesis being rejected can be found in a $\chi^2$ probability table using the test statistic ($\chi^2$) and the degrees of freedom. The degrees of freedom are based on the number of bins in the expected distribution. Only bins with more than 5 observations in the expected distribution are used in the calculation of $\chi^2$. The bin widths were chosen to give approximately 8 degrees of freedom for each variable and the first and last bin included the minimum and maximum value observed for that variable over all sample periods. The results from the $\chi^2$ analysis is found in Section 3.2.2.

**Multiple Linear Regression** Since the $\chi^2$ test tests the significance of one variable at a time, a linear multiple regression was used to determine which combination of variables has the greatest significance on the vertical distribution of copepods. The multiple regression models the dependent variable, $Y_j$ with independent variables, $X_{ij}$ via Equation 2.4, where $m$ is the number of independent variables, $a$ is the value of $Y_j$ when all of the $X_{ij}$ are zero (analogous to a y-intercept for a simple linear regression (m=1)), and $b_i$ are the regression coefficients of the population (*Zar*, 1999). Note that the special case of m=1 gives a simple linear regression.

$$Y_j = a + \sum_{i=1}^{m} b_i X_{ij} \tag{2.4}$$

For my analysis the dependent variable used was copepod abundance and the independent variables used were temperature, density, buoyancy frequency and turbulent dissipation. One of temperature, salinity or density needed to be removed from this analysis to avoid multicollinearity. Since the correlation of the high-resolution data for salinity and density was the highest (0.98), temperature was retained. Salinity was removed from the analysis because the literature suggests density is more important than salinity in affecting the distribution of copepods. Temperature and density were arcsine transformed and the $N^2$ and dissipation were $log_{10}$ transformed into a normal distribution to adhere to the assumption of normality. To determine which factors have the strongest effect on the dependent variable, I calculate the regression for every possible combination of independent variable from all variables (m=5 for this analysis) to including only one independent variable (m=1, a simple linear regression). For each regression calculated from Equation 2.4, an adjusted coefficient of determination, $R_a^2$, can be calculated via Equation 2.5.

$$R_a^2 = 1 - \left(\frac{n-1}{n-m-1}\right)(1-R^2), \tag{2.5}$$

where $n$ is the number of observations, $m$ is the number of independent variables, $R^2$ is the coefficient of determination calculated as $R^2 = \frac{\sum_{i=1}^{n}(f_i - \overline{y_i})^2}{\sum_{i=1}^{n}(y_i - \overline{y_i})^2}$, where $f_i$ are the values of the dependent variable from the regression, $y_i$ are the actual observations of the dependent variable and $\overline{y_i}$ is the mean of $y_i$. The multiple regression with the highest $R_a^2$ represents the equation with the independent variables that have the strongest effect on the dependent variable.

### 2.4.4 Data Analysis: Variation on Mean Copepod Abundance

To examine the effect of the variables on mean abundance at the sample site, a SR was calculated for each sample period. For example, on 19 October, 313 one-metre depth bins were sampled and there were 81 copepods observed within those 313 bins. Hence the SR for 19 October is 81/313 = 0.26.

In order to compare as many physical variables on the same time scale as possible, a 'characteristic sample period value' for each high frequency physical variable was calculated. For the temperature, salinity, density, dissipation and time since low tide, this value was the mean of the variable across depth and time for each day. For the squared buoyancy frequency, the peak $N^2$ value was used by averaging the peak $N^2$ for each cast. The characteristic sample period value for wind was the peak speed during sampling. A simple linear regression was computed for each of the physical variable's characteristic sample period value and were compared to the copepod sample ratio and to each other (Section 3.4).

# CHAPTER 3

# RESULTS

## 3.1 Summary Plots for each Sample Period

From the $1\ \mathrm{m}$ binned dataset, plots of copepod presence, depth, temperature, salinity, density, buoyancy frequency and turbulent dissipation were generated to summarize each sample period. For Figures 3.1 to 3.6, each vertical rectangular box represents one cast. Only measurements during free-fall are plotted and the depths of these casts vary.

### 3.1.1 19 October 2010

The temperature, salinity and density data for 19 October are shown in Figure 3.1. A thermocline can be seen between 10-20 $\mathrm{m}$ (top panel of Figure 3.1). Above the thermocline, the water temperature is $\sim 10\ ^{\circ}\mathrm{C}$ and below it is about $6.5\ ^{\circ}\mathrm{C}$. The salinity profile is very similar to the temperature profile in that there is a halocline near the surface. Near $10\ \mathrm{m}$ depth, the salinity is about $31\ \mathrm{g/kg}$, the water was slightly fresher above and slightly saltier below. Finally, the pycnocline is between 10-20 $\mathrm{m}$, around $1024.4\ \mathrm{kg/m^3}$ (in the bottom plot). Below the pycnocline the waters were heavier, close to $1024.8\ \mathrm{kg/m^3}$ and lighter waters above near $1023.6\ \mathrm{kg/m^3}$. Since the temperature, salinity and density data are highly correlated, they are combined into one plot in subsequent figures. Salinity, which is the least variable, is not plotted, while density is contoured and overlays temperature.

Note that for Figures 3.2 to 3.6 the colour bar is fixed for comparative purposes (panels a-d), hence some observations do not reach the limits of the colour bar. For the wind and tidal data (panels e and f), however, the axes are not consistent from day to day.

The copepod abundance in each depth bin (Figure 3.2 panel a) ranged from 0 up to a maximum of $\sim 3500\ \mathrm{animals/m^3}$(greatest copepod abundance found at any given depth

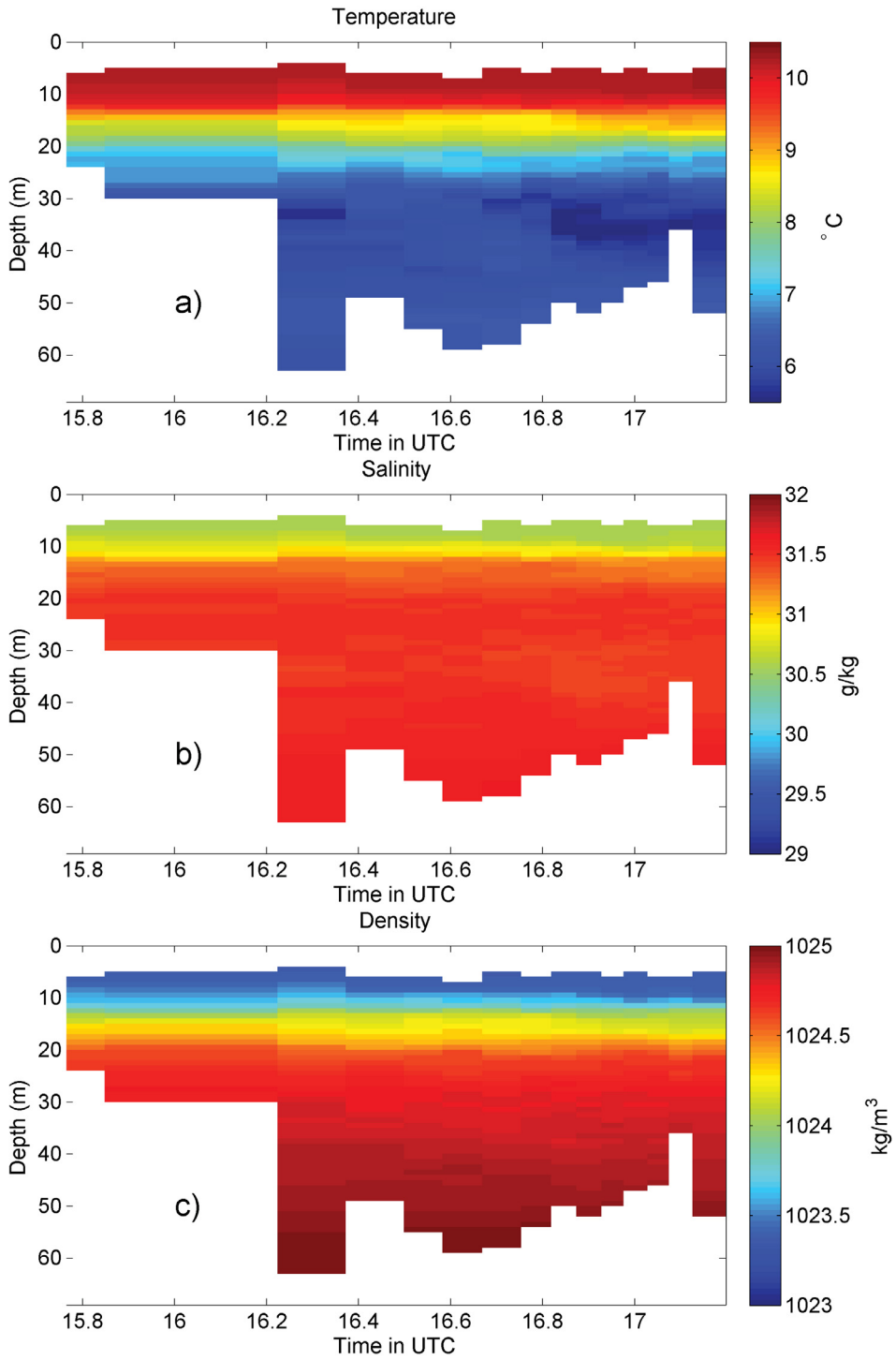


Figure 3.1: Time (UTC) series illustrations of 1 $\mathrm{m}$ depth averaged temperature in $^{\circ}\mathrm{C}$ (panel a), salinity in $\mathrm{g/kg}$ (panel b) and density in $\mathrm{kg/m^3}$ (panel c) in Bedford Basin on 19 October 2010.

for all sample periods). Copepods were observed infrequently and were found throughout the water column. However, they are more scarce at depth, (from time 16.5 hours and onwards in particular, discussed later in Section 3.2.2.1). The temperature profiles, with density contours overlaid (data from Figure 3.1) show the thermocline and pycnocline both occur around 12 $\mathrm{m}$ (Figure 3.2 panel b). The average turbulent dissipation rates range between -6 and -11 $log_{10}$ $\mathrm{W/kg}$ (Figure 3.2 panel c). Notice there are missing (white) data points from within the profiles. These are the dissipation rates that were removed based on the rejection criteria outlined in Section 2.4.1. Higher dissipation rates are near the surface (as expected due to mixing from wind stress), with lower measurements deeper in the water column. The squared buoyancy frequency (Figure 3.2 panel d) peaked at $3 \cdot 10^{-3}$ $1/\mathrm{s}^2$ between 10-20 $\mathrm{m}$ depth. The wind was blowing at a relatively high velocity of 8 $\mathrm{m/s}$ southwest (Figure 3.2 panel e) during sampling (hour 1600) and was weaker before and after sampling. Sampling on 19 October occurred during daylight and during flood tide, just after low tide (Figure 3.2 panel f) and took place in the deepest part of the Basin, away from the sill.

### 3.1.2 26 October 2010

Like the 19 October dataset, the copepod abundance was mainly 0 or 500 $\mathrm{animals/m^3}$ (Figure 3.3 panel a). To observe higher dissipation rates not only at the surface, the location of the ship changed from the centre of Bedford Basin to a location near the mouth of the Basin where there is a 20 $\mathrm{m}$ sill (see Figure 1.3). This accounts for the time gap after the second cast (Figure 3.3). The temperature (Figure 3.3 panel b) is relatively warm near the surface with both the thermocline and pycnocline at about 12 $\mathrm{m}$. Below the thermocline, the temperature is approximately 6 °C and above it is 10 °C. Again, like 19 October, the dissipation rates are highest in the surface layer , but 26 October also had higher and intermediate levels throughout the water column (Figure 3.3 panel c) after the move to near the sill. The squared buoyancy frequencies (Figure 3.3 panel d) were higher above 15 $\mathrm{m}$, especially from hour 14.4 onwards. Below 15 $\mathrm{m}$, the squared buoyancy frequency was close to 0 and varied little. The winds (Figure 3.3 panel e) before sampling were relatively high and decreased to about 4 $\mathrm{m/s}$ throughout the day. During sampling, the tide was just starting to ebb and the most recent low tide was $\sim$ 6 hours earlier. Sampling occurred only during daylight (Figure 3.3 panel f).

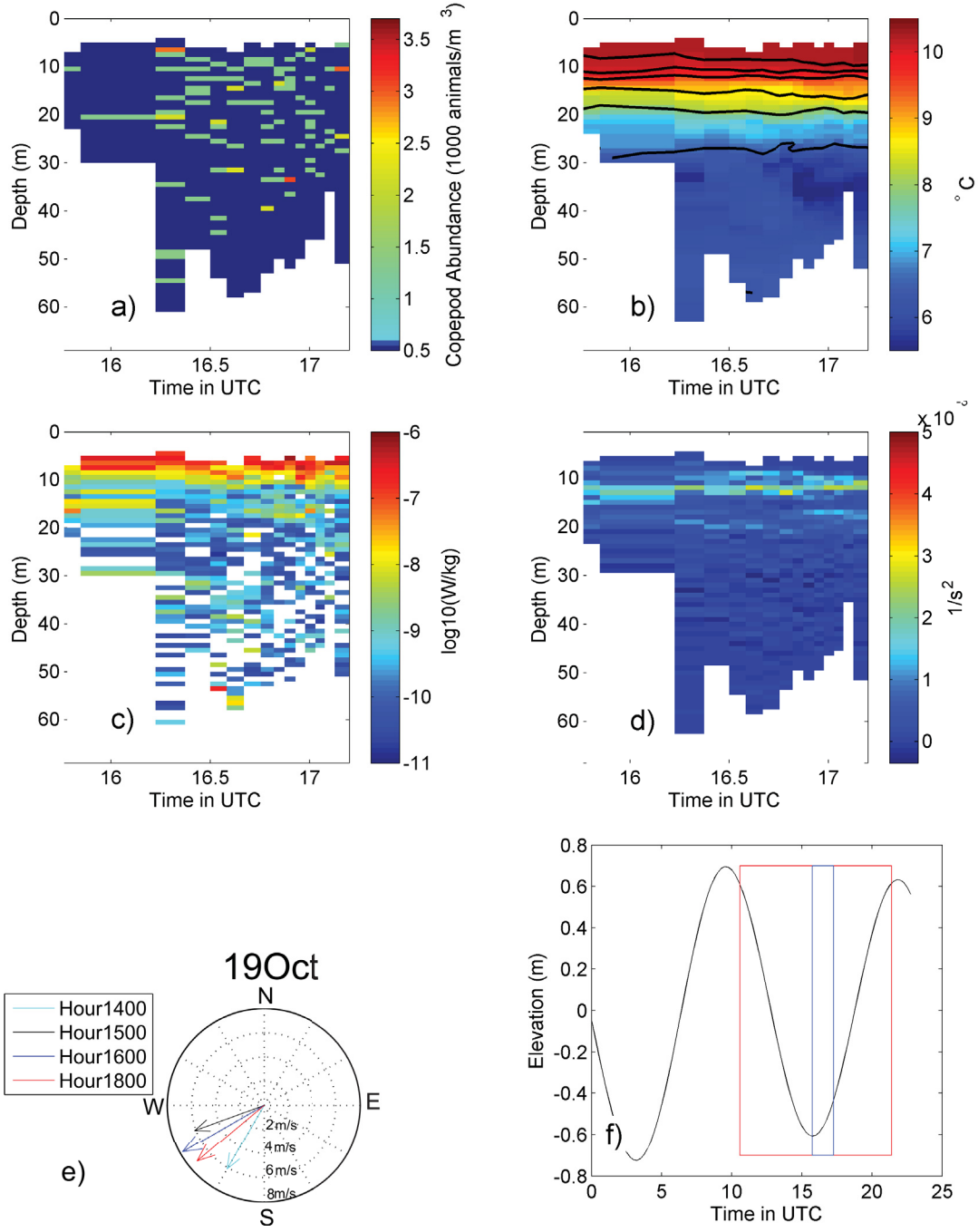


Figure 3.2: Time series summaries of depth averaged a) copepod abundance ($\mathrm{animals/m^3}$), b) temperature ($^\circ$C) with density contours ($\mathrm{kg/m^3}$) (the density contours start at 1023.25 $\mathrm{kg/m^3}$ and increase at 0.25 $\mathrm{kg/m^3}$ to 1024.5 $\mathrm{kg/m^3}$ near 30 $\mathrm{m}$ depth), c) turbulent dissipation rates $log_{10}(\mathrm{W/kg})$, d) squared buoyancy frequency ($\mathrm{1/s^2}$) and the corresponding e) wind speed ($\mathrm{m/s}$) and direction and f) tidal elevation in Bedford Basin on 19 October 2010. The sample period in the tidal cycle is denoted the vertical blue lines and daylight hours are denoted between the vertical red lines.

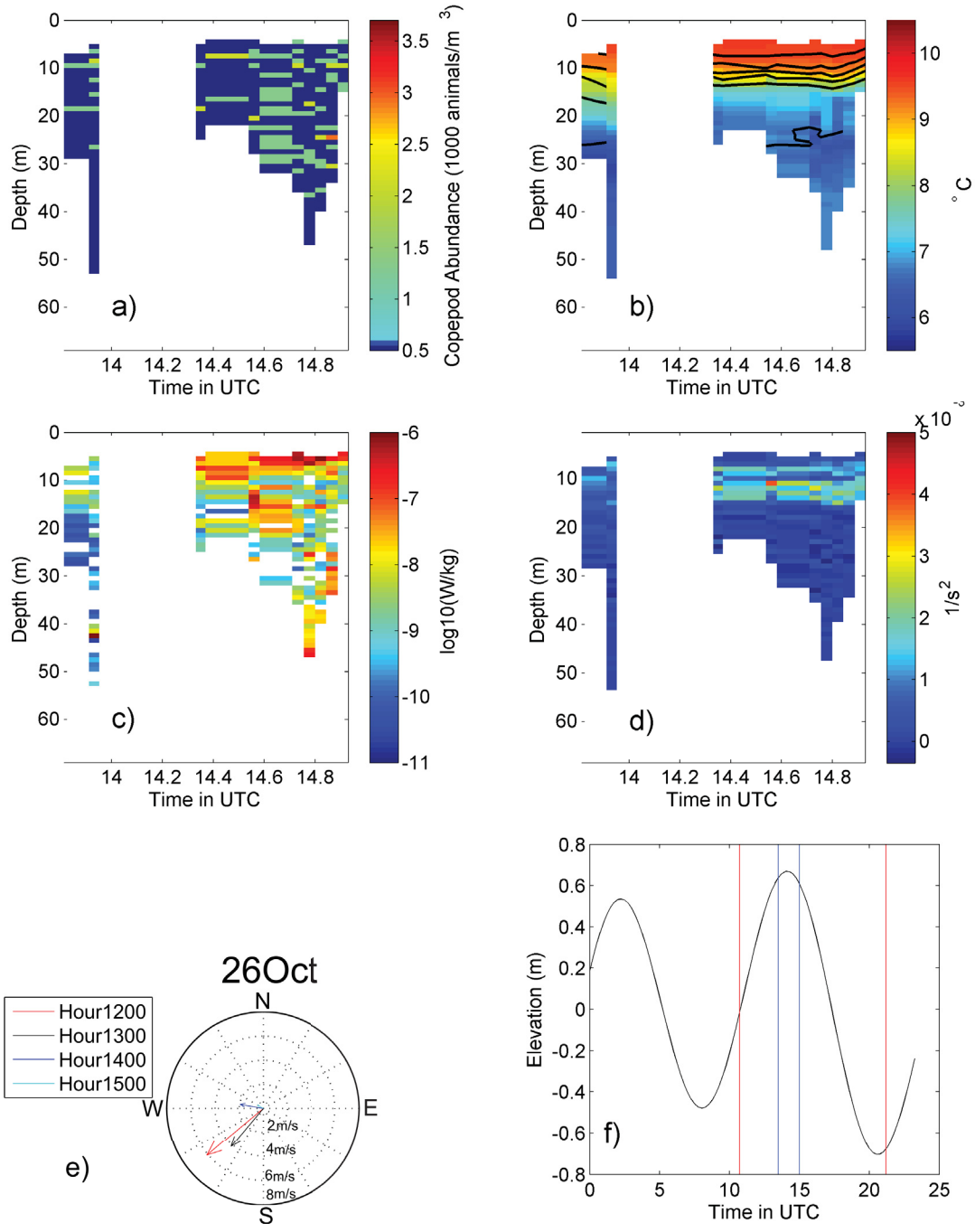


Figure 3.3: Time series summaries of depth averaged a) copepod abundance ($\mathrm{animals/m^3}$), b) temperature ($^\circ$C) with density contours ($\mathrm{kg/m^3}$) (the density contours start at 1023.5 $\mathrm{kg/m^3}$ and increase at 0.25 $\mathrm{kg/m^3}$ to 1024.75 $\mathrm{kg/m^3}$ near 25 $\mathrm{m}$ depth), c) turbulent dissipation rates ($log_{10}(\mathrm{W/kg})$), d) squared buoyancy frequency ($\mathrm{1/s^2}$) and the corresponding e) wind speed ($\mathrm{m/s}$) and direction and f) tidal elevation in Bedford Basin on 26 October 2010. The sample period in the tidal cycle is denoted the vertical blue lines and daylight hours are denoted between the vertical red lines. The gap in the data from about 14 to 14.4 hours is due to the ship's sampling location change.

### 3.1.3 03 November 2010

The number of copepods was lower on 03 November, relative to the earlier two sampling days (Figure 3.4 panel a). Again, there are few copepod observations at depth. The temperature and density plot, (Figure 3.4 panel b), shows the thermocline around 22 $\mathrm{m}$ and is, overall, relatively cooler than the data collected in October, ranging between 5.5 - 8.5 $^{\circ}$C. Compared to the October data, the surface layer has deepened. The pycnocline was shallower than the thermocline, around 7 $\mathrm{m}$. The dissipation rates (Figure 3.4 panel c) are higher throughout both the time series and the water column; very few low $\varepsilon$ values recorded. The squared buoyancy frequencies were larger above 10 $\mathrm{m}$ depth (Figure 3.4 panel d). The winds (Figure 3.4 panel e) during the sample time were mainly westerly and were relatively weak (just over 4 $\mathrm{m/s}$). The tides were ebbing from slack to low, ($\sim$ 11 hours since the last low tide) and sampling occurred during daylight hours (Figure 3.4 panel f) near the sill.

### 3.1.4 04 November 2010

Relative to the previous sampling periods, on 04 November, copepods were more abundant at depth, with multiple observations throughout each cast (Figure 3.5 panel a). The surface temperature was near 8.5 $^{\circ}$C, the thermocline was around 22 $\mathrm{m}$, and deep waters were 6 $^{\circ}$C (Figure 3.5 panel b). As with the 03 November data, the pycnocline was shallower than the thermocline, at 12 $\mathrm{m}$. The dissipation rates vary greatly throughout depth and time, but are generally lower below 27 $\mathrm{m}$ (Figure 3.5 panel c). The squared buoyancy frequency is low throughout (Figure 3.5 panel d), though modest peaks are found around 10-15 $\mathrm{m}$. Winds on 04 November were the lowest of all the sample days: less than 2 $\mathrm{m/s}$, to the west (Figure 3.5 panel e). Sampling on 04 November occurred pre- and post-dawn near the sill. The tidal cycle was ebbing from high to slack tide ($\sim$ 7 hours since low tides) (Figure 3.5 panel f).

### 3.1.5 30 November 2010

Copepods were least abundant on 30 November (Figure 3.6 panel a). The temperature data show a three layer system: surface to 7 $\mathrm{m}$, 7-25 $\mathrm{m}$ and 25 $\mathrm{m}$ to bottom. The temperature in the surface layer is near 7 $^{\circ}$C, 8.5 $^{\circ}$C in the intermediate layer and about 6 $^{\circ}$C in the bottom layer (Figure 3.6 panel b). The dissipation rates spanned a broad range, but were

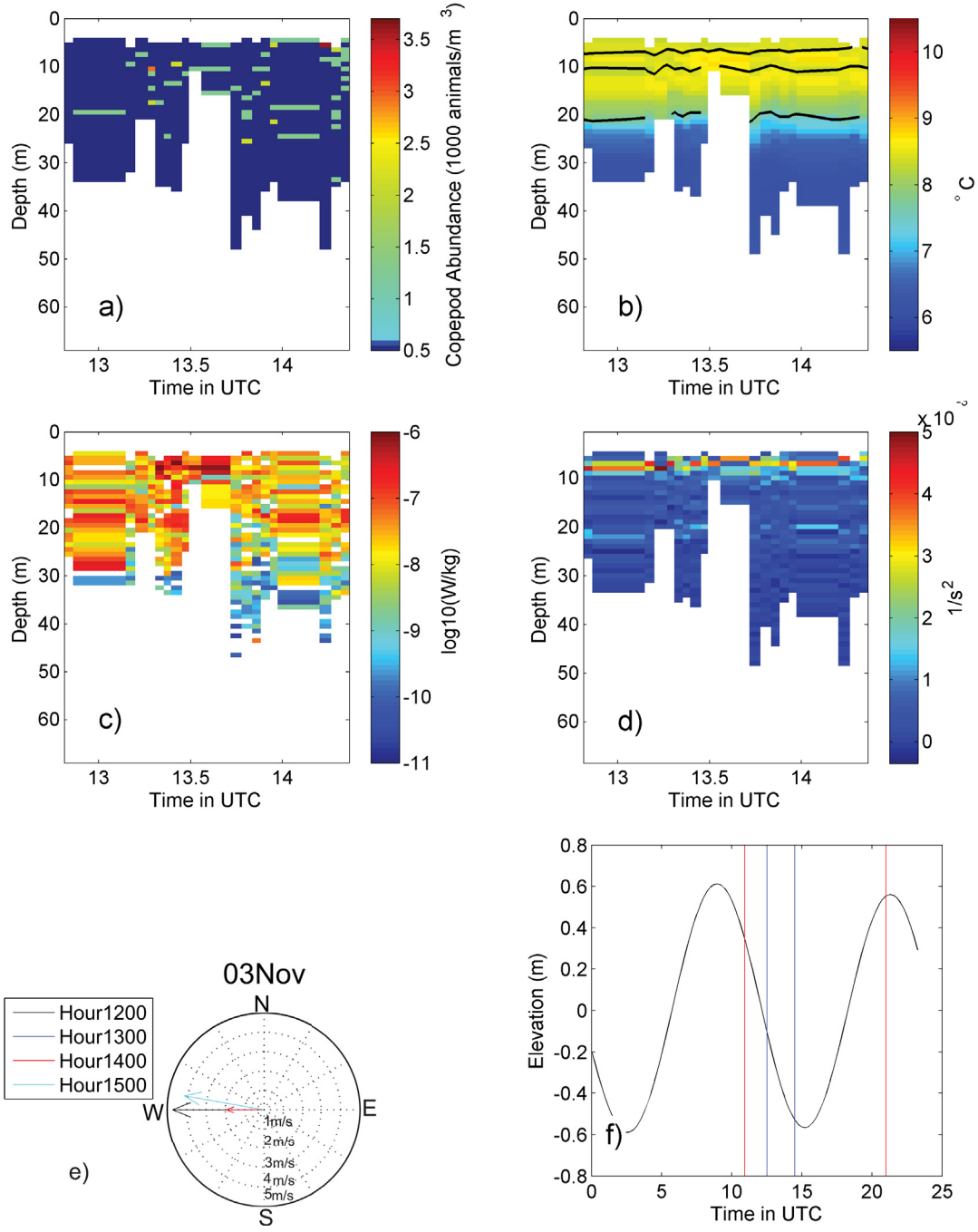


Figure 3.4: Time series summaries of depth averaged a) copepod abundance ($\mathrm{animals/m^3}$), b) temperature ($^{\circ}$C) with density contours ($\mathrm{kg/m^3}$) (the density contours start at 1023.5 $\mathrm{kg/m^3}$ and increase at 0.5 $\mathrm{kg/m^3}$ to 1024.5 $\mathrm{kg/m^3}$ near 20 $\mathrm{m}$ depth), c) turbulent dissipation rates ($log_{10}(\mathrm{W/kg})$), d) squared buoyancy frequency ($\mathrm{1/s^2}$) and the corresponding e) wind speed ($\mathrm{m/s}$) and direction and f) tidal elevation in Bedford Basin on 03 November 2010. The sample period in the tidal cycle is denoted the vertical blue lines and daylight hours are denoted between the vertical red lines.

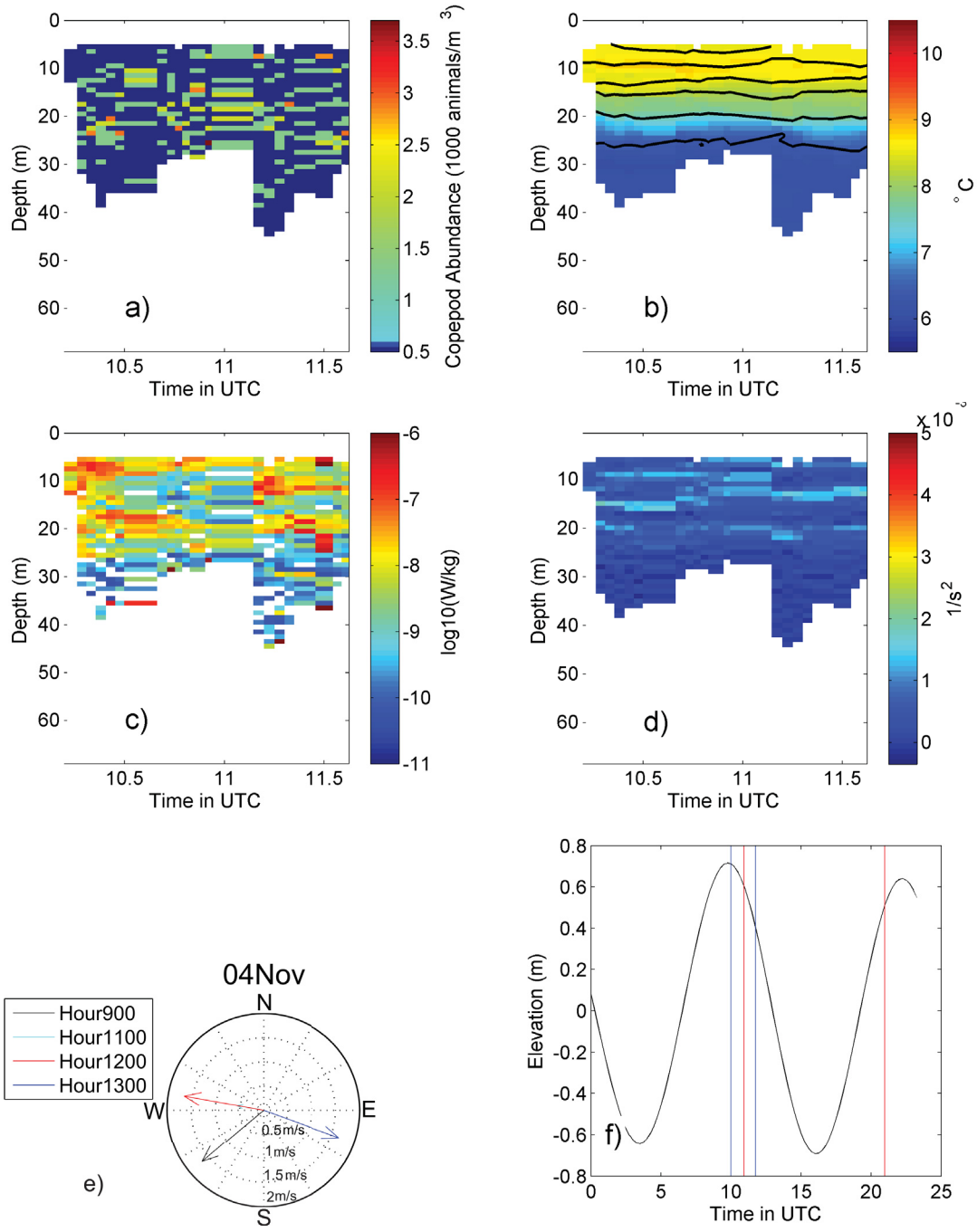


Figure 3.5: Time series summaries of depth averaged a) copepod abundance ($\mathrm{animals/m^3}$), b) temperature ($^\circ$C) with density contours ($\mathrm{kg/m^3}$) (the density contours start at 1023.5 $\mathrm{kg/m^3}$ and increase at 0.25 $\mathrm{kg/m^3}$ to 1024.75 $\mathrm{kg/m^3}$ near 25 ~mdepth), c) turbulent dissipation rates ($log_{10}(\mathrm{W/kg})$), d) squared buoyancy frequency ($\mathrm{1/s^2}$) and the corresponding e) wind speed ($\mathrm{m/s}$) and direction and f) tidal elevation in Bedford Basin on 04 November 2010. The sample period in the tidal cycle is denoted the vertical blue lines and daylight hours are denoted between the vertical red lines.

generally lower below 30 $\mathrm{m}$ (Figure 3.6 panel c). The squared buoyancy frequencies were again low, with modest peaks near 30 $\mathrm{m}$ depth and above 10 $\mathrm{m}$ depth (Figure 3.6 panel d). The winds were mainly northwest and were less than 4 $\mathrm{m/s}$ during sampling (Figure 3.6 panel e). Finally, sampling occurred during daylight and was near slack tide (Figure 3.6 panel f), just after low tide near the sill.

## 3.2 The Distribution of Copepods with respect to High-Resolution Physical Variables

The plots for each sample period show variation of the variables from day-to-day. However, they indicate no clear relationship between the vertical distribution of copepods and any one physical factor. In Chapter 1, I hypothesized that the vertical distribution of copepods is not affected by any physical factor. To test this hypothesis, I determined whether the distributions of the various physical factors changed based on the presence of copepods. First, however, I considered the relationships between all of the physical variables to determine whether any are related.

For each sample period, all of the 1 $\mathrm{m}$ binned observations for each of depth, temperature, salinity, density, buoyancy frequency and turbulent dissipation were plotted against each other. Using the copepod presence data I can do the same for a 'copepod presence' subset. The following figures illustrate the differences in the distributions of the physical variables.

High correlations were observed between temperature and salinity (correlation of -0.74) (Figure 3.7 shows a temperature-salinity plot for all sample periods), temperature and density (correlation of -0.89) and salinity and density (correlation 0.97) (not shown). From Figures 3.8 - 3.10, I can see (as expected) surface waters are warmer, fresher and less dense while deep waters are cooler, saltier and denser.

### 3.2.1 Plots of Physical Data vs Depth: with Copepods and without Copepods

Figures 3.8 - 3.12 are sets of sample ratio (SR) density plots to show how physical variables are related to depth and copepod distribution. The deep blue represents values that were sampled but that had no copepod presence. As the colour bar transitions from blue to red, the relative number of copepod observations to total observations increases, illustrating the

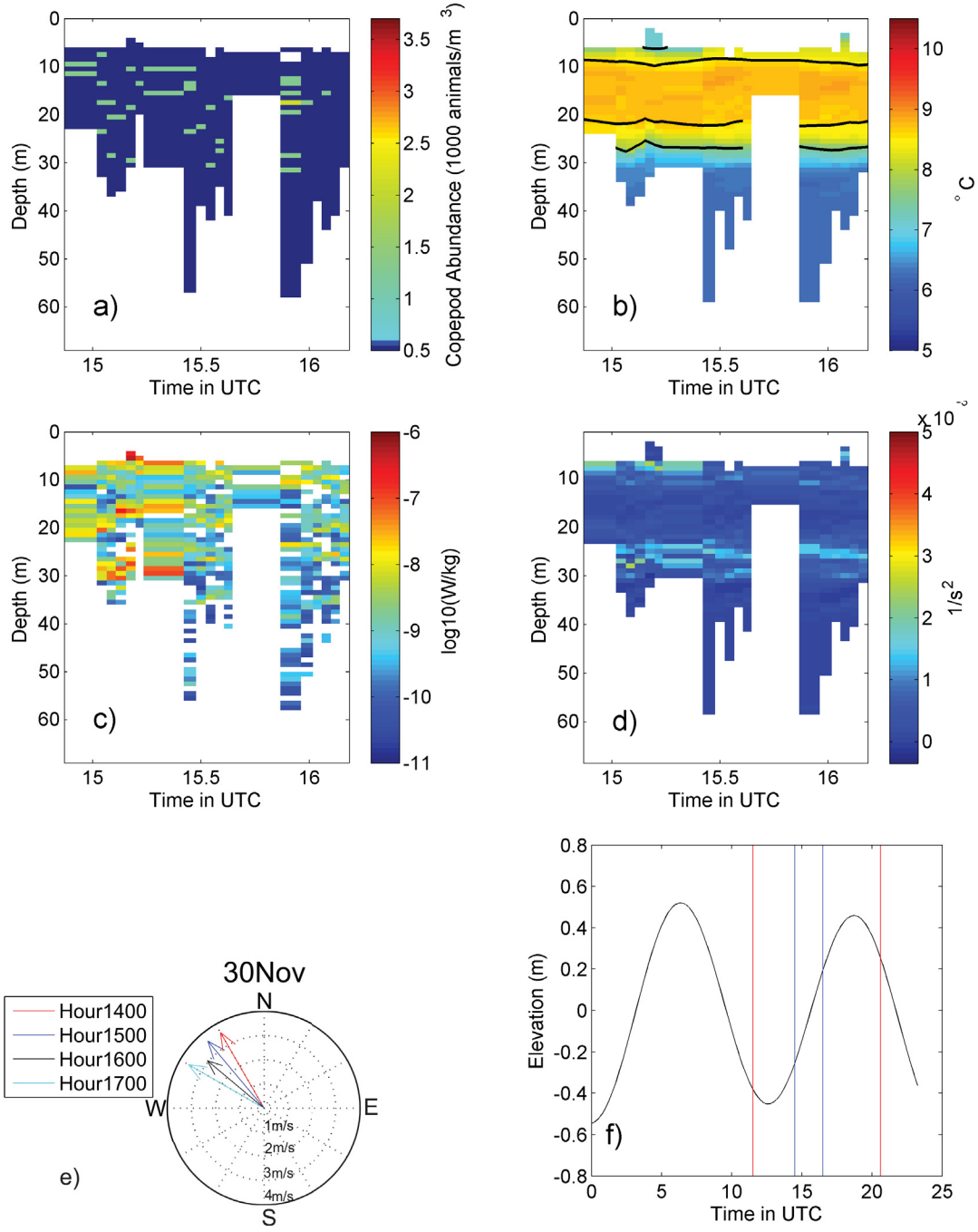


Figure 3.6: Time series summaries of depth averaged a) copepod abundance ($\mathrm{animals/m^3}$), b) temperature ($^\circ$C) with density contours ($\mathrm{kg/m^3}$) (the density contours start at 1023.5 $\mathrm{kg/m^3}$ and increase at 0.5 $\mathrm{kg/m^3}$ to 1024.5 $\mathrm{kg/m^3}$ near 27 $\mathrm{m}$ depth), c) turbulent dissipation rates ($log_{10}(\mathrm{W/kg})$), d) squared buoyancy frequency ($\mathrm{1/s^2}$) and the corresponding e) wind speed ($\mathrm{m/s}$) and direction and f) tidal elevation in Bedford Basin on 30 November 2010. The sample period in the tidal cycle is denoted the vertical blue lines and daylight hours are denoted between the vertical red lines.

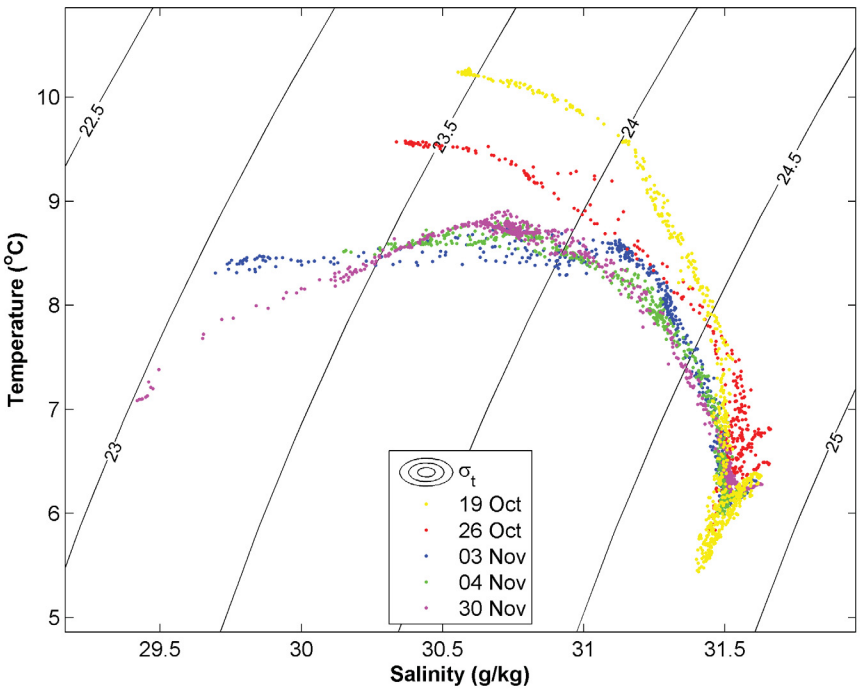


Figure 3.7: Temperature-salinity plot for all sample periods in Bedford Basin for all depths on top of density contours. The x-axis is salinity ($\mathrm{g/kg}$) and the y-axis is temperature ($^{\circ}\mathrm{C}$). The background contours are the density anomaly ($\sigma_t = density - 1000\ \mathrm{kg/m^3}$). The yellow points are observations on 19 October, red from 26 October, blue from 03 November, green from 04 November and magenta from 30 November. This figure shows that while the water mass properties in Bedford Basin have a tight relationship during any given sample period, overall the properties change throughout time.

distribution of copepods with respect to the two variables. The white areas represent no observations.

Temperature data range between $\sim$ 10 and $\sim$ 6 °C and show a consistent thermocline above 30 $\mathrm{m}$ (Figure 3.8). Copepods are most abundant above $\sim$ 35 $\mathrm{m}$ depth. The temperature data correlate with depth (warmer temperatures correspond to shallower waters).

The salinity and depth relationship (Figure 3.9) shows that the salinity varies relatively little, mainly between 30 and 32 $\mathrm{g/kg}$. Salinity data vary with depth, as expected in an estuarine system (fresher waters at the surface due to surface fresh water input). Again, the copepod presence data are concentrated above $\sim$ 35 $\mathrm{m}$. The copepod presence data cover about the same range of values as the all observations data.

The density data (Figure 3.10) show a relationship with depth similar to the salinity data. The denser water is expected to be found deeper in the water column. The copepods are present over the same ranges as the all observations, but there are fewer in deep water ($\sim$ 35 $\mathrm{m}$) compared to the full dataset. Note that Figures 3.8-3.10 suggest that nearly all of the copepods are found in the thermo-, halo- and pycnoclines. All occur over the same depth range, which is no surprise given the strong TS relationships for each sample period (Figure 3.7).

Figure 3.11 compares the buoyancy frequency to the depth data. The $N^2$ values are concentrated at 0 and spread from $-10^{-5}$ to $1.5 \cdot 10^{-3}$ $1/\mathrm{s}^2$ and the depths from $\sim$ 5-20 $\mathrm{m}$. There is not a strong relationship between the squared buoyancy frequency and depth and the copepod data are evenly spread along the squared buoyancy frequency values for all depths $<$ 35 $\mathrm{m}$.

A wide range of dissipation rates were sampled (Figure 3.12) and high dissipation rates were observed more frequently near the surface. As with the squared buoyancy frequency data, there does not appear to be a strong correlation between $\varepsilon$ and depth, the dissipation covers its range for most depths ($<$ 35 $\mathrm{m}$).

The copepod presence distributions for temperature, salinity and density vs. buoyancy frequency and temperature, salinity and density vs. dissipation both cover the same range as the all data distributions (also not shown).

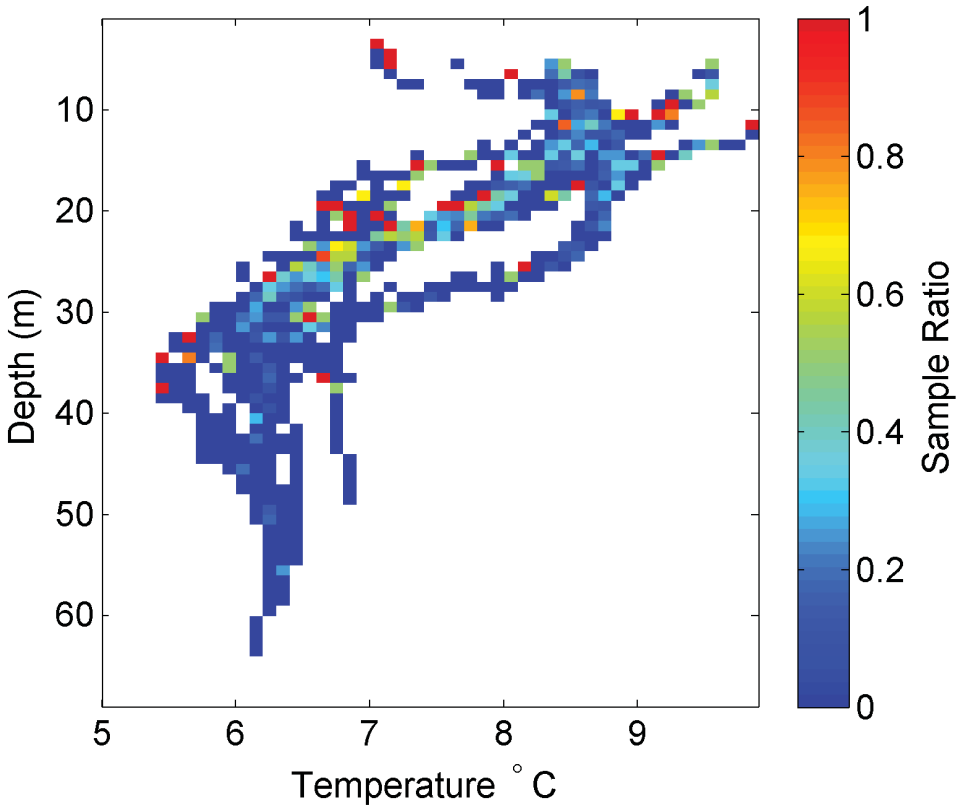


Figure 3.8: SR density plots for temperature vs. depth. The x-axis is temperature (°C) and the y-axis is depth in metres. The colour map represents the sample ratio ($SR = \frac{number\ of\ copepods}{number\ of\ total\ observations}$). The deep blue represents values of temperature and depth that were sampled, but where there were no copepod observations. As the figure colours transition from blue to red, the relative number of copepod observations to total observations increases, providing information about the distribution of copepods in depth and temperature space. The white areas represent no observations (e.g there are no observations of 5 °C in waters at 10 m depth).

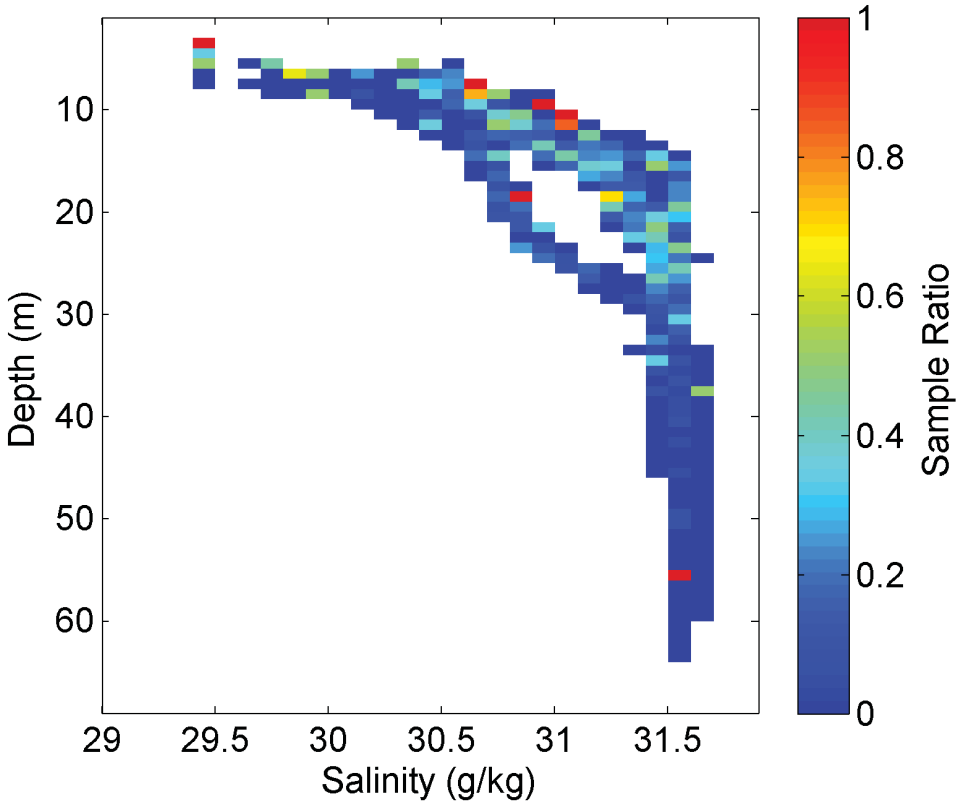


Figure 3.9: SR density plots for salinity vs. depth. The x-axis is salinity ($\mathrm{g/kg}$) and the y-axis is depth in metres. The colour map represents the sample ratio ($SR = \frac{number\ of\ copepods}{number\ of\ total\ observations}$). The deep blue represents values of salinity and depth that were sampled, but where there were no copepod observations. As the figure colours transition from blue to red, the relative number of copepod observations to total observations increases, providing information about the distribution of copepods in depth and salinity space. The white areas represent no observations (e.g there are no observations of 29.5 $\mathrm{g/kg}$ in waters at 30 $\mathrm{m}$ depth).

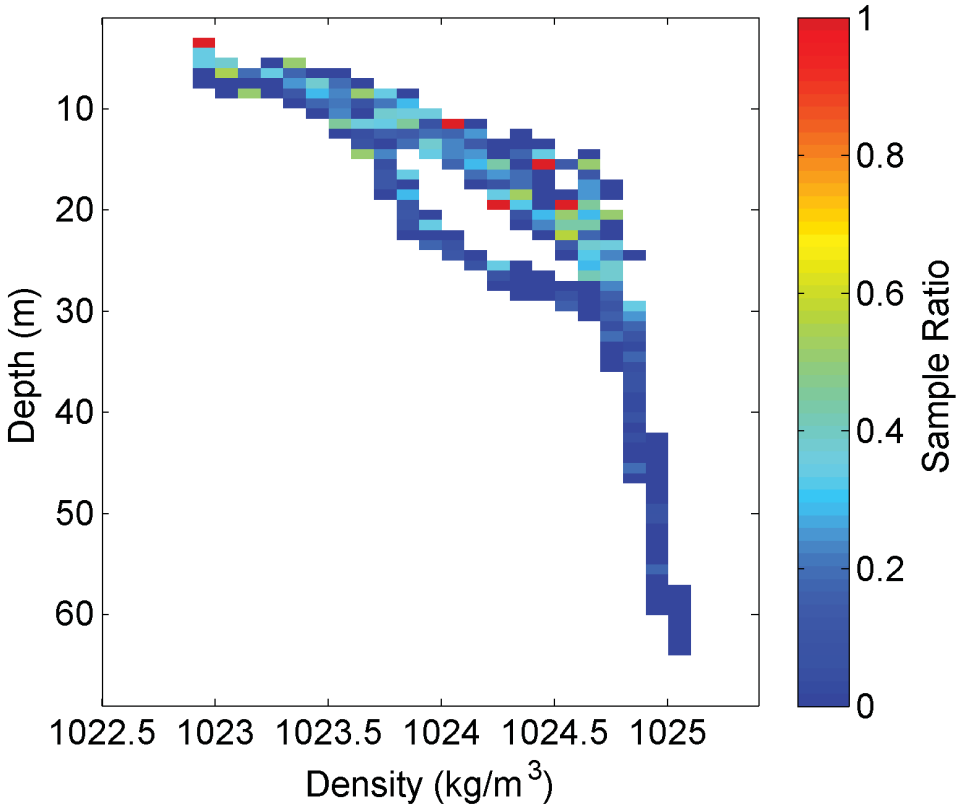


Figure 3.10: SR density plots for density vs. depth. The x-axis is density ($\mathrm{kg/m^3}$) and the y-axis is depth in metres. The colour map represents the sample ratio ($SR = \frac{number\ of\ copepods}{number\ of\ total\ observations}$). The deep blue represents values of density and depth that were sampled, but where there were no copepod observations. As the figure colours transition from blue to red, the relative number of copepod observations to total observations increases, providing information about the distribution of copepods in depth and density space. The white areas represent no observations (e.g there are no observations of 1023 $\mathrm{kg/m^3}$ in waters at 30 $\mathrm{m}$ depth).

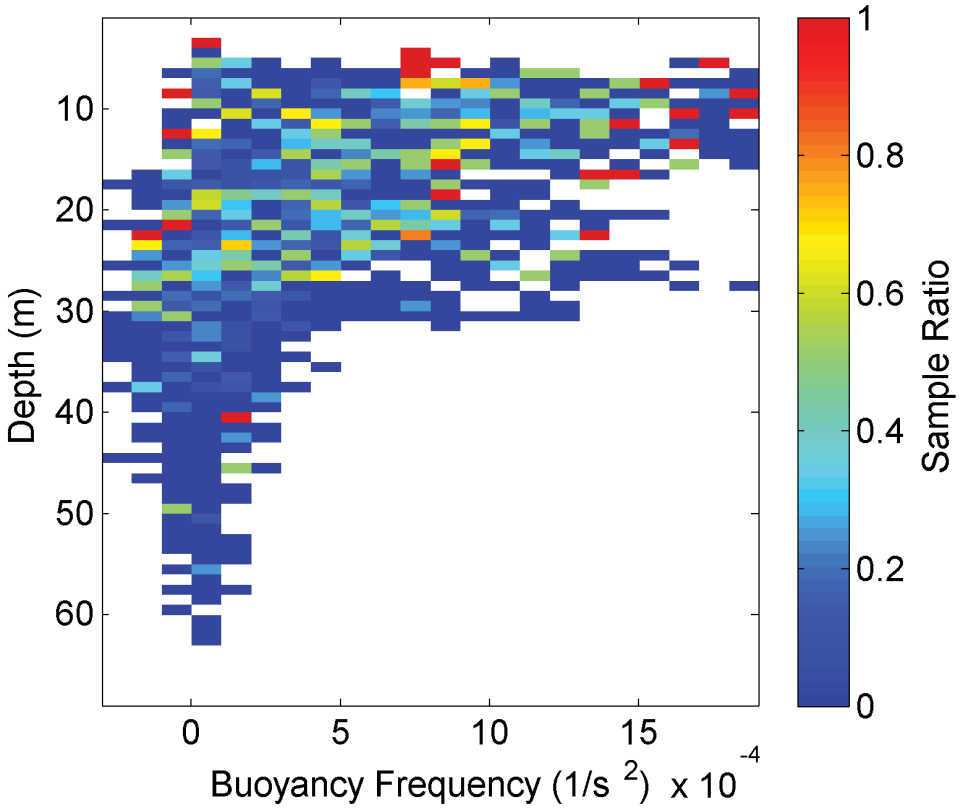


Figure 3.11: SR density plots for squared buoyancy frequency vs. depth. The x-axis is buoyancy frequency squared ( $1/\mathrm{s}^2$) and the y-axis is depth in metres. The colour map represents the sample ratio ($SR = \frac{number\ of\ copepods}{number\ of\ total\ observations}$). The deep blue represents values of squared buoyancy frequency and depth that were sampled, but where there were no copepod observations. As the figure colours transition from blue to red, the relative number of copepod observations to total observations increases, providing information about the distribution of copepods in depth and squared buoyancy frequency space. The white areas represent no observations (e.g there are no observations of $10^{-3}\ 1/\mathrm{s}^2$ in waters at $50\ \mathrm{m}$ depth).

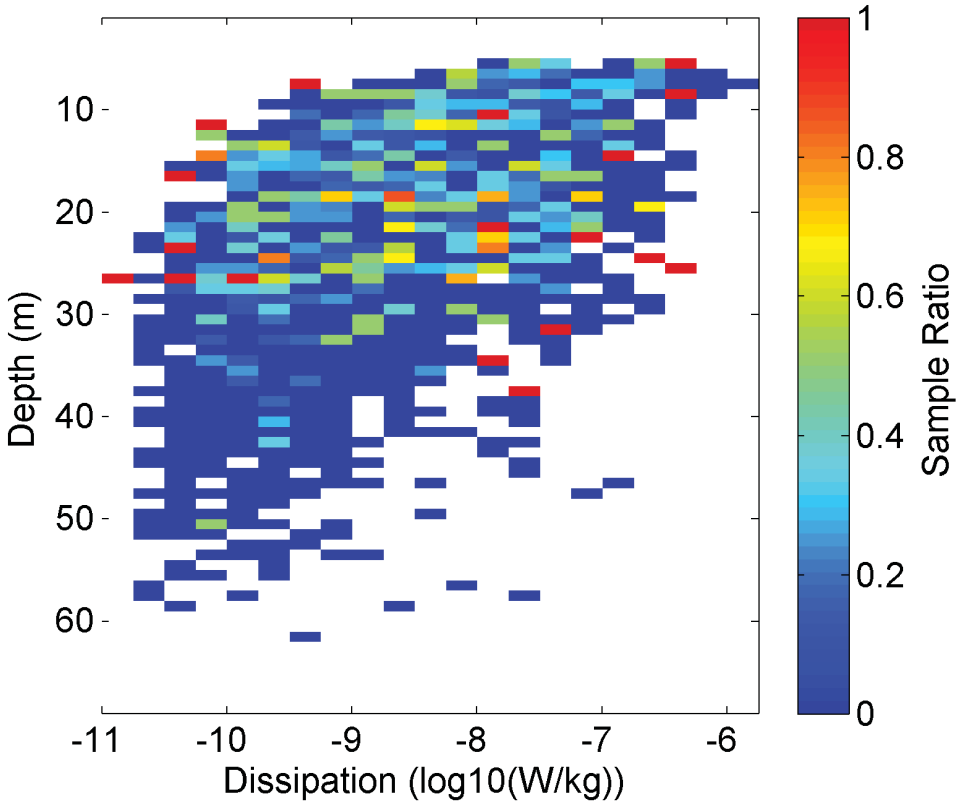


Figure 3.12: SR density plots for $log_{10}$ dissipation vs. depth. The x-axis is $log_{10}$ dissipation ($log_{10}(\mathrm{W/kg})$) and the y-axis is depth in metres. The colour map represents the sample ratio ($SR = \frac{number\ of\ copepods}{number\ of\ total\ observations}$). The deep blue represents values of dissipation and depth that were sampled, but where there were no copepod observations. As the figure colours transition from blue to red, the relative number of copepod observations to total observations increases, providing information about the distribution of copepods in depth and dissipation space. The white areas represent no observations (e.g there are no observations of -7 $log_{10}\,\mathrm{W/kg}$ in waters at 50 $\mathrm{m}$ depth).

### 3.2.2 Bar Graphs of Physical Variables: All Observations and Observations with Copepod Presence

The plots in the last section suggested that copepods were located preferentially in the thermo-, halo- or pycnocline. To assess parameters affecting copepod presence individually, I now compare the natural distribution of each factor with the distribution of each variable while copepods were present. The distribution of the difference between the expected and copepod presence distributions for each physical variable was plotted as bar graphs (Figures 3.15, 3.17-3.21). If a physical variable does not affect the vertical distribution of copepods, I expect the distribution of copepod presence data to be statistically equal to the distribution of all observations, hence the difference in the two distributions would be zero. If the distributions are different (consistently large differences throughout bins), it would suggest that the physical variable affects the vertical distribution of copepods.

#### 3.2.2.1 Depth

Most of the sampling occurred from the depth bins centred at 8 $\mathrm{m}$ to 41 $\mathrm{m}$ (Figure 3.13). There were few observations in the first bins (at 1-3 $\mathrm{m}$) because VMP/VPR casts usually started (i.e. reached free-fall) at a depth of 5 $\mathrm{m}$. There are few observations from the bins centred at 43 $\mathrm{m}$ to 63 $\mathrm{m}$ because much of the sampling was done near the mouth of Bedford Basin where the water depth is only 40 $\mathrm{m}$ (on 19 October, the sampling occurred in the 70 $\mathrm{m}$ deep hole in the centre of the basin). To remove the bias due to the depth distribution, I removed depth bins with few observations in them. Any bins that had less than 20% of the maximum observations in any bin were removed from the analysis. The maximum number of observations (bins 9, 10 and 11 $\mathrm{m}$) was 93, so all bins with less than 75 observations were excluded from the remaining analysis (i.e. data from 0-6 $\mathrm{m}$ and 30-63 $\mathrm{m}$ were removed). Removing these bins excluded 74 copepod observations (13.8% of the copepod observations) from the analysis.

In the resulting distribution, sorted into 2 $\mathrm{m}$ bins, (Figure 3.14 top panel) the sampling depths are more evenly distributed. The copepod presence distribution has a similar overall shape as the full distribution, but copepod presence has much fewer observations (y-axis). Bins centred from 7- 25 $\mathrm{m}$ have $\sim$40 observations, while the two deepest bins, 27 and 29 $\mathrm{m}$, have $\sim$20 and 10 observations respectively.

In the distribution of the difference between the expected and actual observations of copepod presence vs. depth (Figure 3.15), the blue bars represent bins (bins centred at

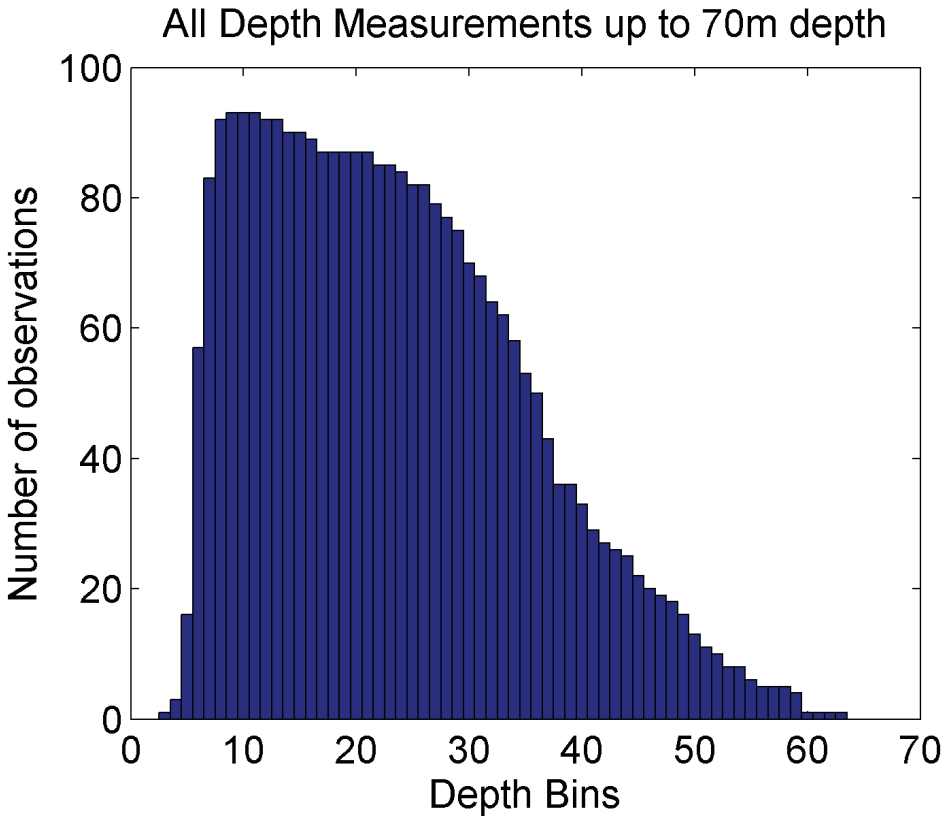


Figure 3.13: The distributions of all observations for depths from 3-63 $\mathrm{m}$ in Bedford Basin. The histogram represents the distribution of all of the 1 $\mathrm{m}$ binned data for that particular variable. The x-axis represents the depth bins sampled. The y-axis is the absolute number of observations. It shows that the sampling distribution is concentrated from $\sim$ 7-29 $\mathrm{m}$ depth.

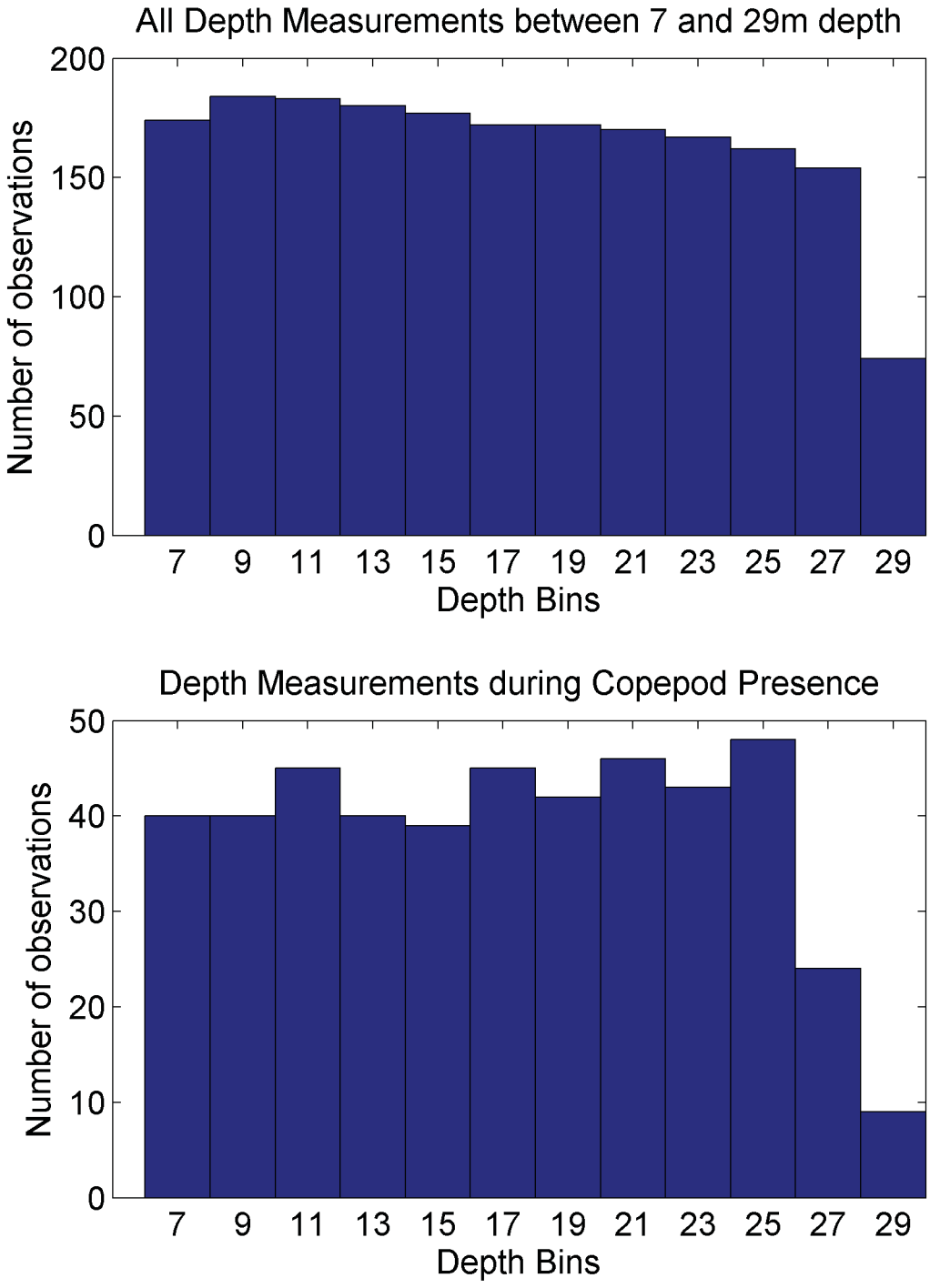


Figure 3.14: The distributions of all observations (top) and copepod presence (bottom) for depths from 7-29 $\mathrm{m}$ in Bedford Basin. The x-axis represents the depth bins sampled. The y-axis is the absolute number of observations. Comparison of the relative abundances of all of the observations compared to the copepod presence observations will give insights into how copepods are distributed with respect to depth.

| Variable | $\chi^2$ | Degrees of Freedom | p-val | Result |
|---|---|---|---|---|
| Depth (7-29 $\mathrm{m}$) | 13.3 | 11 | 0.28 | Not significant |
| Temperature (7-29 $\mathrm{m}$) | 33.8 | 8 | $4.38x10^{-5}$ | Significant |
| Salinity (7-29 $\mathrm{m}$) | 18.1 | 8 | 0.02 | Significant |
| Density (7-29 $\mathrm{m}$) | 18.3 | 8 | 0.02 | Significant |
| Buoyancy frequency (7-29 $\mathrm{m}$) | 9.9 | 7 | 0.19 | Not significant |
| Dissipation (7-29 $\mathrm{m}$) | 11.8 | 8 | 0.16 | Not significant |

Table 3.1: Column 1 is the variable tested against copepod presence. Column 2 is the $\chi^2$ test statistic. Column 3 is the degrees of freedom. Note that it changes per variable due to the number of bins and whether each expected bin has at least 5 observations. Column 4 is the p-value. Any p-value less than 0.05 signifies that the null hypothesis should be rejected and that the two distributions are different. Column 5 is based on Column 4: if a p-value is less than 0.05, then the observed distribution is not the same as the expected distribution and that particular variable is significant in determining the vertical distribution of copepods.

11, 17, 19, 21, 23 and 25 $\mathrm{m}$) where there are more copepods than expected if depth had no effect on the distribution of copepods. In bins with red bars (bins centred at 7, 9, 13, 15, 27 and 29 $\mathrm{m}$) there are fewer copepods than expected if depth had no effect on the distribution of copepods. The statistical test used to determine if these differences are significant over all bins, is the $\chi^2$ goodness-of-fit test (results in Table 3.1). All of the expected bins had more than 5 copepods present, so all of the data were used in calculating the test statistic. The result from the $\chi^2$ test suggests that there is no statistical difference between the distribution of depth for all observations and the distribution of depths with copepod presence (the difference is too small to be significant). This result is surprising since I expected that copepods would not be evenly distributed with respect to depth due to DVM. Therefore, I compared sampling during day and night to determine if depth could affect copepod distributions via DVM as a response to light.

The literature suggested that responses to light may affect the vertical distribution of copepods via DVM. To test whether light had an effect on the vertical distribution of copepods, the distribution of copepod presence during daytime and night-time were compared. A binned sample ratio ($SR = \frac{number\ of\ copepods}{number\ of\ total\ observations}$ per each depth bin) was computed for daytime and night-time (Figure 3.16) for all depth bins sampled (3-63 $\mathrm{m}$). The average binned SR for the depth bins for daytime was 0.11, and 0.16 for night-time.

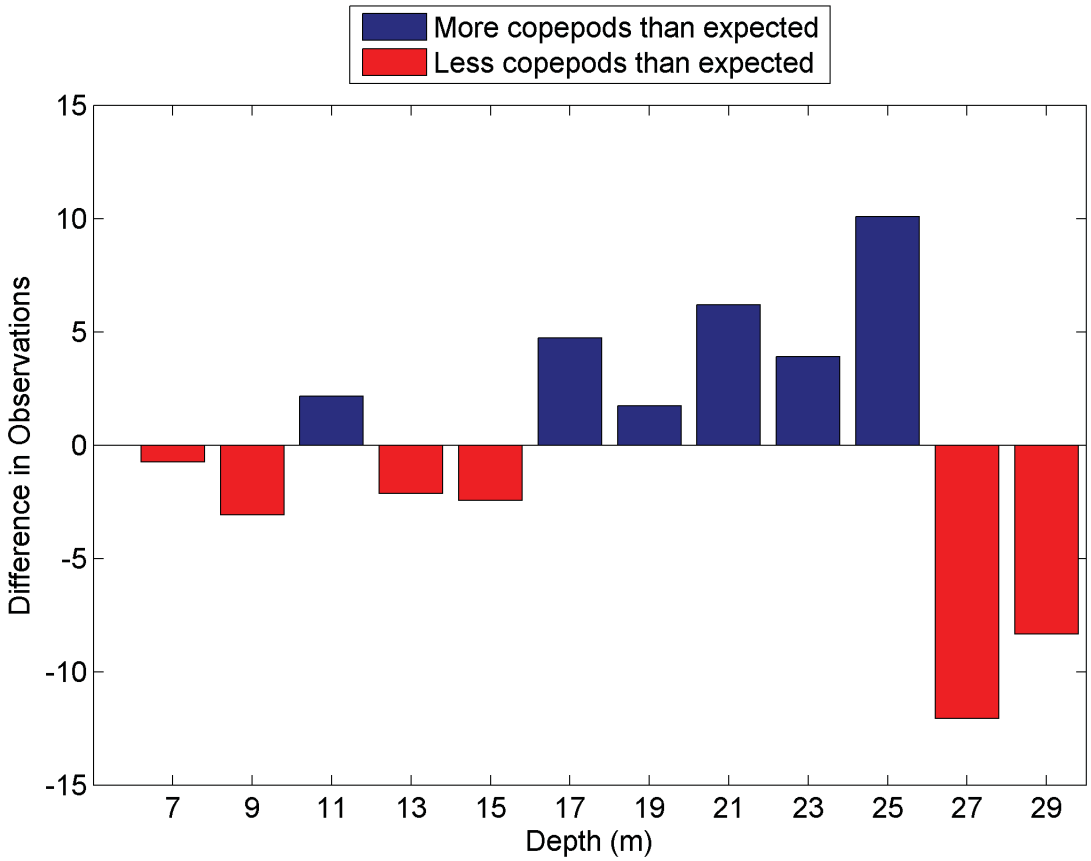


Figure 3.15: Relative differences between the expected and observed observations of copepods per depth bin. The x-axis represents the 2- m depth bin and the y-axis is the difference in observations between the expected (all observations scaled to the number of total copepod observations) and observed (total number of copepods present per depth bin). The blue bars (positive) represent the bins where there are more copepods than expected if copepods were not distributed differently among depth bins. The red bars (negative) represent the bins where there are less copepods than expected if copepods were not distributed differently among depth bins.

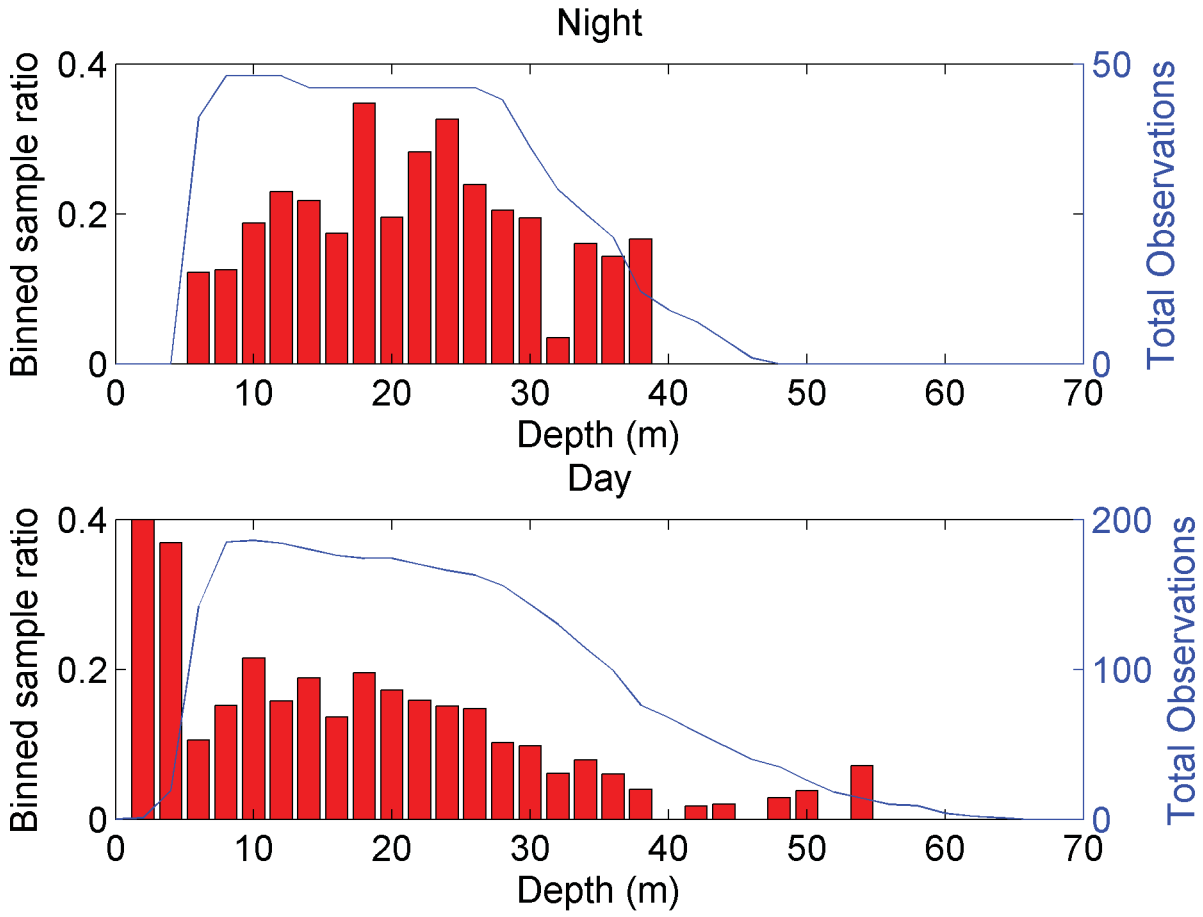


Figure 3.16: A bar graph of the sample ratios for night (top panel) and day (bottom panel). For both plots, the x-axis is the depth bin. The left y-axis is the sample ratio ($SR = \frac{number\ of\ copepods}{number\ of\ total\ observations}$) for each depth bin. The higher a SR, the relatively more copepods are present. The right y-axis (blue) is the absolute number of observations. The red bars show the SR per bin. The blue line represents the total number of observations in each bin to emphasize that during the night, there are proportionally more copepods sampled per bin. This is especially noticeable in the first two bins of the daytime sample, where the SRs are quite high. However, there are only a few total observations in those bins, so the variability in these bins is much higher than in bins with more total observations.

#### 3.2.2.2 Temperature

In the comparison of the difference in the expected and actual copepod presence temperature distribution (Figure 3.17), bins centred at 6 °C, 8.5 °C and 9 °C (red bars) have less copepods than expected if temperature had no effect on the vertical distribution of copepods. There are more copepods than expected in temperature bins centred at 6.5 °C, 7 °C, 7.5 °C, 8 °C, 9.5 °C and 10 °C (blue bars). From the $\chi^2$ test, the distribution of temperature with copepod presence is statistically different from the full distribution of temperature (Table 3.1). All of the expected bins had more than 5 copepods present, so all the data were used in calculating the test statistic.

#### 3.2.2.3 Salinity

Salinity bins with more copepods than expected are centred at 30.65 $\mathrm{g/kg}$, 30.8 $\mathrm{g/kg}$, 31.1 $\mathrm{g/kg}$, 31.25 $\mathrm{g/kg}$ and 31.4 $\mathrm{g/kg}$ (Figure 3.18). The bins with fewer copepods than expected include bins centred at 29.6 $\mathrm{g/kg}$, 29.75 $\mathrm{g/kg}$, 29.9 $\mathrm{g/kg}$, 30.05 $\mathrm{g/kg}$, 30.2 $\mathrm{g/kg}$, 30.35 $\mathrm{g/kg}$, 30.5 $\mathrm{g/kg}$ and 30.95 $\mathrm{g/kg}$. The full salinity distribution is statistically different from the distribution of salinity during copepod presence (Table 3.1). The bins (centred at 29.6 to 30.05 $\mathrm{g/kg}$) with a '*' represent the bins that had less than 5 copepods present, so they were excluded from the calculation of the $\chi^2$ statistic, removing 2 copepod presence points (4.3% of the observations).

#### 3.2.2.4 Density

For the density data, (Figure 3.19), the bins centred at 1023.6 $\mathrm{kg/m^3}$, 1024.4 $\mathrm{kg/m^3}$ and 1024.6 $\mathrm{kg/m^3}$ (blue bars) had more copepods than expected. The bins centred at 1023.2 $\mathrm{kg/m^3}$, 1023.4 $\mathrm{kg/m^3}$, 1023.8 $\mathrm{kg/m^3}$, 1024 $\mathrm{kg/m^3}$, 1024.2 $\mathrm{kg/m^3}$ and 1024.8 $\mathrm{kg/m^3}$ had less copepods than expected. The copepod presence distribution for density is not the same as the full density distribution (see the $\chi^2$ test in Table 3.1). All of the expected bins had more than 5 copepods present, so all of the data were used in calculating the test statistic.

#### 3.2.2.5 Buoyancy Frequency

For the squared buoyancy frequency (Figure 3.20), bins that have more copepods than expected are centred at $3\cdot10^{-4}$ $1/\mathrm{s^2}$, $6\cdot10^{-4}$ $1/\mathrm{s^2}$, $1.2\cdot10^{-3}$ $1/\mathrm{s^2}$ and $1.5\cdot10^{-3}$ $1/\mathrm{s^2}$ (blue bars). There were fewer copepods than expected at bins centred at $0$ $1/\mathrm{s^2}$ and $9\cdot10^{-4}$ $1/\mathrm{s^2}$

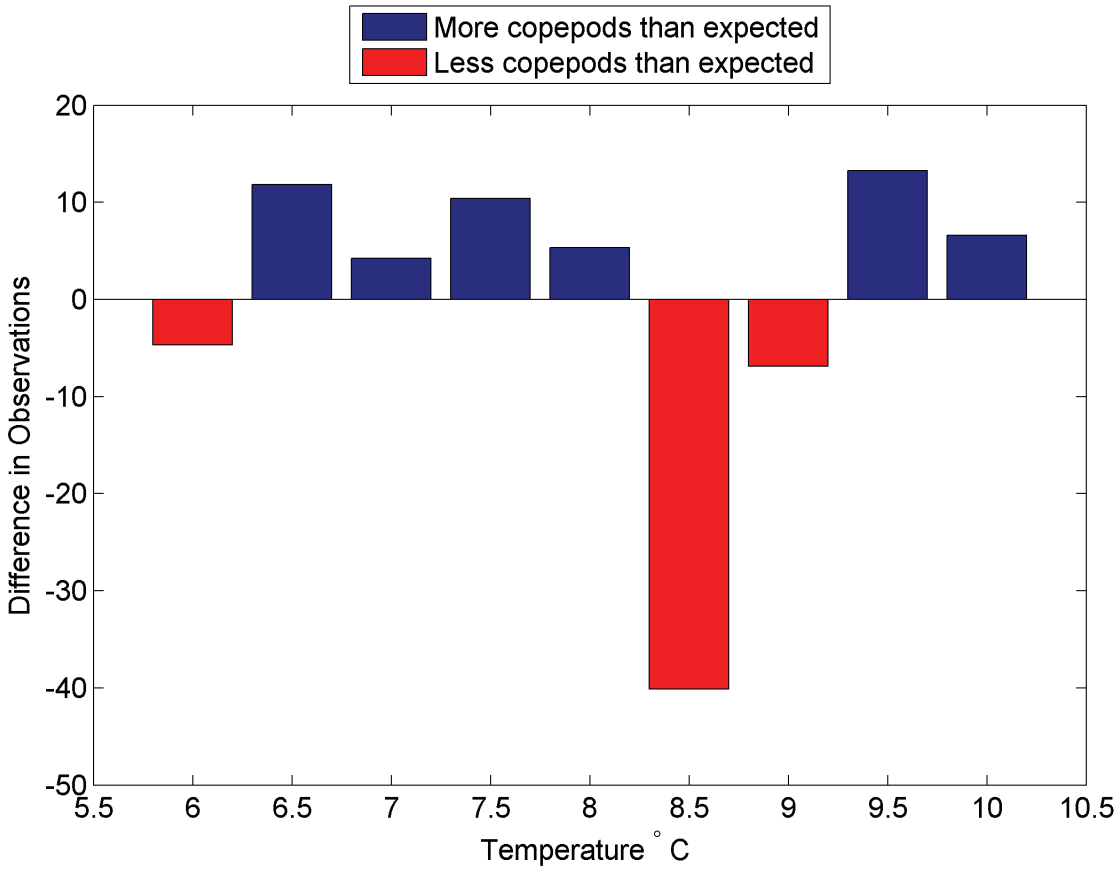


Figure 3.17: Relative differences between the expected and observed observations of copepods per temperature bin. The x-axis represents the 0.5 °C binned temperature and the y-axis is the difference in observations between the expected (all observations scaled to the number of total copepod observations) and observed (total number of copepods present per temperature bin). The blue bars (positive) represent the bins where there are more copepods than expected if copepods were not distributed differently among temperature bins. The red bars (negative) represent the bins where there are fewer copepods than expected if copepods were not distributed differently among temperature bins.

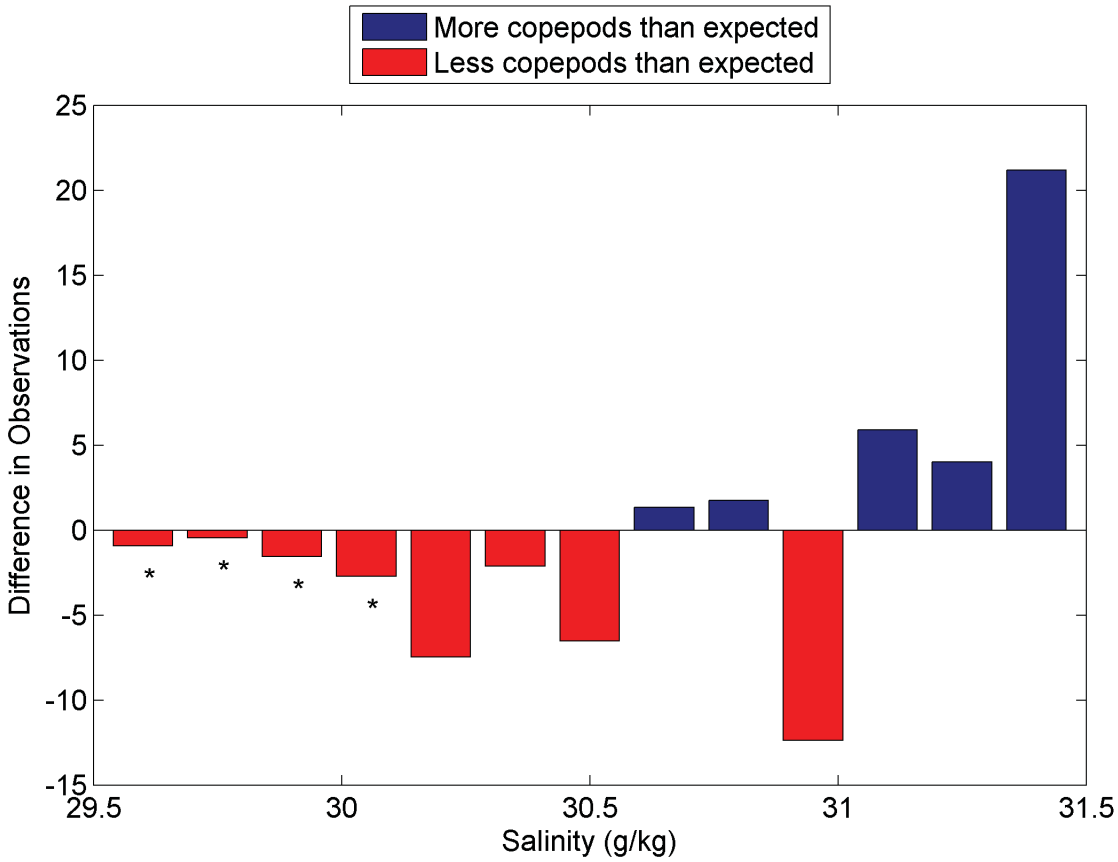


Figure 3.18: Relative differences between the expected and observed observations of copepods per salinity bin. The x-axis represents the 0.3 $\mathrm{g/kg}$ binned salinity and the y-axis is the difference in observations between the expected (all observations scaled to the number of total copepod observations) and observed (total number of copepods present per salinity bin). The blue bars (positive) represent the bins where there are more copepods than expected if copepods were not distributed differently among salinity bins. The red bars (negative) represent the bins where there are fewer copepods than expected if copepods were not distributed differently among salinity bins.

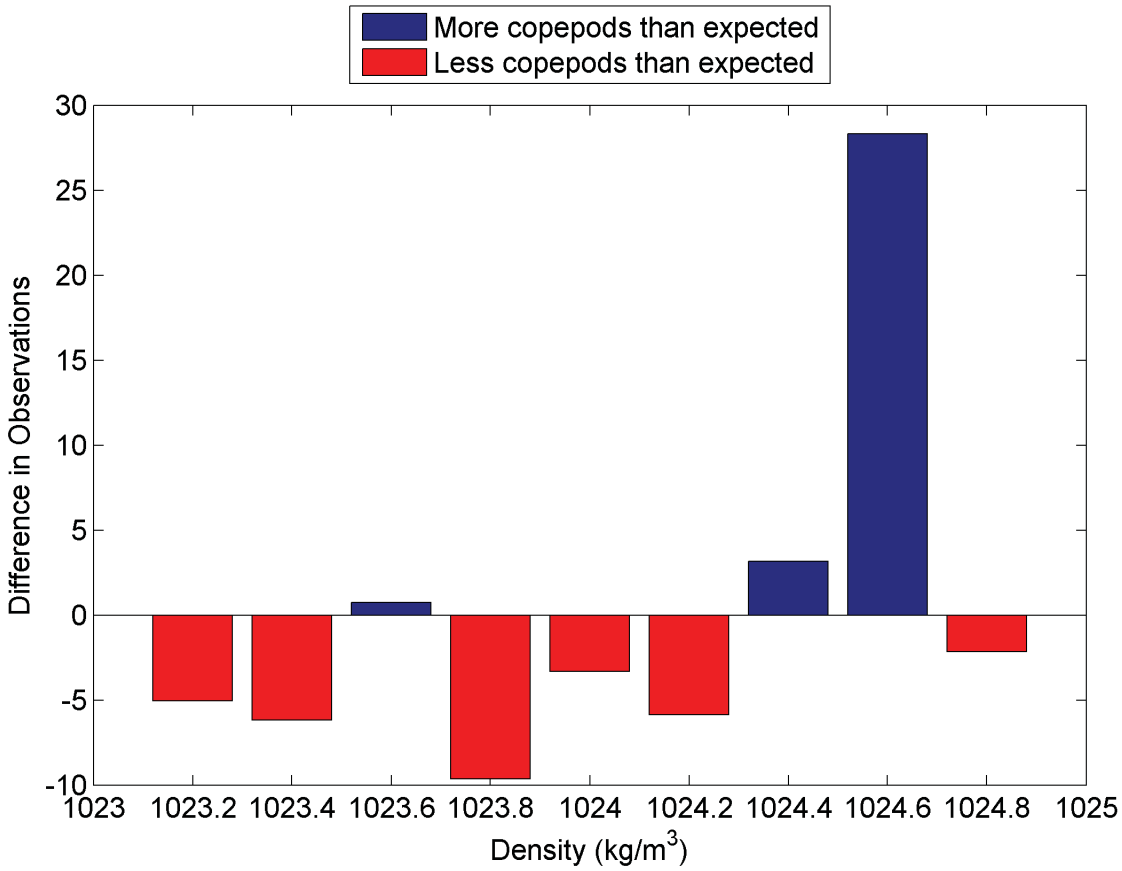


Figure 3.19: Relative differences between the expected and observed observations of copepods per density bin. The x-axis represents the 0.2 $\mathrm{kg/m^3}$ binned density and the y-axis is the difference in observations between the expected (all observations scaled to the number of total copepod observations) and observed (total number of copepods present per density bin). The blue bars (positive) represent the bins where there are more copepods than expected if copepods were not distributed differently among density bins. The red bars (negative) represent the bins where there are fewer copepods than expected if copepods were not distributed differently among density bins.

(red bars). Bins centred at $1.8 \cdot 10^{-3}$ and $2.1 \cdot 10^{-3}$ $1/\mathrm{s}^2$ have about the same number of copepods as expected. Based on the $\chi^2$ test, the copepod presence distribution is not significantly different from the full distribution of buoyancy frequency (Table 3.1). The lowest expected bin had fewer than 5 copepods, so it was removed from the $\chi^2$ calculation.

#### 3.2.2.6 Turbulent Dissipation

Finally, for the $log_{10}$ turbulent dissipation rate distributions (Figure 3.21), bins centred at $10^{-8}$ $\mathrm{W/kg}$, $3.2 \cdot 10^{-9}$ $\mathrm{W/kg}$, $10^{-10}$ $\mathrm{W/kg}$ and $3.2 \cdot 10^{-11}$ $\mathrm{W/kg}$ (red bars) have less copepods than expected, whereas $3.2 \cdot 10^{-7}$ $\mathrm{W/kg}$, $10^{-7}$ $\mathrm{W/kg}$, $3.2 \cdot 10^{-8}$ $\mathrm{W/kg}$, $10^{-9}$ $\mathrm{W/kg}$ and $3.2 \cdot 10^{-10}$ $\mathrm{W/kg}$ have more copepods than expected if dissipation did not effect the vertical distribution of copepods. The result from the $\chi^2$ test suggests that the copepod presence distribution is not affected by dissipation rates (Table 3.1). All of the expected bins had more than 5 copepods present, so all of the data were used in calculating the test statistic.

### 3.2.3 Multiple Linear Regression

The $\chi^2$ test results give insights into whether individual variables affect the copepod abundance, but it may be affected by more than one variable at a time. A multiple linear regression was used to determine which high-resolution independent variable (temperature, density, buoyancy frequency or dissipation) or combinations of these variables, had the strongest effect on the copepod abundance. From the TS plot (Figure 3.7), it can be seen that overall, temperature, salinity and density are not closely related enough to model the three variables with just one variable, thus two must be included in the multiple regression analysis. Multiple regressions were calculated for each possible combination of the factors (temperature, density, $N^2$ and dissipation), resulting in 15 regressions and $R_a^2$ values. Figure 3.22 outlines all of the possible combinations of these variables and the resulting $R_a^2$ values. Using this multiple regression analysis, the combination of temperature and density ($R_a^2 = 8.4 \cdot 10^{-3}$) best models the copepod abundance. The regression was significant (with p-values less than $0.05$) for all cases except with only dissipation only modelling copepod abundance (greyed out).

However, interpretation of the multiple linear regression analysis should be approached with caution, due mainly to the discreteness of the copepod data. Figure 3.23 is a correlation matrix plot, showing all of the simple linear regressions for copepod abundance

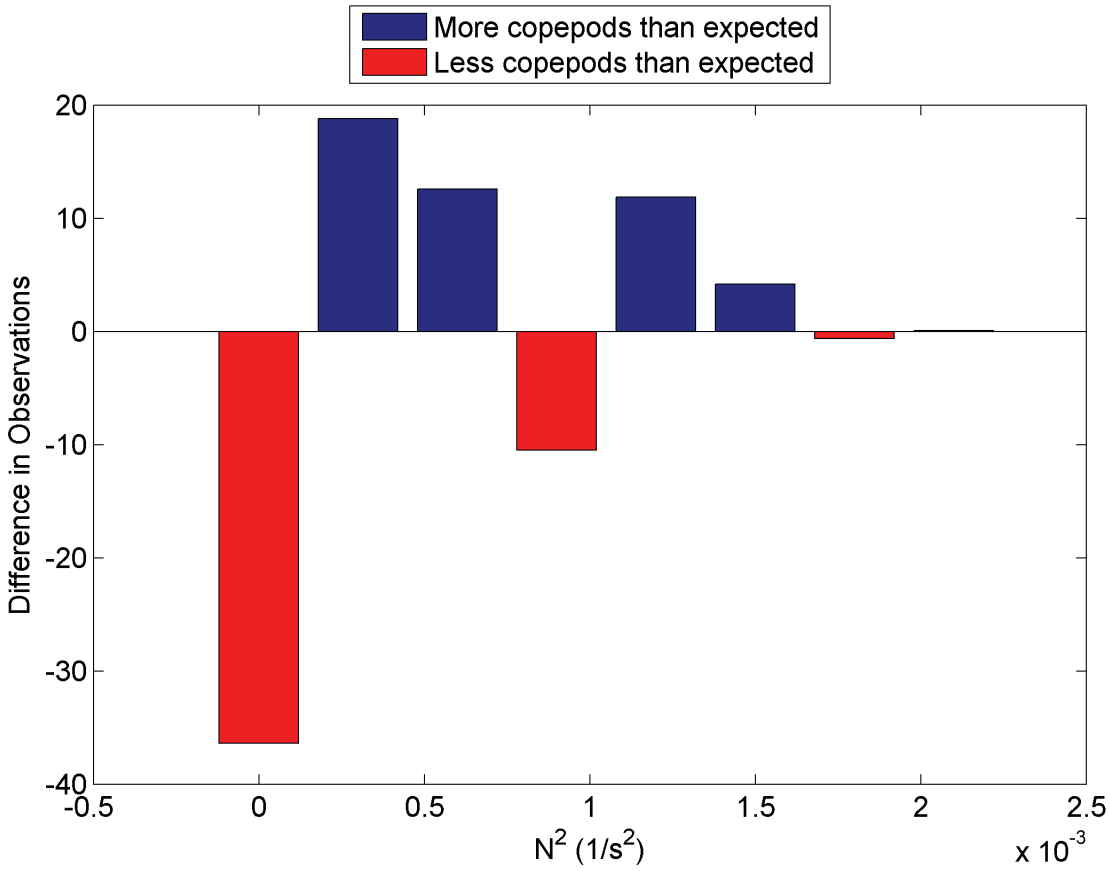


Figure 3.20: Relative differences between the expected and observed observations of copepods per squared buoyancy frequency bin. The x-axis represents the $3 \cdot 10^{-4}$ $1/\mathrm{s}^2$ binned squared buoyancy frequency and the y-axis is the difference in observations between the expected (all observations scaled to the number of total copepod observations) and observed (total number of copepods present per squared buoyancy frequency bin). The blue bars (positive) represent the bins where there are more copepods than expected if copepods were not distributed differently among squared buoyancy frequency bins. The red bars (negative) represent the bins where there are fewer copepods than expected if copepods were not distributed differently among squared buoyancy frequency bins.

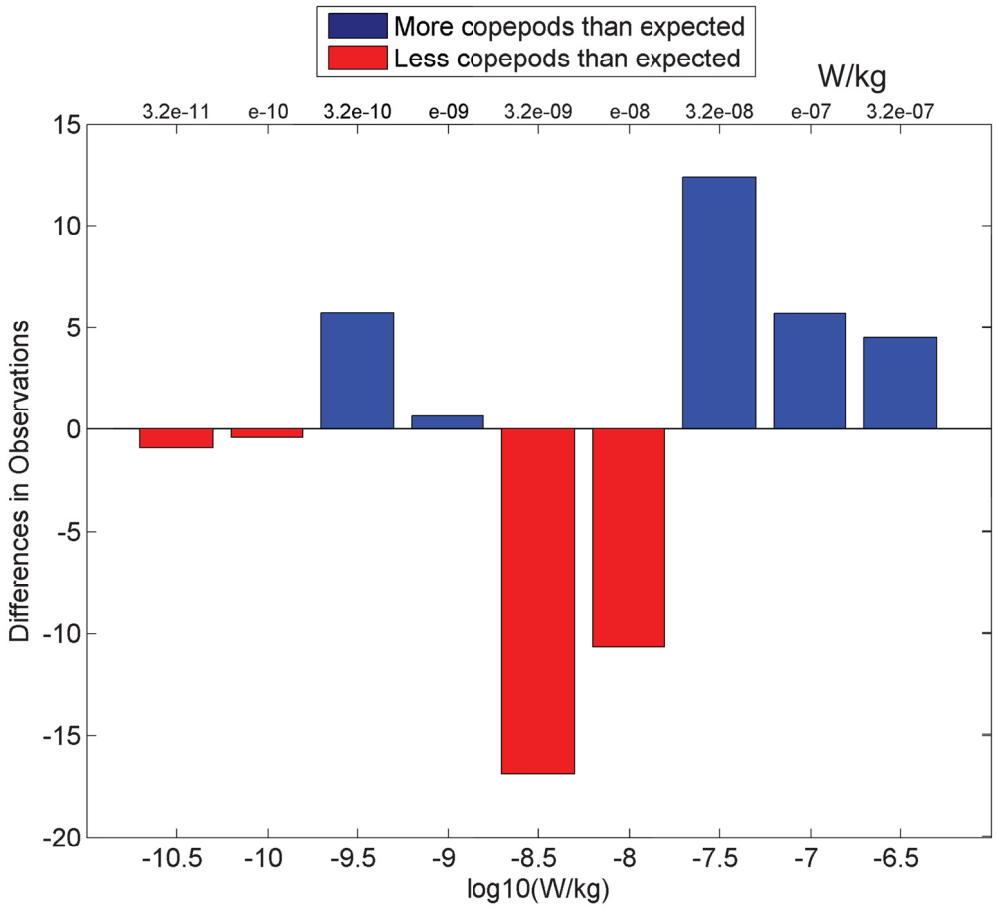


Figure 3.21: Relative differences between the expected and observed observations of copepods per $log_{10}$ dissipation bin. The bottom x-axis represents the 0.5 $log_{10}$ W/kg binned dissipation and the top x-axis is the dissipation arithmetic scale. The y-axis is the difference in observations between the expected (all observations scaled to the number of total copepod observations) and observed (total number of copepods present per $log_{10}$ dissipation bin). The blue bars (positive) represent the bins where there are more copepods than expected if copepods were not distributed differently among $log_{10}$ dissipation bins. The red bars (negative) represent the bins where there are fewer copepods than expected if copepods were not distributed differently among $log_{10}$ dissipation bins.

| Sample Period | In pycnocline # copepods | SR | Below pycnocline # copepods | SR |
|---|---|---|---|---|
| 19 Oct | 79 | 0.25 | 31 | 0.08 |
| 26 Oct | 39 | 0.32 | 45 | 0.21 |
| 03 Nov | 60 | 0.16 | 5 | 0.02 |
| 04 Nov | 176 | 0.40 | 52 | 0.23 |
| 30 Nov | 46 | 0.10 | 2 | 0.01 |

Table 3.2: The copepod SRs for in and below the pycnocline for each sample period.

(1000 $\mathrm{animals/m^3}$), depth ( $\mathrm{m}$), temperature ( $^\circ$C), salinity ($\mathrm{g/kg}$), density ( $\mathrm{kg/m^3}$), buoyancy frequency ( $1/\mathrm{s}^2$) and dissipation ( $\mathrm{W/kg}$) (the multiple linear regression with only one explanatory variable). The top row shows the copepod abundance with respect to each physical variable. The copepod abundance data are discrete while the physical variables are all continuous, resulting in regression fits concentrated at 0 $\mathrm{animals/m^3}$(red line), with weak correlation coefficients ($< 0.13$) but with significant relationships.

## 3.3 Characteristic Sample Period Depths

To determine if the copepod distribution was affected by the location of the pycnocline, the copepod SR was calculated in and below the pycnocline for each sample period (plots shown in Figure 2.7 and Table 3.2). In all cases, the copepod SR was higher in the pycnocline than below it (by as much as a factor of 10), suggesting that the location of the pycnocline affects the vertical distribution of copepods.

The third part of the first objective was to determine if the weighted mean depth of copepods was related to the mean thermocline depth, mean halocline depth, weighted mean squared buoyancy frequency depth or the weighted mean dissipation depth between sample periods. These data were compared using a linear regression (Figures 3.24 and 3.25), with the one-to-one depth relationship shown (red line). The figures show standard error bars, calculated simply $SE = s/\sqrt{n}$ where $s$ is the weighted standard deviation (the standard deviation weighted by $V/\sum_{i=1}^{n} V$ of the observations, $n$ is the number of observations and $V$ is the value of the variable (copepod abundance, buoyancy frequency or dissipation).

For the 19 October and 26 October, the weighted mean copepod depth was below the thermocline (Figure 3.24 left panel) and for the November data (03, 04 and 30), the

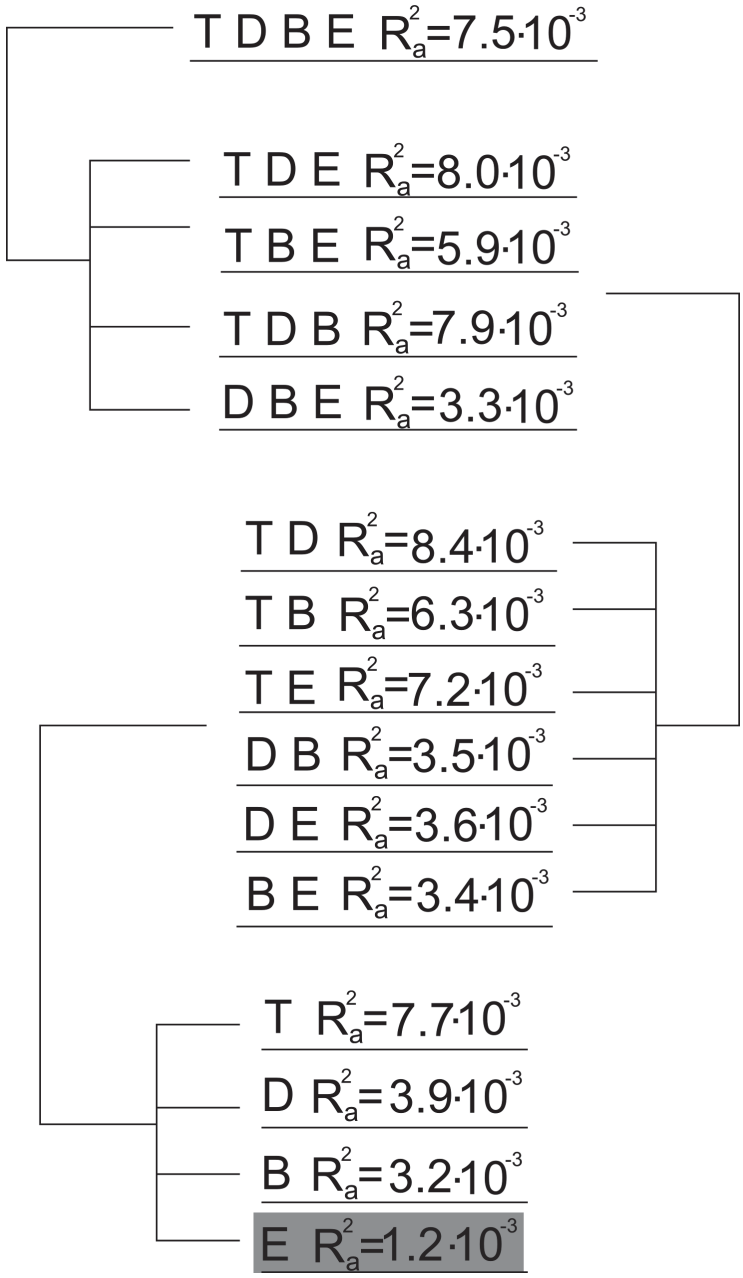


Figure 3.22: Results of the multiple linear regressions. The top line represents the multiple regression including all four variables, temperature (T), density (D), squared buoyancy frequency (B) and dissipation (E), along with the $R_a^2$ value for that particular regression. The second block of lines represent the multiple regressions containing all possible combinations of three variables, along with the $R_a^2$ values. The third block of lines contain multiple regressions for all possible combinations of only 2 independent variables, along with the $R_a^2$ values. The last block shows the results for each variable used in the regression as the only independent variable (simple linear regression).

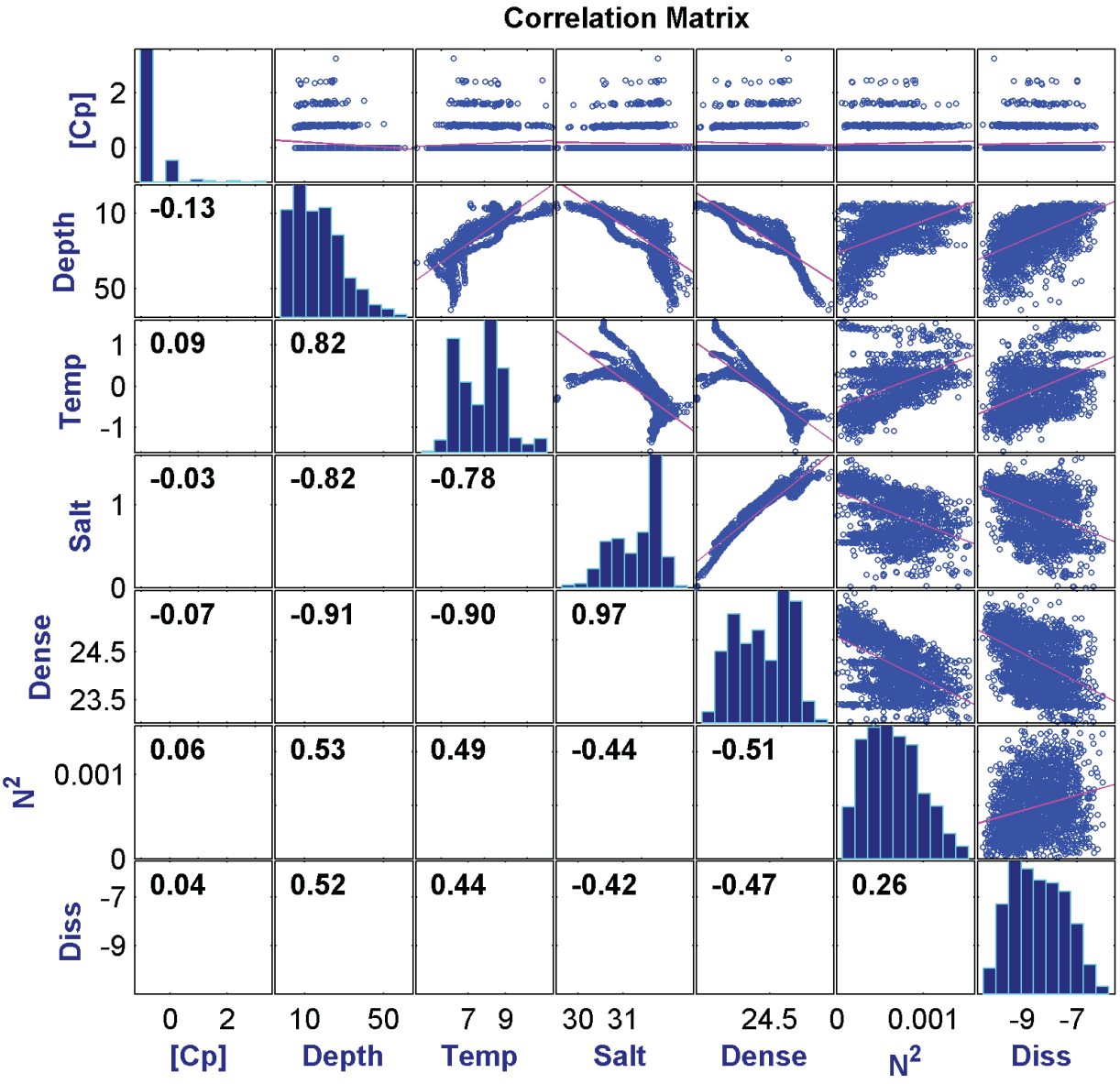


Figure 3.23: A correlation matrix plot to show the simple linear regression between all variables (copepod abundance (1000 $\mathrm{animals/m^3}$), depth ( $\mathrm{m}$), temperature ( $^\circ$C), salinity ($\mathrm{g/kg}$), density ( $\mathrm{kg/m^3}$), buoyancy frequency ( $\mathrm{1/s^2}$) and dissipation ( $\mathrm{W/kg}$)). The diagonal elements show the distribution of the data (temperature, salinity, density, buoyancy frequency and dissipation all transformed as described earlier). The plots above the diagonal show the relationship between the row and column parameters, with the red line representing the regression. The numbers below the diagonal show the correlation coefficient for each regression, mirrored across the diagonal (e.g. correlation in the first column in the second row is for the plot located in the second column and first row). The parameters are listed (top to bottom, left to right): copepod abundance (1000 $\mathrm{animals/m^3}$) [Cp], depth ( $\mathrm{m}$), temperature ( $^\circ$C), salinity ($\mathrm{g/kg}$), density ( $\mathrm{kg/m^3}$), buoyancy frequency ( $\mathrm{1/s^2}$) and dissipation ( $\mathrm{W/kg}$).

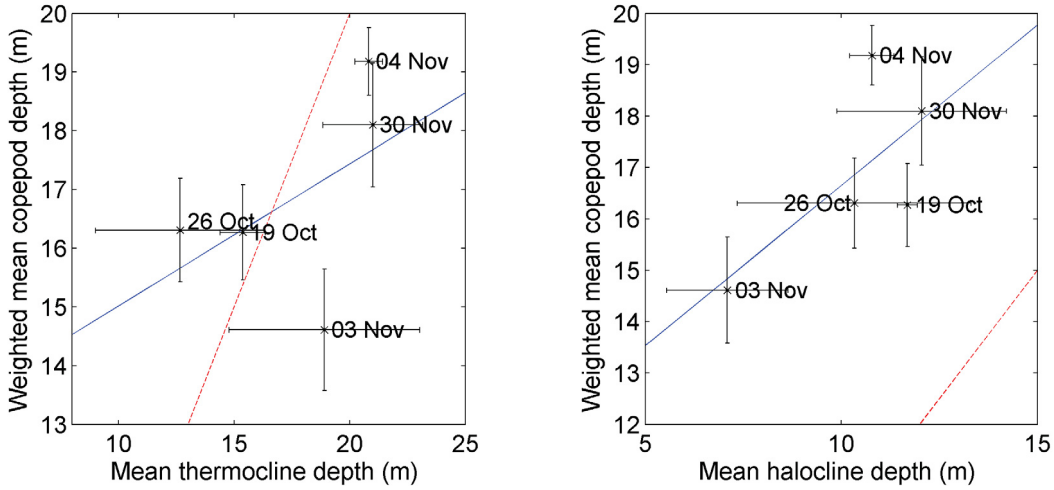


Figure 3.24: Linear regressions for the weighted mean copepod depth vs. the thermocline (left) and halocline (right) depths. Both the x and y-axis are depth in metres. For both plots, the points represent the mean thermocline or halocline depth for each sample period day and the weighted mean copepod depth. The blue line is the linear fit between the two variables. The red line represents the one-to-one line (if the weighted mean copepod depth and mean variable depths aligned). Both plots contain standard errors in the x and the y to show the spread of the data (the copepod weighted mean is minimal because the weights were varied little.)

weighted mean copepod depth was found above the thermocline.

The weighted mean copepod depth was always below the halocline (Figure 3.24 right panel), which tended to be the shallowest mean depth overall ( $< 12$ m for every sample period). The variability from the linear regression was fairly high and the correlation between the mean copepod and halocline depths was 0.69.

For most sample periods (19 October, 26 October, 03 November and 04 November, Figure 3.25 left panel), the weighted mean copepod depth was below the mean peak squared $N^2$, suggesting the copepods stayed below the heightened $N^2$ values. The correlation between the weighted mean copepod depth and weighted mean squared $N^2$ depth was 0.48 (Table 3.3).

On most days, copepods (19 October, 26 October, 03 November and 04 November) stayed below the weighted mean dissipation depth (Figure 3.25 left panel). The correlation between the median copepod depth and mean dissipation depth was 0.39, giving the weakest correlation of all the characteristic sample period depths (Table 3.3).

In all cases, these regressions are not significant (p-values $>> 0.05$), likely a function

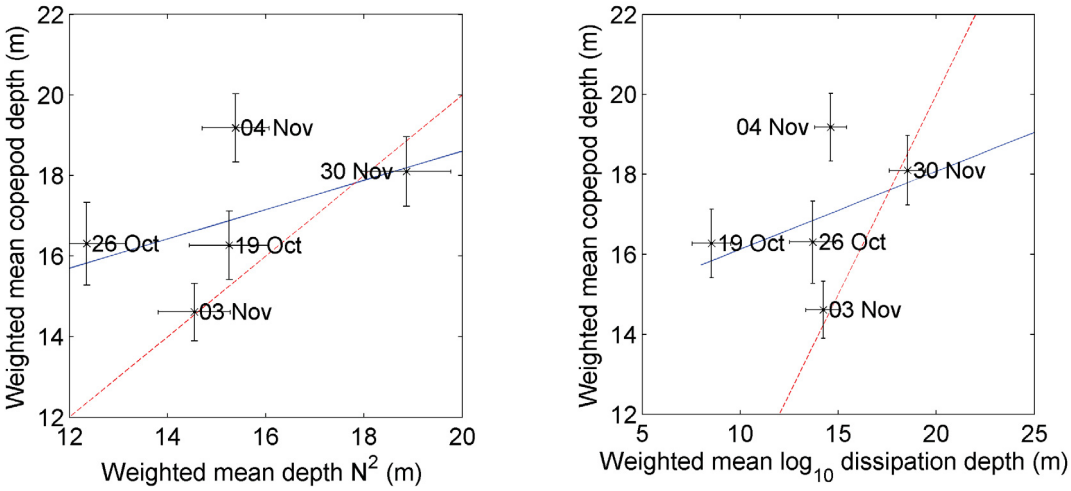


Figure 3.25: Linear regressions for the weighted mean copepod depth vs. the the weighted mean $N^2$ (left) and weighted mean dissipation depths (right). Both the x and y-axis are depth in metres. For both plots, the points represent the weighted mean $N^2$ or dissipation depth for each sample period day and the weighted mean copepod depth. The blue line is the linear fit between the two variables. The red line represents the one-to-one line (if the weighted mean copepod depth and mean variable depths aligned). Both plots contain standard errors in the x and the y to show the spread of the data (the copepod weighted mean is minimal because the weights were varied little).

| | Copepod WMD | Thermocline Depth | Halocline Depth | $N^2$ WMD | Dissipation WMD |
|---|---|---|---|---|---|
| Copepod WMD | 1 | 0.50 | 0.69 | 0.48 | 0.39 |
| Thermocline depth | 0.50 | 1 | $2 \cdot 10^{-3}$ | 0.78 | 0.61 |
| Halocline depth | 0.69 | $2 \cdot 10^{-3}$ | 1 | 0.45 | $-2 \cdot 10^{-3}$ |
| $N^2$ WMD | 0.48 | 0.78 | 0.45 | 1 | 0.50 |
| Dissipation WMD | 0.39 | 0.61 | $-2 \cdot 10^{-3}$ | 0.50 | 1 |

Table 3.3: Correlations between each characteristic sample period depth for copepod abundance, temperature, salinity, $N^2$ and $log_{10}$ dissipation.

of the low number of points (only 5).

## 3.4 Vertically and Sample Period Averaged Data

My second objective was to determine if the mean abundance of copepods was affected by changes in the mean state of the physical variables between sample periods. The total number of copepods observed for each sample period for depths 7-29 $\mathrm{m}$ is shown in Table 3.4 (column 2) and the greatest number of copepods were sampled on 04 November, with 45.5% of the total sample population. However, sampling occurred more frequently that day. Using the sample ratio (SR) outlined in Chapter 2, the copepod data were standardized (Table 3.4 column 4) and reveal that, in decreasing order, 04 November, 26 October, 19 October, 03 November and 30 November have the most copepods per sample potential. To compare the effect of as many of the physical variables as possible on the copepod abundance, characteristic values for each physical variable were also calculated (Table 3.4, again refer to Chapter 2 for details of how each was calculated).

The highest number of copepod observations were collected on 04 November. The variable that changed the most between the sample days was that data collected on 04 November were sampled in both the daytime and the night-time whereas all other days were sampled only during the day. Using another sample ratio (SR) calculation, it was determined that the pre-dawn (data pre-dawn for 04 November) $SR = 0.40$ and that the post-dawn (data from 19 October, 26 October, 03 November, post-dawn 04 November and 30 November) $SR = 0.20$. (Notice that these values are different from the binned SR computed in Section 3.2.2.1 because this SR was calculated for depths 7-29 $\mathrm{m}$ only).

Linear regression plots comparing these data are shown in Figures 3.26-3.29. The correlation between each of these variables and the copepod sample ratio is recorded in Table 3.5. The figures show standard error bars where possible, simply $SE = s/\sqrt{n}$ where $s$ is the standard deviation of the observations and $n$ is the number of observations.

Of the seven physical variables, time since high tide (Table 3.5) has the strongest correlation with the copepod SR (0.73) and wind (-0.36) and $log_{10}$ dissipation have the weakest (0.21). Temperature, salinity, density, buoyancy frequency and wind all have relatively high correlations with the copepod SR. Even though there are some high correlation coefficients, in all cases, these regressions are not significant (p-values always $>> 0.05$, also due to the low number of points, only 5).

| Sample Day | No. of Copepods | No. of 1 m bins | SR | Wind Speed m/s | Time since low tide (h) | Light (day/ night) |
|---|---|---|---|---|---|---|
| 19 Oct | 81 | 313 | 0.23 | 8 | 0.93 | Day |
| 26 Oct | 60 | 205 | 0.27 | 4 | 6.49 | Day |
| 03 Nov | 48 | 372 | 0.13 | 4 | -1.62 | Day |
| 04 Nov | 188 | 475 | 0.41 | 0.5 | 7.40 | Night/Day |
| 30 Nov | 36 | 365 | 0.09 | 4 | 3.07 | Day |
| Sample Day | Temp. °C | Sal. g/kg | Density $\mathrm{kg/m^3}$ | Peak $N^2$ $1/s^2$ | $\varepsilon$ $log_{10}$ (W/kg) | |
| 19 Oct | 8.37 | 31.22 | 1024.22 | $2.2 \cdot 10^{-3}$ | $-7.76$ | |
| 26 Oct | 7.66 | 31.30 | 1024.38 | $2.2 \cdot 10^{-3}$ | $-7.58$ | |
| 03 Nov | 7.85 | 31.14 | 1024.24 | $3.1 \cdot 10^{-3}$ | $-7.12$ | |
| 04 Nov | 7.71 | 31.14 | 1024.25 | $1.4 \cdot 10^{-3}$ | $-7.58$ | |
| 30 Nov | 8.44 | 30.77 | 1023.86 | $1.7 \cdot 10^{-3}$ | $-8.25$ | |

Table 3.4: Data from Bedford Basin during sampling. For the upper table, Column 1 is the sample date. Column 2 is the total number of copepods sampled that day between depth bins 7 and 29 m. Column 3 shows the total number of 1 m depth bins sampled between 7 and 29 m. Column 4 is the SR between 7-29 m depth for the day (column 2 divided by column 3). The maximum wind during sampling is outlined in column 5. Columns 6 displays the average time since low tide. The light index is in column 7, outlining the days when sampling occurred pre- and post-dawn. For the lower table, Column 1 is the sample date. Columns 2-4 represent the mean temperature, salinity and density for each sample period, respectively. Column 5 is the peak $N^2$ and column 6 is the mean dissipation for the day.

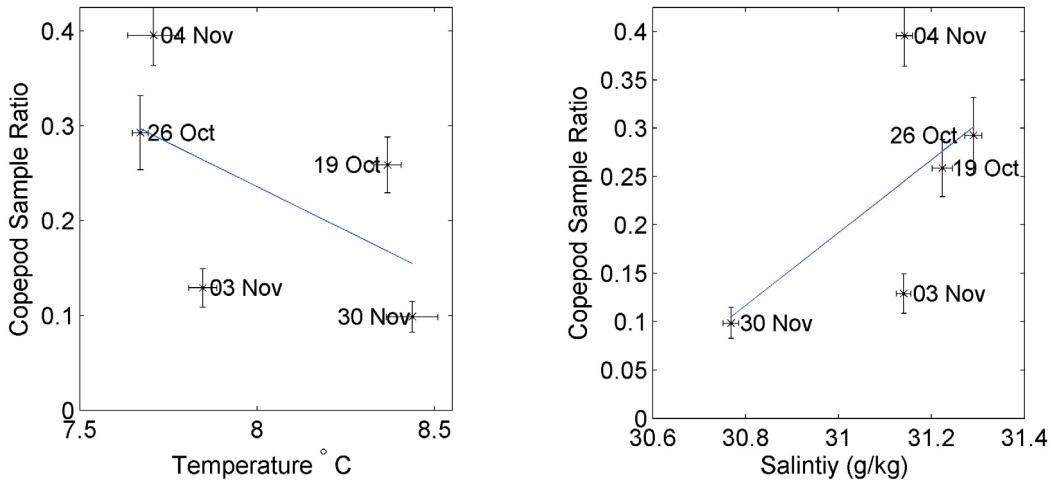


Figure 3.26: Linear regressions between the copepod SR between 7-29 $\mathrm{m}$ depth vs. the mean temperature and salinity over each sample period. The left panel is the the copepod SR vs. the mean temperature for all sample periods. The x-axis is the temperature (in $^{\circ}$C) and the y-axis is the copepod SR (unitless). The right panel is the copepod SR vs. salinity for all sample periods. The x-axis is the salinity ($\mathrm{g/kg}$) and the y-axis is the copepod SR (unitless). For both plots, the points represent copepod SR and the mean temperature or salinity for each sample period. The blue line is the linear fit between the two variables. Both plots contain standard errors in the x and the y to show the spread of the data.

| | Copepod | Temperature | Salinity | Density |
|---|---|---|---|---|
| Copepod | 1 | -0.56 | 0.62 | 0.66 |
| Temperature | -0.56 | 1 | -0.61 | -0.77 |
| Salinity | 0.62 | -0.61 | 1 | 0.97 |
| Density | 0.66 | -0.77 | 0.97 | 1 |
| $N^2$ | -0.46 | -0.18 | 0.36 | 0.34 |
| Dissipation | 0.21 | -0.51 | 0.34 | 0.42 |
| Wind | -0.36 | 0.64 | 0.16 | -0.05 |
| Time since low tide | 0.73 | -0.44 | 0.12 | 0.22 |
| | $N^2$ | Dissipation | Wind | Tide |
| Copepod | -0.46 | -0.20 | -0.36 | 0.73 |
| Temperature | -0.18 | -0.51 | 0.64 | -0.44 |
| Salinity | 0.36 | 0.34 | 0.16 | 0.12 |
| Density | 0.34 | 0.42 | -0.05 | 0.22 |
| $N^2$ | 1 | 0.84 | 0.37 | -0.75 |
| Dissipation | 0.84 | 1 | -0.14 | -0.53 |
| Wind | 0.37 | -0.14 | 1 | -0.59 |
| Time since low tide | -0.75 | -0.53 | -0.59 | 1 |

Table 3.5: Correlation coefficients for the copepod SR and the characteristic value for each physical variables.

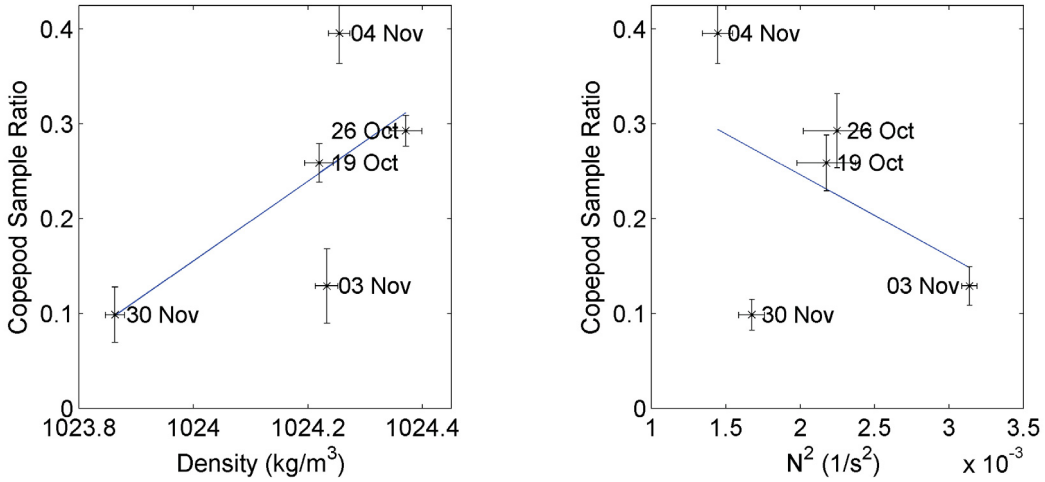


Figure 3.27: Linear regressions between the copepod SR vs. the mean density and mean peak $N^2$ over each sample period. The left panel is the the copepod SR vs. the mean density for all sample periods. The x-axis is the density (in $\mathrm{kg/m^3}$) and the y-axis is the copepod SR (unitless). The right plot is the copepod SR vs. $N^2$ for all sample periods. The x-axis is the squared buoyancy frequency ($1/\mathrm{s}^2$) and the y-axis is the copepod SR (unitless). For both plots, the points represent copepod SR and the mean density or mean peak squared buoyancy frequency for each sample period. The blue line is the linear fit between the two variables. Both plots contain standard errors in the x and the y to show the spread of the data.

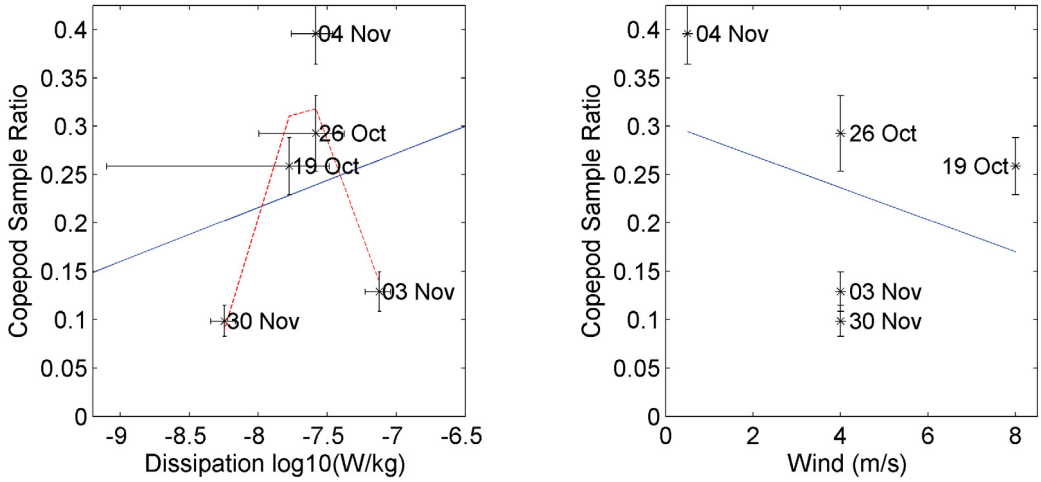


Figure 3.28: Linear regressions between the copepod SR between 7-29 $\mathrm{m}$ depth vs. the mean $log_{10}$ dissipation (left) and maximum wind speed (right) over each sample period. For both plots, the points represent copepod SR and the mean $log_{10}$ dissipation or maximum wind speed for each sample period. The blue line is the linear fit between the two variables. Also included in the left panel (dissipation) is a quadratic fit of the copepod SR to the $log_{10}$ dissipation rates. Both plots contain standard errors in the x and the y to show the spread of the data. No variability is supplied in the wind data because there was only one data point available during each sample period. The variability in the $\varepsilon$ is large because $\varepsilon$ is the most intermittent signal measured and changes significantly between depth bins.

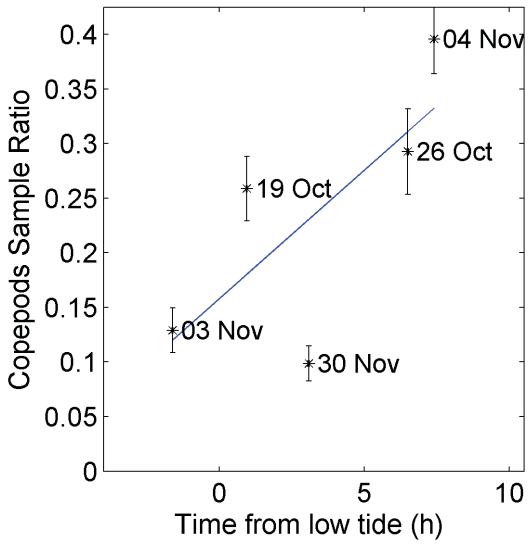


Figure 3.29: Linear regressions between the copepod SR vs. time since low tide over each sample period. The x-axis is the time since low tide (in hours) and the y-axis is the copepod SR (unitless). The points represent copepod SR and time since low tide for each sample period. The blue line is the linear fit between the two variables. Both plots contain standard errors in the x and the y to show the spread of the data.

# CHAPTER 4

# DISCUSSION

The main goal of this project was to determine if the distribution of copepods in Bedford Basin is affected by variables in their physical environment, on both the small (1 m) and large (water column averaged) scales. My results show that the vertical distribution of copepods is controlled by water mass properties (temperature, salinity and density) and their abundance varies with light and tide on larger time scales, suggesting that understanding the distribution of copepods in Bedford Basin requires a multi-variate approach.

## 4.1 Turbulence

In recent years, many researchers have focused on small-scale turbulence and its effect on the vertical distribution of copepods. Results varied from study to study on whether the vertical distribution of copepods was affected by turbulence. Field studies mainly discussed whether turbulence affected the vertical distribution of copepods via avoidance, i.e. copepods avoid high levels of turbulence. As an extension of this avoidance hypothesis, it has also been suggested by *Visser and Stips* (2002) that copepods' population production would be distributed with respect to turbulence in a dome-shape: lower population production at the high and low ends of the spectrum and higher population production in the intermediate levels. All of my results suggest that turbulence does not affect either the vertical distribution of copepods or copepod abundance in Bedford Basin. Copepods in Bedford Basin are evenly distributed with respect to $\varepsilon$ ($\chi^2$ test result) and the weighted mean depth of $\varepsilon$ does not affect the weighted mean depth of the copepods (weak correlation of 0.39). As well, dissipation does not statistically model the abundance of copepods alone,

or with any combination of variables (multiple regression and mean $\varepsilon$ regression with copepod SR).

My results are inconsistent with the cases *Incze et al.* (2001) and *Lagadeuc et al.* (1997) where copepods appear to avoid heightened turbulence in the field. In these studies, there was a 'wind event' (calm waters followed by increased winds back to calm waters) to trigger this avoidance behaviour. The maximum values of $\varepsilon$ measured in my study were similar to the heightened $\varepsilon$ in *Incze et al.* (2001), yet in my field study there was no turbulence avoidance. In the *Incze et al.* (2001) paper, the mean values of $\varepsilon$ reached $10^{-6}$ $\mathrm{W/kg}$, suggesting that the instantaneous values they measured were above $10^{-6}$ $\mathrm{W/kg}$. However, in my study the sample period $\varepsilon$ means were $10^{-8}$ $\mathrm{W/kg}$. Also, the measurements of $10^{-6}$ $\mathrm{W/kg}$ in the *Incze et al.* (2001) paper were maintained over a relatively long period ($\sim$12 hours) whereas my measurements of $10^{-6}$ $\mathrm{W/kg}$ were calculated instantaneously and the high dissipation rate was not consistently maintained during my sampling periods. However, I did not observe a similar event to these wind events. If such a wind event did occur, it might cause the overall instantaneous dissipation rates to reach levels higher than measured and trigger this escape reaction.

My results are also inconsistent with the concept of copepods following a dome-shaped distribution with respect to turbulence, which may be due to the size of the copepods. The physical environment may be dominating the copepod behaviour at the higher $\varepsilon$ levels. For these copepods, high $\varepsilon$ may be the intermediate ranges measured and the low levels, where they are concentrated, may be optimal for encounter rates for these small copepods.

This study focused on measuring small-scale, instantaneous turbulence and assessing its effect on copepods found within the water column. However the mean effect of turbulence, not instantaneous turbulence, may affect the vertical distribution of copepods. For example, despite the fact that *Incze et al.* (2001) had high-resolution turbulence, the turbulence levels were interpreted as high or low near-surface turbulence. I tested both regimes (small-scale with multiple linear regression and large scale with mean $log_{10}$ dissipation depth and mean $log_{10}$ sample period) and neither produced results that suggest copepods are influenced by $\varepsilon$.

Therefore, I conclude that the vertical distribution and mean abundance of copepods in Bedford Basin is not controlled by turbulence, but it may be important in other (perhaps oceanic) environments.

## 4.2 Depth and Light

Diel vertical migration (DVM) very likely affects the vertical distribution of copepods in Bedford Basin. Light is a well known, and studied, trigger for DVM in copepods. This suggests that during daylight hours I would expect to see copepod populations concentrated at depth and sparse numbers at the surface and the opposite for night. The sample ratios (SR) comparing vertical distributions (BSR for night was 0.16 and for day 0.11 for all depths while SR for night was 0.4 and was 0.2 for day for 7-29 $\mathrm{m}$) suggest that light affects the vertical distribution of copepods. This supports the conclusion that light is an important factor affecting the vertical distribution of copepods, suggesting that copepods in Bedford Basin are diel-vertical migrators.

## 4.3 Tides

Tides are likely driving currents that transport copepods into and out of Bedford Basin, affecting their mean abundance and perhaps their vertical distribution. The correlation between the copepod SR and the time that has passed since low tide for the sample period (-0.75) suggests that the time since low tide affects the vertical distribution of copepods; this suggests that tidally-induced currents may be transporting copepods into and out of the basin, depending on the tidal stage (i.e. flood or ebb). To further explore the effect of the tide on the abundance of copepods in Bedford Basin, I calculated a SR for the flood and the ebb tide (number of copepods sampled during each regime over the number of total samples during each regime). The ebb SR (0.28) was larger than the flood SR (0.18), suggesting that the copepod abundance in Bedford Basin is more likely changing due to copepods being flushed out of the basin rather than being flushed into the basin. However, more tidal states need to be measured to remove the possible influence of other factors.

## 4.4 Winds

As with the tide data, it may be expected that the abundance of copepods is affected by wind stress via wind-driven currents in Bedford Basin transporting copepods into or out of the basin. Wind data has also been used in the past as a proxy for $\varepsilon$ (usually in studies where high-resolution shear data are unavailable) but recently *Reiss et al.* (2002) showed

that in their case wind is a poor proxy for estimating dissipation rates, especially far from the surface. The correlation between the copepod SR and the maximum wind speed during the sampling period (-0.36) suggests that either 1) the wind-driven currents are not carrying copepods into or out of the basin or 2) there are not a significant number of copepods transported.

## 4.5 Food Availability and Feeding

From *Jeffries* (1962) results on his study of *E. herdmani*, he suggested that food availability be considered in the description of the vertical distribution of copepods. He suggested that the vertical distribution of copepods could change depending on where food is located within the water column and how much is available. This was tested in *Dam and Peterson* (1993) (for *Temora longicornis*), who concluded that the copepods vertical structure is not determined by the vertical distribution of of chlorophyll, suggesting that food is not a primary factor in determining the vertical distribution of copepods. In a study of Bedford Basin, *Poulet* (1978) also suggests that in most estuaries food is not a limiting factor, hence I assume the vertical distribution of copepods would not change based on food. As well, in their paper analysing a 14 year record of phytoplankton and zooplankton in Bedford Basin, *Li and Harrison* (2008) conclude that there is no significant signal between the changes in the phytoplankton distribution and changes in the copepod distribution. Despite the fact that my work did not include measurements of copepod food sources in Bedford Basin, during the sample periods, the assumption that food is not limited is being made, hence the vertical distribution of copepods unlikely to be solely affected by food.

## 4.6 Water Mass Properties

The copepod species in Bedford Basin may be expected to be found in cooler (*Corkett and McLaren*, 1978), more saline (*Johnson and Allen*, 2005) and higher density gradient waters (*Tiselius et al.*). These three variables are highly correlated (salinity and density in particular for this study) and it is difficult to determine which factor has the greatest effect on the vertical distribution of copepods. However, it is clear they are important to the vertical distribution of copepods, as the copepods were found much more frequently in the pycnocline. Usually surface waters are warmer, less saline and less dense and often

the thermocline, halocline and pycnocline align. The results from the $\chi^2$ test suggested that copepods are not distributed evenly amongst temperature, salinity and density. From the linear regression of the high-resolution data on the copepod abundance, temperature was more important in determining copepod abundance ($R_a^2 = 7.7 \cdot 10^{-3}$) than salinity ($R_a^2 = 4.4 \cdot 10^{-4}$) or density ($R_a^2 = 3.9 \cdot 10^{-3}$), but altogether these three variables best model the high-resolution copepod abundance ($R_a^2 = 2.3 \cdot 10^{-2}$). This is consistent with the correlations between the thermocline and halocline and their regressions with the copepod weighted mean depth (0.5 and 0.69 respectively) as well as the SR values from within and below the pycnocline. These results show that copepods generally tend to be found in the pycnocline, in less dense waters.

Conversely, *Gallager et al.* (2004) observed that *Pseudocalanus* spp. are located well below relatively high $N^2$ (highly stratified) waters, suggesting that copepods avoid highly stratified waters such as the pycnocline. Based on this work, I might expect to see copepods concentrated below the peak $N^2$ depth. The $\chi^2$ test result suggests that copepods are evenly distributed with respect to $N^2$. The comparison of the weighted mean depth of copepods and the weighted mean depth of the $N^2$ show that copepods are generally below the peak $N^2$, where $N^2$ values tend to be near 0. This may explain the $\chi^2$ result: the copepods are distributed evenly in $N^2$ space because most of the copepods are in waters below the peak $N^2$, where $N^2 = 0$. It would be expected that the pycnocline depth and the $N^2$ are related, but the results are conflicting. However, the peak $N^2$ depth is not the same as the pycnocline. The pycnocline is a range of depths, not just one depth value, as I reported the $N^2$ WMD, suggesting why the results are inconsistent. The result from the linear regression correlation (-0.46) is a weak negative relationship suggesting that as the peak $N^2$ increases, the overall copepod abundance decreases. When $N^2$ was used as the only independent variable in the linear regression for the high-resolution data, with copepod abundance as the dependent variable, the $R_a^2$ was extremely small, suggesting that the abundance of copepods is not affected by $N^2$. Therefore I conclude $N^2$ does not describe the copepod distribution in Bedford Basin. Inferences about how the *Pseudocalanus minutus* were distributed from *Gallager et al.* (2004) may help us to further understand my results.

*Gallager et al.* (2004) observed that the copepod population on George's Bank consisted mainly of *Calanus finmarchicus* and some *Pseudocalanus* spp. Their results showed that

phytoplankton were concentrated at peak $N^2$ depths throughout the water column and that the *C. finmarchicus* species were concentrated in density gradients, usually $2\ \mathrm{m}$ above peak $N^2$ values. However, the *Pseudocalanus* spp. were not concentrated near these peak $N^2$ values, and were in fact much lower in the water column, suggesting that they may be avoiding their competition (*C. finmarchicus*). Thus, since the *Pseudocalanus* spp. copepods may be responding to their food or competition, which are distributed with respect to $N^2$, there may be a relationship between $N^2$ and *Pseudocalanus* spp.. However, as I discussed previously, *Pseudocalanus* spp. copepods in Bedford Basin may not align themselves with phytoplankton because the supply of food within the basin may be abundant enough that *Pseudocalanus* spp. do not need to seek out high concentrations of food. Also, the population of *C. finmarchicus* in Bedford Basin is minimal compared to the *Pseudocalanus* spp. and other small copepod species. Therefore, based on these inferences regarding the distribution of food and competition, I might not expect to see the same relationship between the vertical distribution of copepods and buoyancy frequency in Bedford Basin.

# CHAPTER 5

# CONCLUSIONS

Studying in situ, bio-physical relationships is complicated and these relationships cannot be explained simply by only one physical variable controlling changes in copepod distributions. Copepods live in a highly dynamic world and are affected by the physics controlling their environments on different length scales.

The overall goal of this project was to determine if the vertical distribution of copepods in Bedford Basin is affected by its physical environment, in particular turbulence. To accomplish this I tested whether copepods were evenly distributed with respect to high-resolution physical variables (using a $\chi^2$ test) and tested whether the weighted mean depth of the copepods was affected by a characteristic depth for high-resolution physical variables (using linear regressions and correlations). I concluded that turbulence does not affect the vertical distribution of copepods in Bedford Basin and that it is explained best by light through DVM and by a combination of temperature and density.

The second overall goal of this thesis was to determine if the copepod abundance is affected by physical variables on a large-scale. To accomplish this goal, I tested whether the copepod abundance changed between sample periods based on the physical environment (linear regressions for copepod abundance with high-resolution physical variables and linear regressions of copepod abundance sample ratios with characteristic physical variable values). I concluded that tidal currents flushing copepods out of Bedford Basin and light have the strongest effect on the overall copepod abundance.

The results from this work show the necessity for coincident high-resolution observations to improve the understanding of bio-physical relationships. One of the most important aspects of this work is the addition of high-resolution observations of turbulence and

copepod abundances to the field of research. Even though these results conclude that turbulence does not have an effect on the vertical distribution of copepods in Bedford Basin, this adds important data to a field in which data is scarce and the prospective projects using this novel approach are exciting.

## 5.1 Suggestions for Future Work

To continue studying the relationship between copepods and their physical environment, I would suggest the following additions and changes to a sampling program. First, the number of copepods sampled was quite small due to the small sample volume of the camera. To increase the sample population, sampling should occur: over a longer time period (more casts), during the peak copepod population season and over more days (to have more daily mean data to analyse). If sampling were to continue in Bedford Basin, I would suggest sampling once a week over the course of many seasons (a full year if possible) to observe all possible copepod abundances in Bedford Basin, as well as to observe changes in the physical environment that come with the different seasons (e.g. in the summer temperatures are higher. How will that effect the vertical distribution of copepods?). I would also suggest sampling during daytime and nighttime again, particularly well before twilight to ensure that any copepods exhibiting DVM would not have started descending. I would also use a light sensor to measure the amount of light during the sample period to distinguish between sampling during sunny and cloudy days as well as between daylight, twilight and night-time. To determine the extent of the horizontal advection of copepods into or out of the basin (if there is any), a moored ADCP, to observe the tidal currents, along with an Optical Plankton Counter (OPC), both located at the mouth of Bedford Basin would be interesting. To directly compare to other field studies, sampling during a wind event may produce similar results, though predicting a wind event would not be trivial. Finally, adding chlorophyll measurements to the dataset could address the idea that the distribution of food affects the vertical distribution of copepods in estuaries.

# APPENDIX A

# TURBULENCE

Turbulence in the ocean is ubiquitous. By definition, a turbulent flow is characterized by (*Baumert et al.* (2005) and *Kundu and Cohen* (2008)):

- Randomness: The flow is unpredictable and irregular. Two flows whose starting states are slightly different will evolve into two completely different flows and both would be impossible to describe as a function of space and time.
- 3-Dimensional vorticity: The structures found in the flow are broadly termed "eddies" and span a large length scale, from scaling order O($10^{-2}$)m to O($10^{5}$)m, which are represented in all three physical dimensions.
- Dissipation: The flow is strongly affected by vortex stretching which transfers energy and vorticity from large eddies to increasingly smaller scales.
- Diffusivity: Through rapid mixing, the flow transfers both momentum and heat.

The Reynold's number is used to determine whether or not a flow is considered turbulent. It arises from the fluid momentum equations (*Kundu and Cohen* (2008)):

$$\rho(\frac{d\vec{u}}{dt} + \vec{u} \cdot \nabla\vec{u}) = -\nabla P + \rho\vec{g} + \mu\nabla^2\vec{u} - 2\rho\vec{\Omega} \times \vec{u} \tag{A.1}$$

$$\vec{\nabla} \cdot \vec{u} = 0 \tag{A.2}$$

where $\rho$ is the density, $\vec{u}$ is the velocity of the flow, $P$ is the pressure, $\vec{g}$ is the acceleration due to gravity, $\mu$ is the dynamic viscosity of the water and $\vec{\Omega}$ is the angular velocity due to

the Coriolis force. The local acceleration term is $\rho\frac{d\vec{u}}{dt}$, $\rho(\vec{u}\cdot\nabla\vec{u})$ is the inertial term, $-\nabla P$ is the pressure gradient, $\rho\vec{g}$ is the buoyancy term, $\mu\nabla^2\vec{u}$ is the viscous/friction term and $-2\rho\vec{\Omega}\times\vec{u}$ is the Coriolis term.

The Reynold's number is the ratio of the inertial forces to the viscous forces and simplifies to:

$$Re = \frac{UL}{\nu} \tag{A.3}$$

where U is a typical velocity of the flow, L is a typical length scale of the flow and $\nu = \frac{\mu}{\rho}$ is the kinematic viscosity of the fluid. Flows which have high Reynold's numbers ($Re >> 1$) are characterized as turbulent and a flow is laminar (or non-turbulent) for low Reynold's numbers ($Re << 1$).

#### A.0.0.1 Derivation of the dissipation rate

If we consider the fluid momentum equations A.1 and A.2 and apply a Reynold's decomposition (on u and P), which assumes the total flow can be represented as, Total Flow ($\tilde{u}$) = Turbulent Fluctuations ($u'$) + Average Flow ($\bar{u}$), then:

$$\rho\frac{D\overrightarrow{(u'+\bar{u})}}{Dt} = -\nabla(p'+\bar{P}) + \rho\vec{g} + \mu\nabla^2\overrightarrow{(u'+\bar{u})} \tag{A.4}$$

Where the left-hand side of equation A.1 has taken the form $\frac{D\vec{u}}{Dt} = \frac{\partial\vec{u}}{\partial t} + \vec{u}\cdot\nabla\vec{u}$. There is no Coriolis term in equation A.4; turbulent dissipation rates are measured on scales small enough to ignore it.

Let the equation of state have the form $\rho' = -\rho_0\alpha(T'+\bar{T}-T_0)$ and apply the Boussinesq approximation ($\frac{\rho'}{\rho_0} << 1$, where $\rho'$ and $\rho_0$ are the densities of the fluctuations and average flow respectively. The thermal expansion coefficient for water is $\alpha$). Averaging equation A.4 over time gives (in tensor notation):

$$\frac{D(u'+\bar{u})}{Dt} = -\frac{1}{\rho_0}\frac{\partial(p'+\bar{p})}{\partial x_i} - g[1-\alpha(T'+\overline{T}-T_0)]\delta_{i3} + \nu\frac{\partial^2(u'+\bar{u})}{\partial x_i^2} \tag{A.5}$$

Since we are interested in the turbulent terms, subtract $\bar{u}$ from $\tilde{u}$ to get $u'$:

$$\frac{\partial u_i'}{\partial t} + \bar{u_j} u_{i,j}' + u_j' \bar{u}_{i,j} + u_j' u_{i,j}' - (\overline{u_i' u_j'})_{,j} = -\frac{1}{\rho_0} p_{,i}' + g\alpha T' \delta_{i3} + \nu u_{i,jj}' \tag{A.6}$$

where $u_{i,j} = \frac{\partial u_i}{\partial x_j}$

To calculate the average turbulent energy flux, multiply equation (A.6) by $u_i'$ and average over time again to get:

$$\frac{D}{Dt}(\overline{\frac{1}{2}(u_i')^2}) + \overline{u_i' u_j'} \bar{u}_{i,j} = -\frac{1}{\rho_0} \overline{u_i' p_{,i}'} + g\alpha \bar{w} \bar{T}' + 2\nu(\overline{u_i' e_{ij}'})_{,j} - 2\nu \overline{e_{ij}' e_{ij}'} \tag{A.7}$$

where $e_{ij}' = \frac{1}{2}(u_{i,j}' + u_{j,i}')$. The term $2\nu e_{ij}' e_{ij}'$ is the turbulent energy dissipation rate $\varepsilon$. It is used as an indicator of turbulence because it includes both the mixing rate and frictional effects. (*Lueck et al.*, 2002, page 154). If isotropic conditions are applied ($u_i u_j = u_0^2 \delta ij$) (*Oakey*, 1982, page 256) then,

$$\varepsilon = \frac{15}{2} \nu (\overline{\frac{\partial u'}{\partial z}})^2 \tag{A.8}$$

The $\frac{\partial \bar{u'}}{\partial z}^2$ term is the variance in the vertical gradient of turbulent fluctuations which the instrument measures via shear probes. This variance of the shear can be used to directly estimate the dissipation rate (*Osborn*, 2007, page 140). The units of Equation A.8 are $\mathrm{W/kg}$.

Kolmogorov also defined two very useful relationships: one relating the Kolmogorov length scale $\eta$ to the dissipation rate $\varepsilon$ and viscosity $\nu$ (Equation A.9) and a velocity scale (known as the Kolmogorov velocity), relating the velocity to the dissipation rate $\varepsilon$ and viscosity $\nu$ (Equation A.10):

$$\eta = (\frac{\nu^3}{\varepsilon})^{1/4} \tag{A.9}$$

$$v = (\varepsilon \nu)^{1/4} \tag{A.10}$$

At the large eddy scale, turbulent energy is produced (through breaking waves, winds, etc.) and at the Kolmogorov length scale, the turbulent energy is dissipated. The range

in between this range is called the inertial subrange (*Kundu and Cohen*, 2008). For homogeneous flows, the turbulent energy distribution can be represented in terms of wavenumbers.

$$E(k) = v^2 \nu E_e(k, \varepsilon, \nu) \tag{A.11}$$

Where $v$ is the velocity of the flow, $\nu$ is the viscosity, $E_e$ is a dimensionless energy, $\varepsilon$ is the dissipation rate and $k$ is the wavenumber (ie. length of the flow in wavenumber space). In the inertial subrange, $E_e$ must take a form such that the right hand side of Equation A.9 is independent of $\nu$. Thus,

$$E(k, t) = \alpha \eta (\eta k)^{-5/3} \tag{A.12}$$

Substituting Equations A.9 and A.10 into Equation A.12 gives:

$$E(k) = C_k \varepsilon^{2/3} k^{-5/3} \tag{A.13}$$

Which is Kolmogorov's famous $-5/3$s law (*Batchelor*, 1953).

# BIBLIOGRAPHY


Batchelor, G. K., *The theory of homogeneous turbulence*, Cambridge University Press, 1953.

Baumert, H. Z., J. H. Simpson, and J. Sunderman, *Marine Turbulence: Theories, Observations and Models*, Cambridge University Press, Cambridge, UK, 2005.

Bollens, S., B. Frost, and J. Cordell, Chemical, mechanical and visual cues in the vertical migration behavior of the marine planktonic copepod acartia hudsonica, *Journal of Plankton Research*, *16*, 555–564, 1994.

Buskey, E., Swimming pattern as an indicator of the roles of copepod sensory systems in the recognition of food, *Marine Biology*, *79*, 165–175, 1984.

Clarke, G. L., Factors affecting the vertical distribution of copepods, *Ecological Monographs*, *4*, 530–540, 1934.

Corkett, C. J., and I. A. McLaren, The biology of *Pseudocalanus*, in *Advances in Marine Biology*, vol. 15, pp. 1–231, Academic Press, 1978.

Cury, P., and C. Roy, Optimal environmental window and pelagic fish recruitment success in upwelling areas, *Canadian Journal of Fisheries and Aquatic Sciences*, *46*, 670–680, 1989.

Dam, H., and W. Peterson, Seasonal contrasts in the diel vertical distribution, feeding behavior, and grazing impact of the copepod temora longicornis in long island sound, *Journal of marine research*, *51*, 561–594, 1993.

Fader, G. B. J., and R. Miller, Surficial geology, halifax harbour, nova scotia, *Geological Survey of Canada Bulletin*, *590*, 2008.

Frost, B., and S. Bollens, Variability of diel vertical migration in the marine planktonic copepod pseudocalanus newmani in relation to its predators, *Canadian Journal of Fisheries and Aquatic Sciences*, *49*, 1137–1141, 1992.

Gallager, S. M., H. Yamazaki, and C. S. Davis, Contribution of fine-scale vertical structure and swimming behavior to formation of plankton layers on georges bank, *Marine Ecology Progress Series*, *267*, 27–43, 2004.

Goodman, L., E. R. Levine, and R. G. Lueck, On measuring the terms of the turbulent kinetic energy budget from an AUV, *JOURNAL OF ATMOSPHERIC AND OCEANIC TECHNOLOGY*, *23*, 2006.

Greenberg, D. A., *Atlas of Tidal Currents for Halifax Harbour*, 1999.

Greenberg, D. A., T. S. Murty, and A. Ruffman, A numerical model for the halifax harbour tsunami due to the 1917 explosion, *Marine Geodesy*, *16*, 1993.

Gregory, D., B. Petrie, F. Jordan, and P. Langille, Oceanographic, geographic and hydrological properties of scota-fundy and southern gulf of st. lawerence inlets., *Canadian Technical Report of Hydrography and Ocean Sciences*, *143*, 1–248, 1993.

Herman, A. W., D. D. Sameoto, and A. R. Longhurst, Vertical and horizontal distribution patterns of copepods near the shelf break south of nova scotia, *Canadian Journal of Fisheries and Aquatic Sciences*, *38*, 1065–1076, 1981.

Incze, L., D. Herbert, N. Wolff, N. Oakey, and D.Dye, Changes in copepod distributions associated with increased turbulence from wind stress, *Marine Ecology Progress Series*, *213*, 229–240, 2001.

Jeffries, H., Salinity-space distribution of the estuarine copepod genus eurytemora, *Internationale Revue der gesamten Hydrobiologie und Hydrographie*, *47*, 291–300, 1962.

Johnson, W. S., and D. M. Allen, *Zooplankton of the Atlantic and Gulf Coasts*, The John Hopkins University Press, 2005.

Kundu, P. K., and I. M. Cohen, *Fluid Mechanics*, fourth ed., Academic Press: Elsevier, 2008.

Lagadeuc, Y., M. Boule, and J. Dodson, Effect of vertical mixing on the vertical distribution of copepods in coastal waters, *Journal of Plankton Research*, *19*, 1183–1204, 1997.

Li, W. K. W., and W. G. Harrison, Propagation of an atmospheric climate signal to phytoplankton in a small marine basin, *Limnology and Oceanography*, *53*, 1734–1745, 2008.

Lueck, R. G., F. Wolk, and H. Yamazaki, Oceanic velocity microstructure measurements in the 20th century, *Journal of Oceanography*, *58*, 2002.

McDougall, T., and P. Barker, *Getting started with TEOS-10 and the Gibbs Seawater (GSW) Oceanographic Toolbox*, 2011.

McLaren, I., Effects of temperature on growth of zooplankton, and the adaptive value of vertical migration, *Journal of the Fisheries Board of Canada*, *20*, 685–727, 1963.

Nasmyth, P. W., Oceanic turbulence, Ph.D. thesis, University of British Columbia, 1970.

NationalResearchCouncil, *National Research Council Canada Sunrise/sunset calculator*, 2010.

Oakey, N., and J. Elliott, Dissipation within the surface mixed layer, *J. Phys. Oceanogr.*, *12*, 171–185, 1982.

Oakey, N. S., Determination of the rate of dissipation of turbulent energy from simultaneous temperature and velocity shear microstructure measurements, *Journal of Physical Oceanography*, *12*, 1982.

Osborn, T., Applicability of turbulence measurement technology to small-scale plankton studies, *Marine Ecology Progress Series*, *347*, 2007.

Pinkerton, M. H., A. N. Smith, B. Raymond, G. W. Hosie, B. Sharp, J. R. Leathwick, and J. M. Bradford-Grieve, Spatial and seasonal distribution of adult *Oithona similis* in the southern ocean: Predictions using boosted regressiosn trees, *Deep-Sea Research I*, *57*.

Platt, T., A. Prakash, and B. Irwin, Phytoplankton nutrients and flushing of inlets on the coast of nova scotia, *Le Naturaliste Canadien (QUE)*, *99*, 253–261, 1972.

Poulet, S., Comparison between five coexisting species of marine copepods feeding on naturally occurring particulate matter, *Journal of Limnology and Oceanography*, *23*, 1126–143, 1978.

Poulet, S., and P. Marsot, Chemosensory grazing by marine calanoid copepods (arthropoda: Crustacea), *Science*, *200*, 1403–1405, 1978.

Reiss, C., A. Anis, C. T. Taggart, J. Dower, and B. Ruddick, Relationships among vertically structured in situ measures of turbulence, larval fish abundance and feeding success and copepods on western bank, scotian shelf, *Fisheries Oceanography*, *11*, 156–174, 2002.

Ross, T., A video-plankton and microstructure profiler for the exploration of in situ connections between zooplankton and turbulence, *Limnology and Oceanography: Methods*, 2013.

Rothschild, B., and T. Osborn, Small-scale turbulence and plankton contact rates, *Journal of Plankton Research*, *10*, 465–474, 1988.

Ruddick, B., A. Anis, and K. Thompson, Maximum likelihood spectral fitting: The batchelor spectrum, *Journal of Atmospheric and Oceanic Technology*, *17*, 1541–1555, 2000.

Shan, S., Numerical study of three-dimensional circulation and hydrography in halifax harbour using a nested-grid ocean circulation model, Master's thesis, Dalhousie University, 2010.

Shan, S., J. Sheng, K. Thompson, and D. Greenberg, Simulating the three-dimensional circulation and hydrography of halifax harbour using a multi-nested coastal ocean circulation model, *Ocean Dynamics*, pp. 1–26, 2011.

Svensen, C., and T. Kiørboe, Remote prey detection in oithona similis: hydromechanical versus chemical cues, *Journal of Plankton Research*, *22*, 1155–1166, 2000.

Syvitski, J., K. Asprey, and K. Leblanc, In-situ characteristics of particles settling within a deep-water estuary, *Deep Sea Research Part II: Topical Studies in Oceanography*, *42*, 223–256, 1995.

Tiselius, P., G. Nielsen, and T. G. Nielsen, Microscale patchiness of plankton within a sharp pycnocline, *Journal of Plankton Research*.

Visser, A. W., and A. Stips, Turbulence and zooplankton production: insights from provess, *Journal of Sea Research*, *47*, 317–329, 2002.

WeatherOffice, *National Climate Data and Information Archive*, 2010.

Webster, D., A. Brathwaite, and J. Yen, A novel apparatus for simulating isotrophic oceanic turbulence at low reynolds number, *Journal of Limnology and Oceanography*, pp. 1–12, 2004.

Yen, J., K. Rasberry, and D. Webster, Quantifying copepod kinematics in a laboratory turbulence apparatus, *Journal of Marine Systems*, *69*, 283–294, 2008.

Zar, J. H., *Biostatistical Analysis*, 4 ed., Prentice-Hall Inc., 1999.